The dissertation Committee for Jong-In Youn certifies that this is the approved version of the following dissertation:

NON-INVASIVE OPTICAL DIAGNOSTICS OF CARTILAGE

Committee:

Thomas E. Milner, Supervisor

Ashley J. Welch

Kenneth R. Diller

Brian J. F. Wong

Emil N. Sobol

NON-INVASIVE OPTICAL DIAGNOSTICS OF CARTILAGE

by

JONG-IN YOUN, B.S., M.S.E.

DISSERTATION

Presented to the Faculty of the Graduate School of

The University of Texas at Austin

in Partial Fulfillment

of the Requirements

for the Degree of

DOCTOR OF PHILOSOPHY

The University of Texas at Austin

December 2002

Dedicate to my fiancé and family,

particularly, in loving memory of my father Tae-Sun Youn

ACKNOWLEDGEMENTS

This dissertation wouldn't exist without the assistance from my supervising professor, Dr. Thomas E. Milner who has inspired me to the world of biomedical optics and guided me in the all aspects of the science and technical issues. In addition, I express my gratitude to Dr. Ashley J. Welch who taught me the fundamental knowledge of laser-tissue interactions in tissue. I also thank other committee members, Drs. Kenneth R. Diller and Emil N. Sobol, for fruitful discussions and suggestions and Dr. Brian Wong, who taught me the nasal septal cartilage extraction technique provided many suggestions and comments for my research. Also, I would like to extend my gratitude to Dr. Gracie Vargas for her assistance to complete the PS-OCT measurements.

No less do I wish to thank my professors in the Biomedical Engineering department at Inje University, who taught and inspired me the broad knowledge of biomedical engineering and Dr. Sung-Soo Kim in Korea Research Institute of Chemical Technology, who guided me in various research projects in biomaterials. I also nod appreciatively to my friends and officemates for their friendship.

Finally, I dedicate this dissertation to my fiancé, Anna Hyun, sister, You Jung Youn, and dear mother, Wae Soo Kim, for their patience and understanding, and, especially, my late father for the uncompromising principles that guided his life and his role model for the development of my personal philosophy of life.

NON-INVASIVE OPTICAL DIAGNOSTICS OF CARTILAGE

Publication No._____

Jong-In Youn, Ph.D.

The University of Texas at Austin, 2002

Supervisor: Thomas E. Milner

With progressive use of lasers in medical applications, a recent focus of cartilage research has resulted in many reports on the investigation of the photobiological effects as well as development of non-invasive optical diagnostic techniques. Studies of the physical process underlying laser-induced stress relaxation have shown a number of mechanical, thermal and optical effects following laser reshaping of cartilage that need to be better understood to optimize the reshaping procedure for clinical applications. In the study of pathological degradation of cartilage such as osteoarthritis, understanding the kinetics of swelling and deformational behavior as well as morphological changes that occur in response to applied electric stimulation will be important to delineate the electro-mechanical mechanisms and rate-limiting processes that govern electromechanical behavior. Studies described in my dissertation are directed toward development of optical feedback control techniques for laser-assisted cartilage reshaping, and optical diagnosis for osteoarthritis. Although my work was directed toward these objectives, solution of many associated problems in the

course of my work require scientific and engineering developments that may have benefits outside of those demonstrated here. In feedback control for laser assisted cartilage reshaping, preliminary photothermal effect assessment was performed using Fourier transform infrared spectroscopy. Results of this study may be useful for quantitative investigation of the relationship between the clinically important phenomenon of accelerated stress relaxation and kinetics of macromolecular denaturation in cartilage. For feedback control for laser assisted cartilage reshaping, the depth-resolved phase retardation measurements were performed using polarization sensitive optical coherence tomography (PS-OCT). The measurements of phase retardation changes in cartilage accompanying laser irradiation may be useful to better identify the biophysical transformation responsible for stress relaxation in cartilage and develop an optical feedback control procedure. In optical diagnosis for osteoarthritis, electrokinetic surface displacement and optical phase delays depending on applied excitation voltage and frequency were measured in cartilage using differential phase optical coherence tomography (DP-OCT). The electrokinetic measurements with application of electric voltage to excite deformation show the measured interferometric surface displacement increased with increasing applied voltage and decreased with increasing excitation frequency. In the electrokinetic response of cartilage, measured optical phase delay between the surface displacement response and excitation waveform varies inversely to the excitation frequency. The investigation of electrokinetic behavior using DP-OCT may be used to develop a non-invasive optical technique for providing a sensitive indicator of cartilage viability on the molecular-level and possibly detecting early degradative changes in cartilage associated with osteoarthritis.

Table of Contents

LIST OF FIGURES

LIST OF TABLES

CHAPTER 1: INTRODUCTION

1.1. CARTILAGE BIOLOGY

Cartilage is an important tissue that provides structural support, withstands loads, and allows bones in opposition to move smoothly against one another. In the human body, four varieties of cartilage are recognized: (1) morphological cartilage - a genetically sculpted tissue that helps to shape the body features such as the nose; (2) fibrocartilage - a tissue notable for its tensile strength and ability to resist breakage such as the intervertebral disks; (3) articular cartilage - a tissue that enables bones to move smoothly with respect to each other in addition to providing resilience (e.g. joints); and (4) elastic cartilage - a tissue that contains elastic fibers and interconnecting sheets of elastic material and gives elastic properties in addition to the resilience and pliability (e.g. the external ear, and the front of the rib cage) [1-3]. The various types of cartilage are composed of similar chemical structures including water, collagen and proteoglycans. In most cartilage, water contributes 80% by mass while the macromolecules contribute about 20% including 13% collagen and 7% proteoglycan [1]. Collagen in cartilage provides tensile stiffness and strength while proteoglycan aggregates

give resistance to compressional deformation. The negatively charged sulfate (SO_3^-) and carboxyl (COO^-) groups are fixed along the proteoglycan molecules and contribute significantly to the mechanical properties of cartilage. Figure 1.1(A) depicts schematically cartilage structure at the molecular level showing that proteoglycan aggrecan is randomly distributed along collagen fibers in the extracellular matrix. Figure 1.1(B) shows a proteoglycan subunit that contains keratan sulfate rich thin segment and chondroitin rich thick segment.

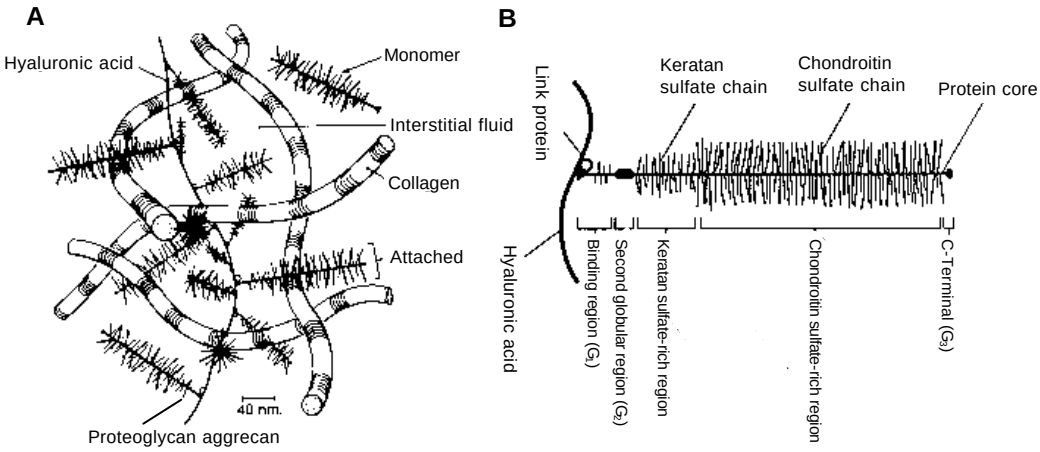

Figure 1.1: Schematic of cartilage structure (A) and proteoglycan subunit (B) [4].

When pressure is applied to cartilage, water is forced away from the sulfate and carboxyl groups, reducing the separation between negative charges thereby increasing the repulsive Coulomb force that resists further compression. Release

of pressure allows the proteoglycan molecules to relax and water to return to the charged domains [1-4].

1.2. STATEMENT OF THE PROBLEMS AND SIGNIFICANCE

(1) Optical Diagnosis for Non-Invasive Laser-Assisted Cartilage Reshaping: In conventional cartilage reconstructive surgery, an autologous cartilage graft is used to replace deformed or damaged cartilage, but may result in associated problems with damage to normal healthy tissue due to carving or suturing. In 1993, Sobol *et al*. introduced laser-assisted cartilage reshaping, demonstrating that under the effect of controlled photothermal heating, mechanically deformed cartilage undergoes a temperature dependent phase transformation, resulting in accelerated stress relaxation [5-17]. The advantage of this technique for surgical applications is that local laser irradiation may be used to change the shape of cartilage without tissue removal as seen in Figure 1.2.

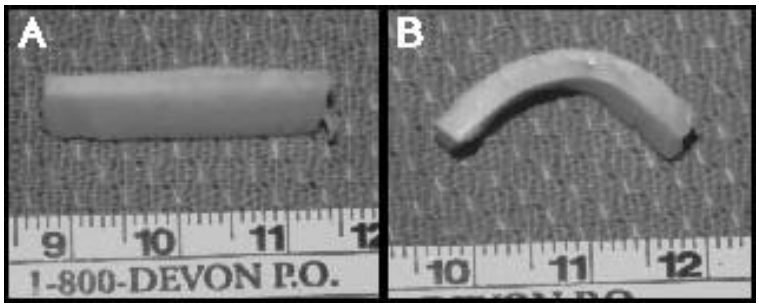

Figure 1.2: Modification of porcine nasal septal cartilage shape before (A) and after (B) laser irradiation.

Clinically, laser reshaped cartilage tissue can be used to recreate the underlying cartilaginous framework of structures in the head and neck such as ear, larynx, trachea, and nose [5-14]. Therefore, optimization of the laser-assisted cartilage reshaping process requires identification of the optical, thermal and mechanical transformations responsible for stress relaxation in cartilage accompanying heating. Currently, a clinical research study has been completed in Moscow, Russia including 110 patients aged 11 to 66 years with symptomatic nasal obstruction due to septal deviation. Patients enrolled in the study underwent an office-based laser nasal septal cartilage reshaping procedure [18]. The study concluded 84 patients (76 %) showed stable improvement in nasal airways and disappearance of the attendant symptoms at 18-month average duration of follow-up [18]. More recently, a US company is being formed to develop commercial instrumentation to complete the laser-assisted cartilage reshaping procedure in the clinic.

- Proposed cartilage reshaping mechanisms: Since demonstration of laser-assisted stress-relaxation is relatively recent (1993), important details of the mechanism of why and how the reshaping occurs are still under investigation. Three possible mechanisms for laser-assisted cartilage reshaping are recognized (Fig. 1.3).

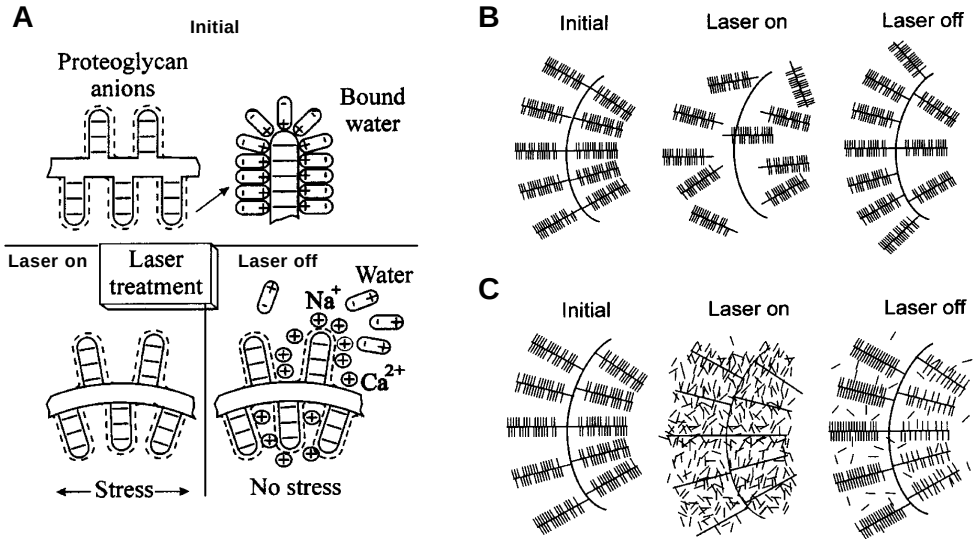

Figure 1.3: Proposed cartilage reshaping mechanisms [15].

First, local mineralization of cartilage that is caused by neutralization of negatively charged groups by sodium and calcium without altering any collagen and proteoglycan (PG) microstructure (Fig. 1.3A). In initial condition, the electrostatic repulsion between the negatively charged ions results in an expansion of the PG molecules and the molecules occupy the large molecular domain with holding bound water molecules. After laser irradiation, the free counter ions (Na^+ and Ca^{++}) in solution balance the negative charge density and the mechanical stress relaxation occurs; second, local depolymerization of PG aggregates and reformation of the PG structure following laser irradiation without pronounced denaturation that results in dramatic structural changes of the cartilage matrix

(Fig. 1.3B); and third, separation of chondroitin sulfate (CS) chains from a protein core and reassembly of CS chains following laser irradiation (Fig. 1.3C). Each hypothesis can be investigated by obtaining the information on both the degree and the characteristic length scale of local structural alteration as well as monitoring the local mineralization of the tissue followed by laser irradiation. Sobol *et al.* demonstrated some indirect evidence of the first mechanism (Fig. 1.3A) using atomic force microscopy (AFM) [15]. The results showed that small crystals (sodium carbonate) were formed following CO_2 ($\lambda = 10.6\ \mu m$) laser irradiation and disappeared in a few days [15]. Sobol *et al.* suggested that the local mineralization with sodium carbonate could be responsible for the short-term stability of laser-treated cartilage [15]. To demonstrate the second and third mechanisms (Figs. 1.3B and 1.3C), Sobol *et al.* used size exclusion chromatography coupled to multi-angle laser scattering and sedimentation velocity measurements in an analytical ultracentrifuge [15]. Irradiated cartilage was compared with non-irradiated specimens and the results showed that laser irradiation decreases the molecular weight of chondroitin sulfate and induces diffusion of macromolecules into the medium [15]. Sobol *et al.* concluded that since the proteoglycan aggregates cannot diffuse through the interstitial fluid, the mechanism of laser induced stress relaxation could be connected with separation and motion both of proteoglycan units and chondroitin sulfate chains [15]. The

further investigation of these and similar molecular level studies will provide valuable information to identify and characterize cartilage reshaping mechanisms.

- Effective laser dosimetry for laser-assisted cartilage reshaping: Determination of the optimal laser dosimetry parameter space for cartilage reshaping requires evaluation of irradiance and exposure time for candidate laser wavelengths (Fig. 1.4.) [16]. Sviridov *et al.* demonstrated that conditions exist that allow laser reshaping without chondrocyte death [16]. They showed that laser heating with lower laser fluences and shorter time of irradiation produced only minimal cell damage but, unfortunately, ineffective reshaping [16]. On the other hand, when the flux in laser energy is increased or the treatment time prolonged, significant nuclear condensation in chondrocytes occurred [16]. Studies also revealed that the distribution of chondrocyte damage varies throughout the cartilage thickness: the more superficial cells showed morphological evidence of damage, while many of the cells in the cartilage bulk remained undamaged [16]. Therefore, use of a different cartilage thickness, laser wavelength, irradiation time, or other conditions may alter the 'therapeutic window' (Fig. 1.4) at which stress relaxation occurs while minimizing non-specific tissue damage. Although laser-assisted reshaping without any chondrocyte death has not been demonstrated, a careful balance exists between optimal reshaping and minimal non-specific injury. Therefore, the laser-assisted

cartilage reshaping process should be optimized with investigating the optical, thermal, and biophysical transformations responsible for stress relaxation in cartilage accompanying local laser heating.

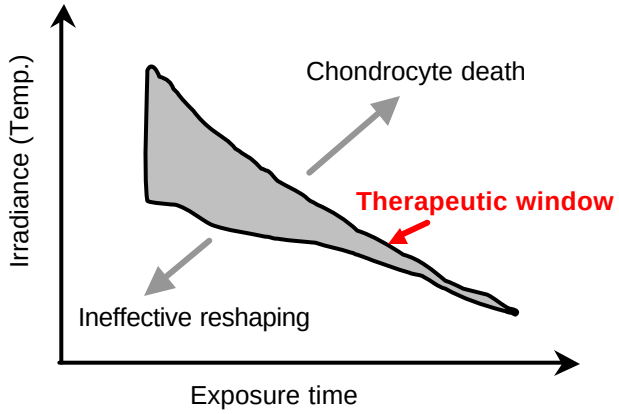

Figure 1.4: Shaded area represents parameter space for effective laser dosimetry for reshaping of cartilage [16].

Since protein denaturation, coagulative necrosis, and subsequent cell death are a function of the time-dependent heating profile generated during laser irradiation, the rigorous evaluation of optical, thermal and mechanical properties of cartilage is required. Fortunately, changes in molecular structure during laser heating can be measured using many techniques in real time [5-16]. Several theoretical models of light distribution, heat and mass transfer during laser heating have been developed [17-20]. Bagratashvili *et al.* developed the thermal and diffusion model with the view of mass transfer in cartilage being governed by a

process of successive adsorption and desorption of water molecules by proteoglycans [17]. Madsen *et al.* investigated optical properties of fresh and cryopreserved cartilage at a wavelength of 632.58 nm [19]. Youn *et al.* measured the spectral dependence of optical absorption and reduced scattering coefficients and thermal conductivity and diffusivity of porcine nasal septal cartilage [20].

Two non-invasive optical diagnostic techniques, Fourier transform infrared spectroscopy and polarization sensitive optical coherence tomography, may be used to investigate the biophysical transformations responsible for stress relaxation and investigate the relationship between kinetics of macromolecular denaturation and accelerated stress relaxation in cartilage accompanying local laser irradiation.

(2) Optical Measurements of Mechano-Electrochemical Properties: Mechano-electrochemical properties of cartilage in the physiological wet condition are determined by mobile electrolyte ions in the interstitial fluid and by fixed negatively ionized charged moieties such as sulfate (SO_3^-) and carboxyl (COO^-) groups in proteoglycan aggrecans within cartilage [21,22]. Within the interstitial fluid, proteoglycan aggrecans with abundant negatively charged groups attract mobile cations such as Na^+ and Ca^+ in the interstitial fluid to maintain the electroneutrality of the tissue [22]. The mechano-electrochemical properties are dependent upon the relative amount of the solid matrix and the mechano-electrical

interaction between the components within the extracellular matrix. Many mechano-electrochemical phenomena such as anomalous osmosis and electro-osmosis, ion-induced swelling, and streaming potential and current are attributed to the electrostatic and frictional interactions between the fixed charge groups and mobile ions [22].

One of the most common diseases of cartilage, osteoarthritis is a heterogeneous disease of uncertain etiology and is characterized by progressive loss of articular cartilage. The earliest and most important chemical features of osteoarthritis, which precede gross pathological changes, include non-uniform loss of proteoglycan molecules and grow-out of bone spurs from the edge of bone with an associated increase in synovial fluid and fibrillation of the collagen network (Fig. 1.5(B)) compared to normal healthy cartilage (Fig. 1.5(A)). Loss of proteoglycans decreases the ability of cartilage to withstand compressive loading and results in a tissue that is softer and more susceptible to wear and fibrillation [21,24].

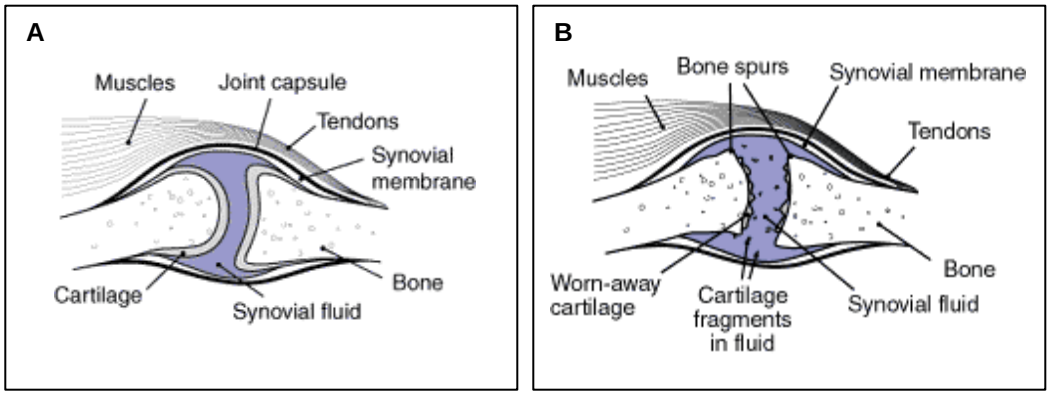

Figure 1.5: A healthy joint (A) and a joint with osteoarthritis (B) [25].

Over the past few decades, many researchers have attempted to observe early indications of the pathological conditions that result in cartilage degeneration using a variety of techniques such as mechanical property measurements [26], chemical assay [27], and electromechanical measurements [28]. Among mechanical property measurements, Setton *et al.* reported the fundamental relationships between mechanical behavior and the composition and structure of healthy cartilage and proposed mechanisms for changes associated with degeneration [26]. They observed that in cartilage with osteoarthritis, tensile, compressive and shear behaviors were dramatically altered and presented decreases in the modulus or stiffness of cartilage in tension, compression and shear loading, and the increases in the propensity to swell as compared to healthy cartilage [26]. Chemical analysis can provide the most direct estimate of the total number of ionizable groups that may be reduced by osteoarthritis. Venn

and Maroudas measured the number of charged groups of wet articular cartilage [27]. They assayed the glycosaminoglycans (GAG) carboxyl and sulfate group content using hexamine and uronic acid analysis and demonstrated that in post-mortem cartilage, water content decreased from a maximum at the surface to a minimum in the deep zones [27]. In contrast, however, water content in the osteoarthrotic specimens was greatest in the middle zones [27]. Furthermore, GAG content increased with depth in healthy controlled cartilage, but GAG content in the osteoarthrotic specimens was reduced compared to normal controls throughout the depth of cartilage. With increasing degeneration, increased water content and decreased GAG content was observed [27]. However, despite the accuracy and utility of these chemical assay procedures, their application is often irreversible and destructive to the test specimen. In addition, the total number of available dissociable groups does not necessarily reflect the effective charge density. Site binding and/or counter-ion condensation may also reduce the effective charge density below the total density of fixed, ionizable sites [21,29]. In electromechanical measurements, Berkenblit *et al.* measured the current-generated stress with a piezoelectric sensor positioned at the surface of articular cartilage [28]. The results of their experiment supported the feasibility of surface measurements as a means of assessing electromechanical transduction in cartilage [28]. Although Berkenblit *et al.*'s electromechanical surface spectroscopy provides a measure of cartilage material properties and may allow

detection of degradative changes accompanying early stages of osteoarthritis, only surface displacement information is detected.

Sensitive electrokinetic response measurements as well as surface displacements using a depth-resolved optical imaging instrument - differential phase optical coherence tomography (DP-OCT) may provide a sensitive indicator of cartilage viability. Detection of depth-resolved electromechanical stress gradients in cartilage may be useful to monitor non-invasively cartilage degeneration and allow arresting progression of the disease using, for example, pharmacological intervention.

1.3. RESEARCH OBJECTIVES

The primary objectives of my dissertation research are:

Evaluate thermally induced macromolecular changes in cartilage using Fourier transform infrared spectroscopy: The photothermal effects of cartilage can be investigated using an infrared focal plane array camera and a Fourier transform infrared (FT-IR) spectrometer. The methodology may be useful for quantitative investigation of the relationship between the clinically important phenomenon of accelerated stress relaxation and the kinetics of macromolecular denaturation.

Measure and characterize thermally induced phase retardation changes in cartilage using polarization-sensitive optical coherence tomography (PS-OCT):

The investigation of the thermodynamic induced changes in birefringence of cartilage may find laboratory and clinical applications to characterize internal dynamics of the extracellular matrix (mainly water) and macromolecules such as collagen and proteoglycans. Moreover, the phase retardation changes accompanying laser irradiation may possibly be used to identify the biophysical transformations responsible for stress relaxation in cartilage.

Measure and characterize electrokinetic stress gradients in cartilage using differential phase optical coherence tomography (DP-OCT): Since the streaming potential and other electrokinetic effects in cartilage are directly related to proteoglycan density, application of an electric field in cartilage combined with depth-resolved phase sensitive optical measurements may provide a sensitive indicator of cartilage viability. Detection of electromechanical stress gradients in cartilage using DP-OCT may be useful to identify non-invasively regions of cartilage degeneration.

1.4. DISSERTATION ORGANIZATION

Following an overview of cartilage biology, the significance of my dissertation research in cartilage and sample harvest and preparation, in Chapter 1, several experiments were conducted to identify and characterize the physiological

transformations in cartilage accompanying laser irradiation and electrical stimulation.

In Chapter 2, photothermal effects following laser irradiation of cartilage are investigated using an infrared focal plane array camera and a Fourier transform infra-red (FT-IR) spectrometer to record radiometric temperature profile in response to local laser heating and to analyze absorption peaks, respectively. Spectral differences due to dehydration between the controlled and laser-irradiated cartilage was observed by recording FT-IR spectra. Observation of spectral absorption changes due to macromolecules such as collagen and proteoglycans due to phase transformation and/or conformational changes following laser irradiation are reported. The methodology may be useful for quantitative investigation of the relationship between the clinically important phenomenon of accelerated stress relaxation and the kinetics of macromolecular denaturation.

In Chapter 3, thermally induced changes in birefringence of nasal septal cartilage following Nd:YAG laser irradiation were investigated using a polarization-sensitive optical coherence tomography (PS-OCT) system. From the experiments, phase retardation changes observed in cartilage are primarily due to dehydration. Since dehydration is the principal source for the observed changes in cartilage, use of PS-OCT as a feedback control methodology for non-

ablative cartilage reshaping is primarily sensitive to the detection of water loss rather than thermal denaturation of the macromolecules.

In Chapter 4, the electrokinetic response measurements as well as surface displacements were performed in nasal septal cartilage using differential phase optical coherence tomography (DP-OCT) and the dependence of the measured stress on the amplitude of the applied voltage was characterized. Since the streaming potential and other electrokinetic effects in cartilage are directly related to proteoglycan density, application of an electric field in cartilage combined with depth-resolved phase sensitive optical measurements may provide a sensitive indicator of cartilage viability and possibly be utilized to detect early degradative changes in cartilage associated with osteoarthritis.

Following all of the experiments, Chapter 5 summarizes and analyzes the data obtained from all measurements. Conclusions and future directions for investigation in non-invasive optical diagnostics of cartilage are discussed.

1.5. CARTILAGE SAMPLE HARVEST AND PREPARATION

Porcine has been widely used to obtain biological tissue specimens. In this study, porcine nasal septal cartilage was used for all the experiments because of its ready availability, relatively large specimen size, and reasonable cost. The nasal septal cartilage extraction procedure utilized here was approved by the Animal Resource Center of the University of Texas at Austin (Protocol #:

99020101). A fresh porcine head was obtained from a local abattoir and cartilage was extracted 2-hours postmortem before experiment. The prepared porcine head was placed on an operating table and explored for an incision line. The skin was removed from the upper side of the head through the bilateral nasal side. Bilateral nasal bone osteotomies were performed along the line of incision using a standard carpenter's hammer and chisel. The hard bone was removed from the site, being careful not to damage the nasal septal cartilage, and the specimen was removed using a chisel (Fig. 1.6). After extraction, soft tissue including perichondrium was peeled away from the cartilage specimen and the sample was rinsed in tap water for approximately 15 minutes to remove hemocytes. By using a scalpel, the cartilage specimens were sliced in rectangular parallelepiped shapes ($28 \times 31 \times 5$ mm^3) and placed on a sample plate. Samples were stored in physiological saline solution at 4 ^oC just prior to experimentation.

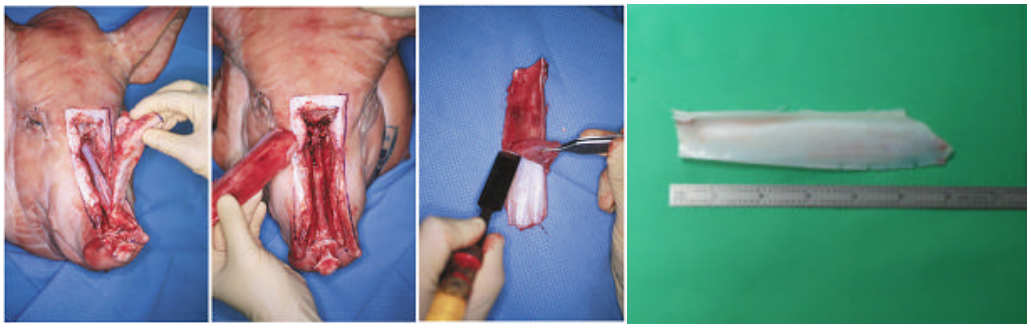

Figure 1.6: Porcine nasal septal cartilage extraction procedure (Left) and extracted specimen (Right).

- Cartilage Sample Cutting Device

A mechanical device was designed and constructed to cut extracted cartilage specimens to a uniform thickness (t = 0.75 mm or 1.5 mm) (Figs. 1.7 and 1.8).

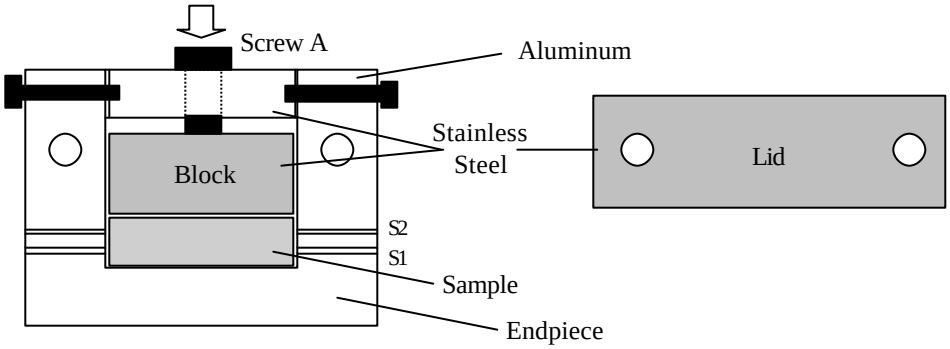

Figure 1.7: Cartilage sample cutting device design layout.

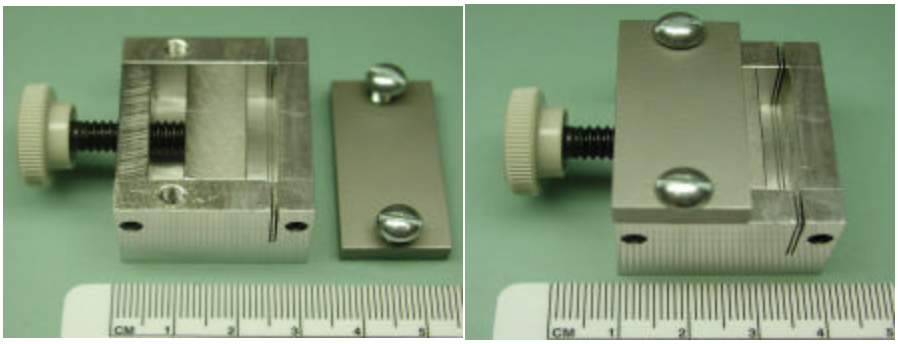

Figure 1.8: Cartilage sample cutting device.

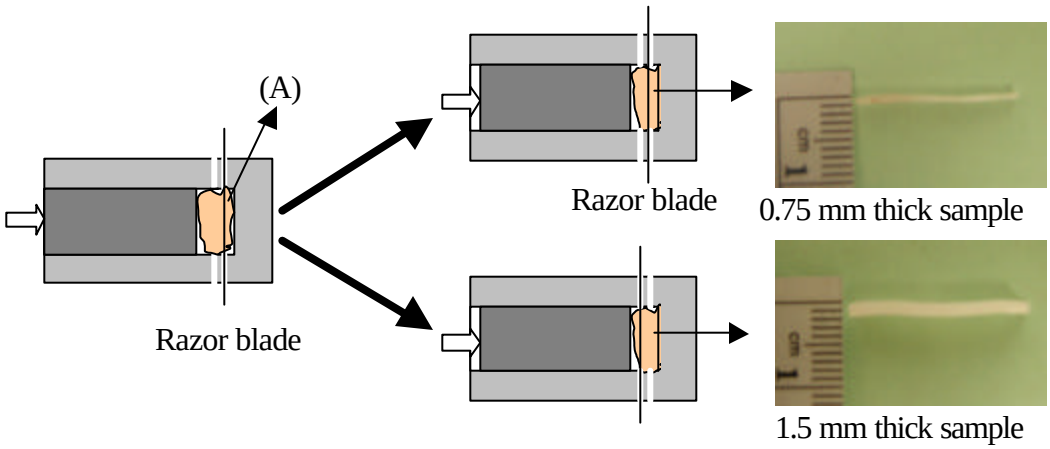

Figure 1.9: Cartilage sample cutting steps for a desired thickness.

After the lid is fastened to the frame, a cartilage specimen is placed in the space between the endpiece and block (Fig. 1.9). Rotating screw-A (Fig. 1.9) maintains the cartilage sample against the endpiece. A razorblade slices the cartilage specimen at the bottom spacer (S1 in Fig. 1.7) and produces a smooth surface. After the piece (A) (Fig. 1.9) is removed and screw A (Fig. 1.7) is fastened again, the razorblade slices at S1 or S2 (Fig.1.7) to obtain a desired uniform sample thickness (t = 0.75 mm or 1.5 mm) (Fig. 1.9). The specimen is removed from the slicer and stored in physiological saline (4 ^{o}C).

1.6. REFERENCES

1. Gray H., "*Gray's Anatomy*", Gramercy Books, New York, 1977

2. Hall B. K., "*Cartilage: Structure, Function, and Biochemistry*", vol. 1, Academic Press, New York, 1983

3. Caplan A. I., "Cartilage", *Scientific American*, **251(4)**: 84-94, 1984

4. Mow V. C., "*Injury and Repair of the Musculoskeletal Soft Tissues*", American Academy of Orthopaedic Surgeons, 1988

5. Sobol E. N., Bagratashvili V., Omel'chenko A., Sviridov A., Hwlidonis E., Kawalos G., Christodoulou P., Naoumidi I., Velegrakis G., Ovchinnikov Y., Shechter A., "Laser Shaping of Cartilage", *Proc. SPIE*, **2128**: 43-49, 1994

6. Sobol E. N., Bagratashvili V., Sviridov A., Omel'chenko A., Kitai M., Jones N., Zenger V., Nasedkin A. Isaev M., Karlov V., Schechter A., "Study of Cartilage Reshaping with Holmium Laser", *Proc. SPIE*, **2623**: 544-547, 1996

7. Sobol E. N., Bagratashvili V., Sviridov A., Omel'chenko A., Ovchinnikov Y., Svistushkin A., Isaev M., Shechter A., Phenomenon of cartilage shaping using moderate heating and its applications in otorhinolaryngology", *Proc. SPIE*, **2623**: 548-552, 1996

8. Sobol E. N., Sviridov A., Bagratashvili V., Omel'chenko A., Ovchinnikov Y., Shechter A., Downes J., Howdle S., Jones N., Lowe J., "Stress Relaxation and Cartilage Shaping under Laser Radiation", *Proc. SPIE*, **2681**: 358-363, 1996

9. Sobol E. N., *"Phase Transformations and Ablation in Laser-Treated Solids"*, John Wiley & Sons, New York, 1998

10. Sobol E. N., Kitai M., Jones N., Sviridov A., Milner T. E., Wong B. J. F., "Theoretical Modeling of Heating and Structure Alterations in Cartilage under Laser Radiation with regard of Water Evaporation and Diffusion Dominance", *Proc., SPIE*, **3254**: 54-63, 1998

11. Wong B. J. F., Milner T. E., Anvari B., Sviridov A., Omel'chenko A., Bagratashvili V., Sobol E. N., Nelson J. S., "Thermo-Optical Response of Cartilage During Feedback Controlled Laser-Assisted Reshaping", *Proceedings SPIE*, **2970**: 380-391, 1997

12. Wong B. J. F., Milner T. E., Anvari B., Sviridov A., Omel'chenko A., Bagratashvili V., Sobol E. N., Nelson J. S., "Measurement of Radiometric Surface Temperature and Integrated Back-Scattered Light Intensity During Feedback Controlled Laser-Assisted Cartilage Reshaping", *Lasers in Med. Sci.*, **13**: 66-72, 1998

13. Wong B. J. F., Milner T. E., Kim H. K., Telenkov S., Chew C., Kuo T., Smithies D. J., Sobol E. N., Nelson J. S., "Critical Temperature Transitions in Laser Mediated Cartilage Reshaping", *Proceedings SPIE*, **3425**: 161-172, 1998

14. Wong B. J. F., Milner T. E., Kim H. H., Nelson J. S., Sobol E. N., "Stress Relaxation of Porcine Septal Cartilage during Nd:YAG ($\lambda = 1.32\mu m$) Laser Irradiation: Mechanical, Optical, and Thermal Response", *J. of Biomed. Opt.*, **3(4)**: 409-414, 1998

15. Sobol E. N., Sviridov A., Omel'chenko A., Bagratashvili V., Kitai M., Harding S. E., Jones N., Jumel K., Mertig M., Pompe W., Ovchinnikov Y., Shekhter A., Svistushkin V., "Laser Reshaping of Cartilage", *Biotech. Gen. Eng. Rev.*, **17**: 539-564, 2000

16. Sviridov A., Sobol E. N., Jones N. S., Lowe J., "Effect of Holmium Laser Radiation on Stress, Temperature, and Structure Alterations in Cartilage", *Lasers in Med. Sci.*, **13**:73-77, 1998

17. Bagratashvili V., Sobol E. N., Sviridov A., Popov V. K., Omel'chenko A., Howdle S. M., "Thermal and Diffusion Processes in Laser-Induced Stress Relaxation and Reshaping of Cartilage", *J. Biomech.*, **30**: 813-817, 1997

18. Ovchinnikov Y., Sobol E. N., Shekhter A., Bagratashvili V., Svididov A., "Laser Septochondrocorrection", *Arch Facial Plast. Surg.*, **4**:180-185, 2002

19. Madsen S. J., Chu., Wong B. J. F., "The Optical Properties of Porcine Nasal Cartilage", *IEEE J. Selected Topics Quantum Elec.*, **5**:1127-1133, 1999

20. Youn J. I., Telenkov S. A., Kim E., Bhavaraju N. C., Wong B. J. F., Valvano J. W., Milner T. E., "Optical and Thermal Properties of Nasal Septal Cartilage", *Lasers Surg. Med.*, **27**:119-128, 2000

21. Grodzinsky, A. J., "Electromechanical and Physicochemical Properties of Connective Tissue", *CRC Crit. Rev. Biomed. Eng.*, **9**: 133-199, 1983

22. Sun D. N., Gu, W. Y., Guo X. E., Lai W. M., Mow V. C., "A Mixed Finite Element Formulation of Triphasic Mechno-Electrochemical Theory for Charged, Hydrated Biological Soft Tissues", *Int. J. Numer. Meth. Eng.*, **45**: 1375-1402, 1999

23. Maroudas A., "Physicochemical Properties of Articular Cartilage", *Adult Articular Cartilage*, Freeman, M.A.R. ed., Pitman Medical, Kent, England, 2nd ed., 215-290, 1979

24. Berkenblit S. I., Frank E. H., Salant E. P., Grodzinsky A. J., "Nondestructive Detection of Cartilage Degeneration using Electromechanical Surface Spectroscopy", *Trans. ASME*, **116**: 384-392, 1994

25. NIAMS, “Handout on Health: Osteoarthritis”, *NIH Publication No. 99-4617*, June, 1999

26. Setton L. A., Elliott D. M., Mow V. C., “Altered Mechanics of Cartilage with Osteoarthritis: Human Osteoarthritis and an Experimental Model of Joint Degeneration”, *Osteoarthritis & Cartilage*, **7**:2-14, 1999

27. Venn M., Maroudas A., “Chemical Composition and Swelling Pressure of Normal and Oseteoarthrotic Femoral Head Cartilage”, *Ann. Rheum. Dis.*, **36**:121-129, 1977

28. Berkenblit S. I., Frank E. H., Salant E. P., Grodzinsky A. J., “Nondestructive Detection of Cartilage Degeneration using Electromechanical Surface Spectroscopy”, *Trans. ASME*, **116**: 384-392, 1994

29. Manning G.S., “The Molecular Theory of Polyelectrolyte Solutions with Applications to the Electrostatic Properties of Polynucleotides”, *Quart. Rev. Biophy. II*, **11**:179-246, 1978

CHAPTER 2: PRELIMINARY EVALUATION OF THERMALLY INDUCED MACROMOLECULAR CHANGES IN CARTILAGE USING FT-IR SPECTROSCOPY

2.1. ABSTRACT

Photothermal effects following laser irradiation of cartilage are investigated using an infrared focal plane array (IR-FPA) camera and a Fourier transform infra-red (FT-IR) spectrometer. The IR-FPA camera records radiometric temperature profile while the local laser heating is applied to the sample while the FT-IR spectrometer analyzes absorption peaks of cartilage constituents. Since the major effect of photothermal heating in cartilage is water evaporation, spectral changes due to dehydration between control and laser-irradiated cartilage are recorded by FT-IR spectrometer measurements. Additionally, another interest was observation of the spectral changes from macromolecules such as collagen and proteoglycans due to phase transformation and/or conformational changes following laser irradiation. The methodology may be useful for quantitative investigation of the relationship between the clinically important phenomenon of accelerated stress relaxation and the kinetics of macromolecular denaturation.

2.2. INTRODUCTION

Fourier transform infrared (FT-IR) spectroscopy has been used to study the structure and orientation of constituents in cartilaginous tissues. Camacho *et al*. investigated the spatial distribution of collagen orientation in different zones of cartilage using an FT-IR spectrometer to provide a framework for study of complex pathological changes [1]. Bagratashvili *et al.* studied the thermodynamic characteristics of the 'bound-to-free' phase transformation of water in laser-induced reshaping of cartilage with differential microcalorimetry and FT-IR spectroscopy [2]. They concluded that the dehydration and rehydration processes in cartilage are reversible but depend on the temperature of preliminary dehydration caused by laser heating [2]. Although Bagratashvili *et al.* investigated the spectral range from 5,500 cm^{-1} to 1,500 cm^{-1}, they only concentrated on water diffusion process in cartilage under the heating without any analysis on the absorption spectra of macromolecules below 2,000 cm^{-1}.

The major effect of photothermal heating is water evaporation and thermal denaturation of macromolecules in cartilage such as collagen and proteoglycans due to phase transformation and/or conformational changes following laser irradiation [2]. Because the highly charged proteoglycans in cartilage provide the internal restoring forces necessary to balance externally applied loads, accelerated stress relaxation following laser irradiation is thought to originate in thermal modification of these large macromolecules. The goal of this study is to

investigate the photothermal kinetics accompanying laser irradiation, and to differentiate the effects of dehydration and thermal denaturation using an IR-FPA camera and a FT-IR spectrometer.

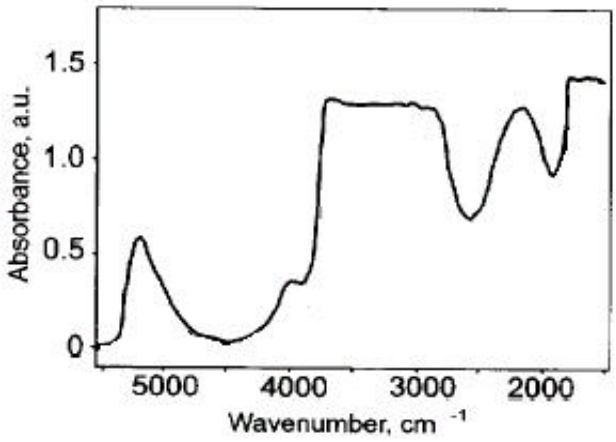

Figure 2.1: FT-IR absorption spectrum of cartilage from 5500 to 1500 cm^{-1} [2].

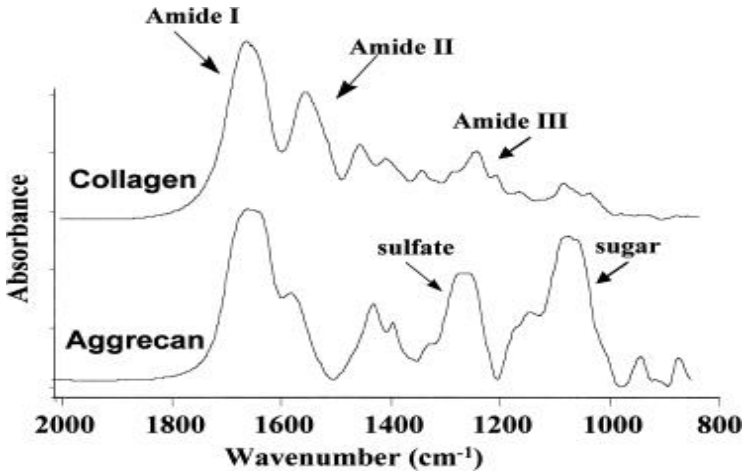

Figure 2.2: FT-IR spectra of collagen and proteoglycan aggrecan model constituents [1].

FT-IR absorption spectra of cartilage and major constituents in cartilage are presented (Figs. 2.1 and 2.2). As seen in Figure 2.1, three major peaks (5200, 3300, and 2200 cm^{-1}) due to water absorption are observed in the range from 5500 cm^{-1} to 2000 cm^{-1} [2, 4]. The main absorption bands of collagen arise from the peptide bond vibration: 3330 cm^{-1}, 1655cm^{-1}, 1550 cm^{-1}, and 1250 cm^{-1} due to Amide A, I, II and III, respectively [1] (Fig. 2.2). The spectrum of proteoglycan aggrecan exhibits features arising from sulfate (1245 cm^{-1}), sugar (1125-920cm^{-1}, 850cm^{-1}), and protein entities (1640 cm^{-1}, 1545 cm^{-1} due to Amide I and II) [1] (Fig. 2.2). Since any loss of m`acromolecules in cartilage following laser heating may cause decrease of the absorption peaks, monitoring FT-IR spectrum of cartilage may be useful for clinical applications to investigate the spatial distribution of collagen and proteoglycans and their interaction with water molecules pre- and post-laser irradiation.

2.3. EXPERIMENTAL METHODS

A FT-IR spectrum represents a fingerprint of a sample with absorption peaks that correspond to the frequencies of vibrations between the bonds of the atoms/molecules making up the material. Because each state in the biological sample during heating is a unique combination of atoms and the environment, no two constituents produce exactly the same infrared spectrum. Therefore, infrared spectroscopy can result in a positive identification/qualitative analysis of the

material state. In addition, magnitude of the spectral peaks is an indication of the amount of a particular constituent material present [5].

Figure 2.3 shows the schematic layout of the FT-IR spectrometer used in my studies (Nicolet Magna IR-560).

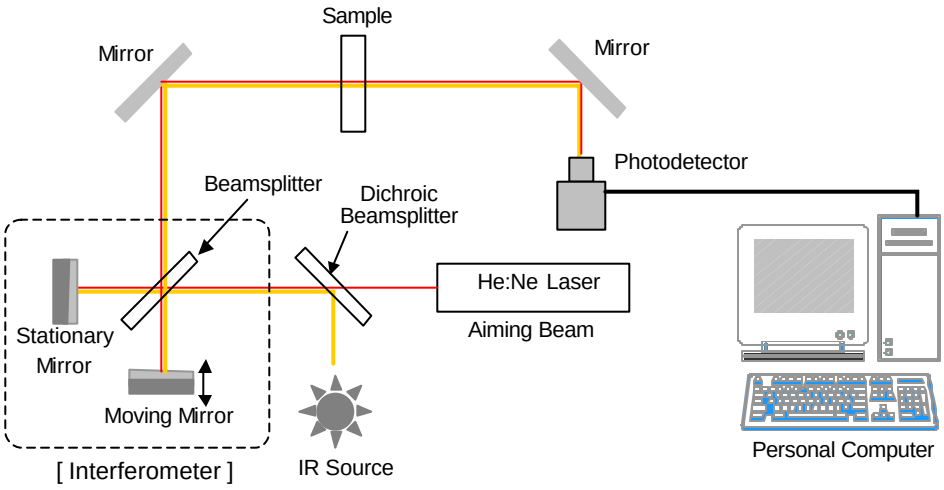

Figure 2.3: FT-IR schematic layout [5].

The FT-IR spectrometer employed a simple Michelson interferometer for the fast scanning process that is capable of measuring all of the infrared frequencies simultaneously. Beamsplitter in the interferometer amplitude divides the incoming infrared beam into two paths. One beam reflects off a fixed flat mirror and the other beam reflects off of a flat mirror, which is on a translation stage that allows this mirror to move a very short distance away from the beamsplitter. The two beams reflect off of their respective mirrors and are recombined at the

beamsplitter. Because the path that one beam travels is a fixed length and the other is constantly changing as the mirror moves, the signal which exits the interferometer is the result of these two beams interfering with each other. The resulting signal has information about every infrared frequency that comes from the source. As the signal is measured, all frequencies are being measured simultaneously. Since optical frequency spectrum is required to identify constituents in the material, the measured signals is interpreted via Fourier transform to plot the intensity at each individual frequency [5].

Before the measurements, cartilage slices of about 100 μm in thickness were stored in a physiological buffered saline (PBS) solution at 4 ^{o}C. Since the photothermal effects with laser irradiation are mainly dehydration and denaturation of macromolecules, the experimental procedures are divided to study three effects; (1) dehydration, (2) thermal denaturation, and (3) photothermal heating. For spectroscopic monitoring of dehydration, the cartilage specimen was placed in the sample chamber of the FT-IR spectrophotometer and an absorption spectrum was recorded every 5 minutes for 20 minutes. After dehydration, the sample was placed into physiological saline for rehydration for 5 minutes and absorption spectrum measured again (Fig. 2.4(A)). To investigate thermal denaturation effects without any dehydration, the sample was placed into hot physiological buffered saline (PBS) solution at 90 °C by monitoring the

temperature with a thermocouple (HH202A, Omega) for 20 minutes and the absorption spectrum measured every 5 minutes (Fig. 2.4(B)).

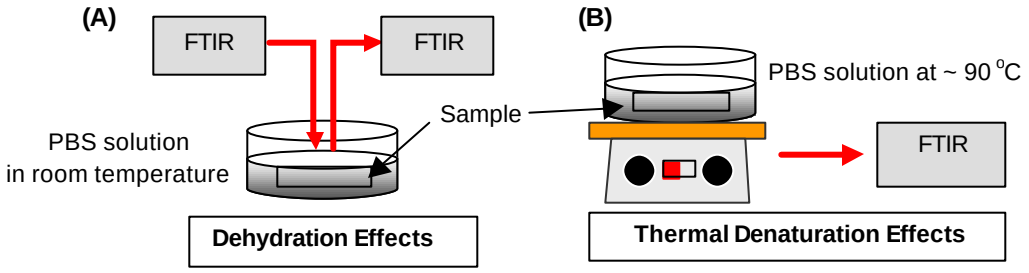

Figure 2.4: Experimental layout for study of dehydration effects (A) and thermal denaturation effects (B).

For study of photothermal effects, the rehydrated samples were used for irradiation with a Ho:YAG laser (λ = 2.1μm) with different laser dosimetry (1W and 2W for 6 seconds, spot size = 4 mm) followed by FT-IR absorption spectrum measurements. During laser irradiation, radiometric temperature was measured by an InSb IR-FPA camera (Merlin, Indigo Systems Inc., 320×240 pixels) at the frame rate of 20 Hz (Fig. 2.5) for 8 seconds. IR-FPA camera was calibrated with a comercial black body source (M310, Mikron Instruments Co.) and the radiometric temperature was determined by averaging pixels in a square area (2 mm × 2 mm) in the accquired images over time. After averaging pixels in

the 2 mm × 2 mm area in each frame, we ploted the average radiometric tempeature versue time.

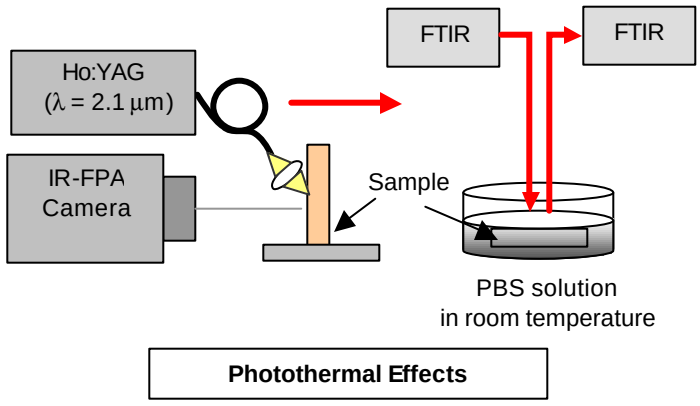

Figure 2.5: Experimental layout for studying photothermal effects.

2.4. RESULTS

Figure 2.6 shows the recorded FT-IR absorption spectra of cartilage in response to dehydration. The spectrum of hydrated cartilage arises from overlapping spectral features from each constituent and the only distinguishable absorption band is at around 2100 cm^{-1} due to water. After dehydration, overall absorbance as well as strength of the water absorption band at 2100 cm^{-1} decreases. However, the absorption bands of cartilage macromolecules at 1650 cm^{-1} (Amide I), 1560 cm^{-1} (Amide II), 1260 cm^{-1} (sulfate/Amide III), and 1080

cm^{-1} (sugar) become distinguishable. Because FT-IR spectra of cartilage after rehydration in PBS solution for 5 minutes are similar to those observed before dehydration, the dehydration process appears reversible.

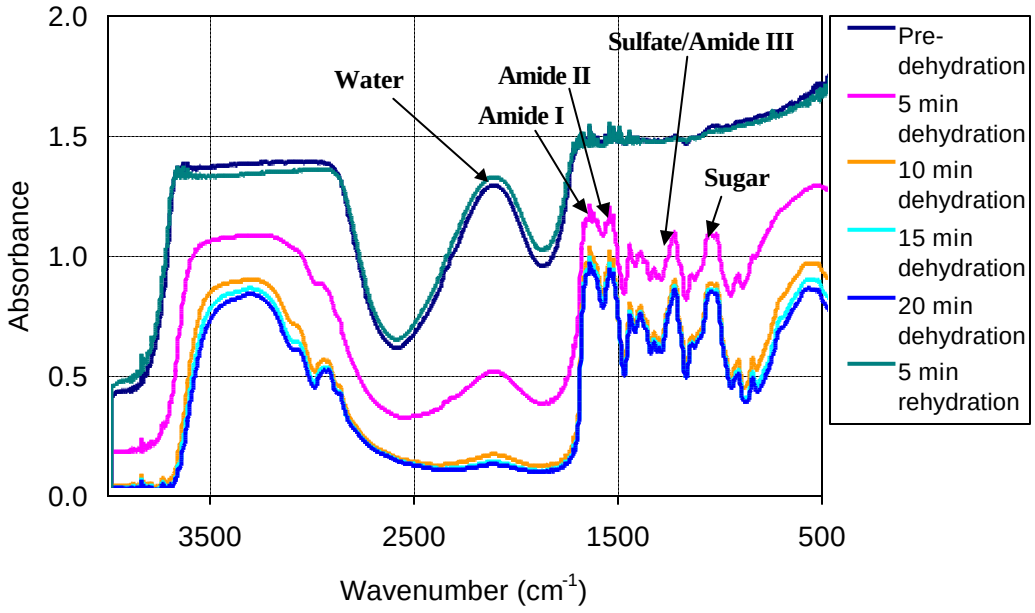

Figure 2.6: FT-IR absorption spectra of cartilage in response to dehydration.

To investigate thermal denaturation without dehydration, the cartilage sample was heated in hot (90 ^{o}C) PBS solution for 20 minutes and FT-IR absorption spectra in Figure 2.7 shows the decrease of water absorption peak at 2100 cm^{-1} compared to the pre-dehydration water absorption peak in Figure 2.6.

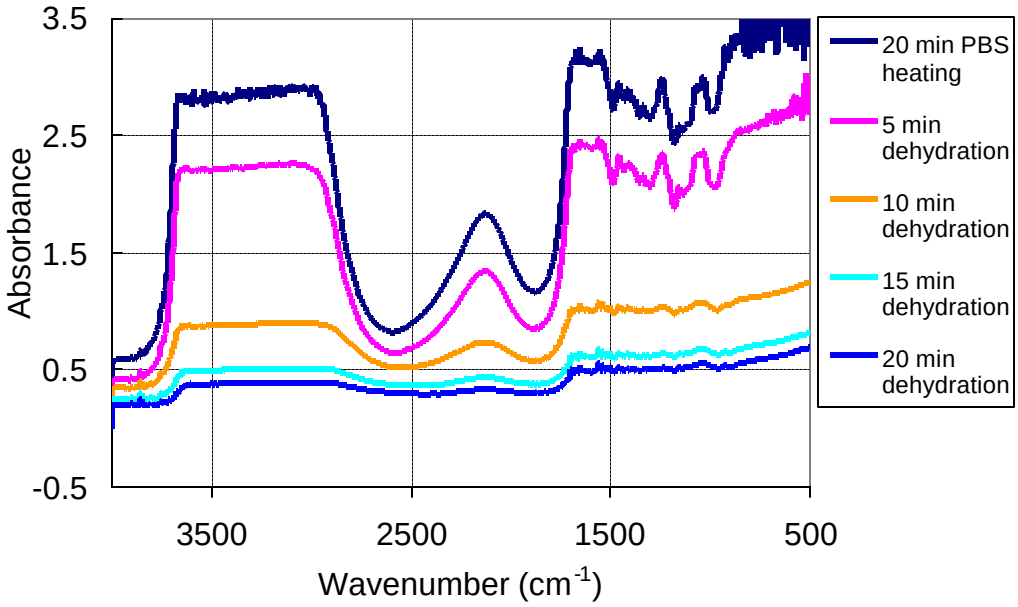

Figure 2.7: FT-IR spectra of cartilage for thermal denaturation effects and dehydration for 20 minutes after PBS solution heating.

To detect changes in the absorption spectra of water and macromolecules in cartilage, the heated specimen was dehydrated in air for various time (5, 10, 15, 20 minutes), and the spectra were compared with those of dehydrated cartilage without heating (Figure 2.8). In the absorption spectra of water at 3200 cm^{-1}, the dehydrated cartilage with PBS solution heating shows more substantial decreases than that of the only dehydrated cartilage. The absorption spectra of the macromolecules with PBS solution heating below 1700 cm^{-1} disappeared, but the peaks without heating can be clearly distinguishable.

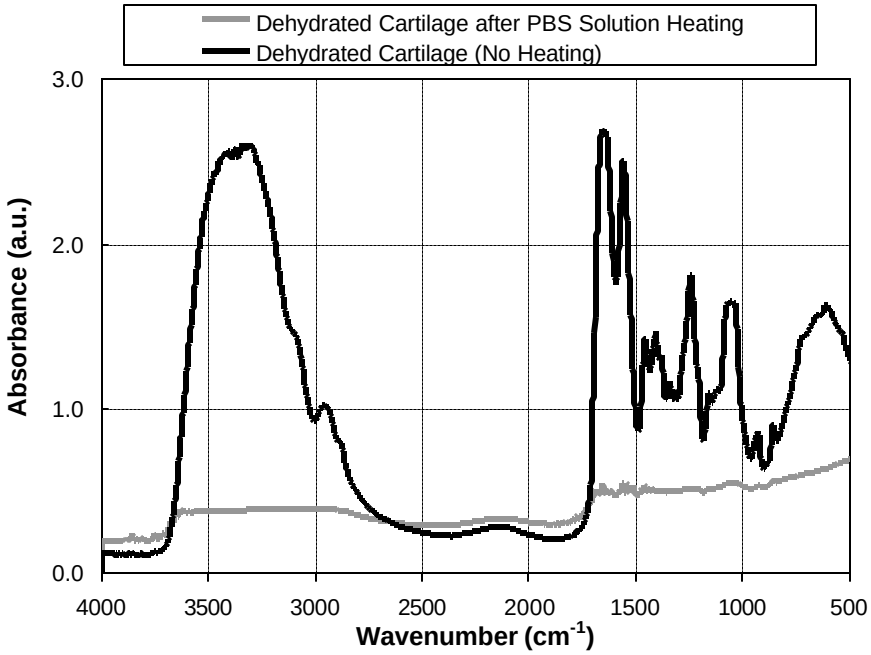

Figure 2.8: FT-IR absorption spectra of dehydrated cartilage after PBS solution heating and dehydrated cartilage.

Figures 2.9 and 2.10 present the photothermal effects following laser irradiation compared with dehydration effects. When the sample was heated (λ = 2.1 μm, 1W, 6 sec) to a radiometric temperature of 70 ^{o}C (Figure 2.9B), dehydration effects by the decrease in the magnitude of water absorption at 2100 cm^{-1} occurred. The absorption peaks from the macromolecules below 1700 cm^{-1} appear to smear out, but do not decrease significantly compared to the water peak (Figure 2.9(A)).

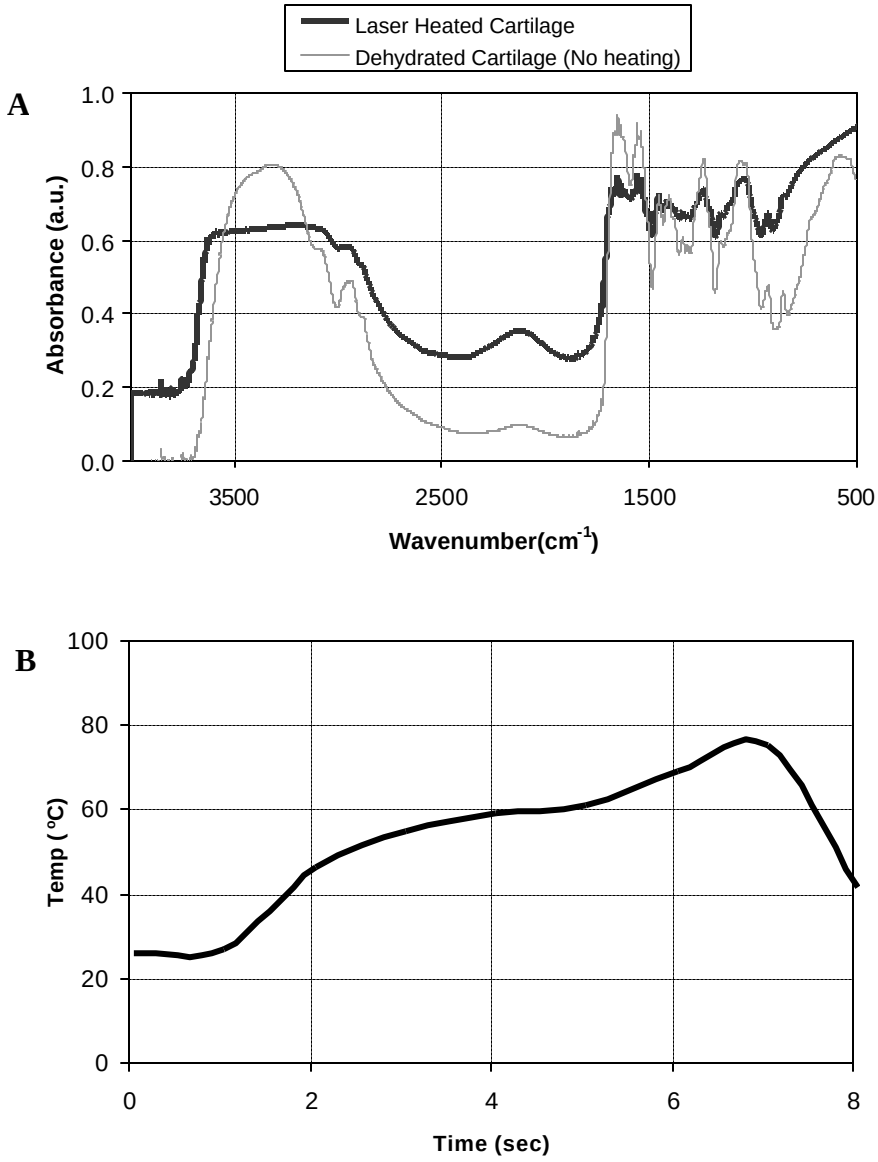

Figure 2.9: FT-IR absorption spectra of dehydrated without heating and laser irradiated (λ = 2.1 μm, 1W, 6 sec) cartilage (A) with radiometric temperature profile (B).

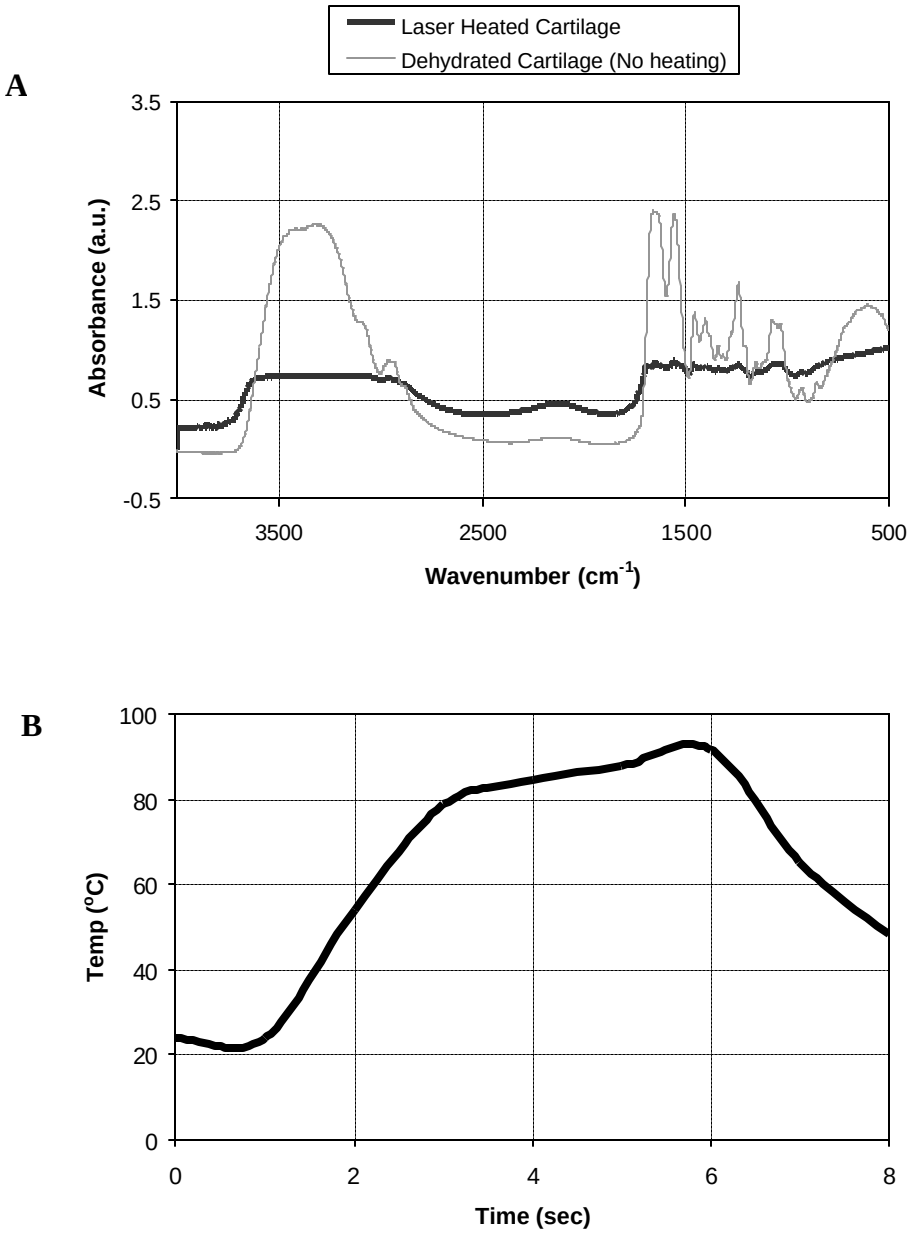

Figure 2.10: FT-IR absorption spectra of dehydrated without heating and laser-irradiated (λ = 2.1 μm, 2W, 6 sec) cartilage (A) with radiometric temperature profile (B).

When incident laser power is increased, radiometric temperature of the sample increased to 90 ^{o}C (Figure 2.10B) and the water absorption peak at 2100 cm^{-1} disappeared in Figure 2.10A that indicates more dehydration occurred than that in Figure 2.9A. The magnitude of macromolecule absorption spectra below 1700 cm^{-1} in Figure 2.10A also shows dramatic decrease compared to Figure 2.9A.

2.5. DISCUSSION AND CONCLUSIONS

In most cartilage, the water contributes 80% and the macromolecules contribute about 20% with 13% collagen and 7% proteoglycans [3]. Water is the most concentrated constituent in cartilage and the strongest absorber in the IR range. The water molecule vibrates in a number of modes and overtones with characteristic absorption bands [4, 6]. Also, macromolecules such as collagen and proteoglycans can contribute to the absorption spectrum of cartilage (sulfate (1245 cm^{-1}), sugar (1125-920cm^{-1}, 850cm^{-1}), and protein entities (1640 cm^{-1}, 1545 cm^{-1} due to Amide I and II) [1]). Although the isolated constituents of cartilage have unique spectral features, their spectra are considerably overlapped and it may be difficult to determine quantitatively the changes in the spectra of the individual constituents and their interactions due to photothermal modification of the macromolecules without application of a more sophisticated model-based spectral analysis.

As seen in the results, the spectra of cartilage arise from known absorption bands. The water peak around 2100 cm^{-1} is well isolated and can be used to characterize water content in cartilage such as the investigation of the magnitude changes and the shift of the water absorption band upon heating.

In macromolecular constituents in proteins, the two strong amide bands centered near 1656 (Amide I) and 1548 cm^{-1} (Amide II) have been the major constituents to study thermal induced structural transitions because of their distinguishable peaks. The amide I band arises primarily from C=O stretching vibration of the peptide linkage and is known to be sensitive to the secondary structural composition and conformal changes in proteins [7]. The amide II band arises mainly from an out-of-phase combination of N-H in-plane bending and C-N stretching vibrations of peptide linkage and is less useful in protein structural analysis [7]. Carroll *et al.* investigated the infrared spectrum and water binding of collagen depending on relative humidity from 0 to 95% at 25 ^{o}C and observed the gradual decrease in the intensities of characteristic amide bands due to the conformational changes in the binding of water molecules to the macromolecular structures [8]. Doyle *et al.* also observed the downward shift of the amide bands as well as the absorption peak decreases in collagen upon heating suggesting that the amide absorption band of collagen is characteristic of some level of collagen structure which is lost due to the denaturation of macromolecules [9]. In recent years, many researchers have been involved to

obtain detailed structural information on the denatured states of proteins [10-12]. Fabian and Mantsch undertook an infrared spectroscopic study to test for the presence of native-like structures in thermally denatured Ribonuclease A by observing amide I band which is one of the constituents in cartilage and reported that Ribonuclease A did not aggregate at high temperatures (above 75 ^{o}C) and the infrared spectrum showed a completely featureless amide I band contour [10]. Panick and Winter also studied the temperature dependence of the amide I FT-IR spectrum of RNase and observed the increase of temperature 82 ^{o}C lead to a shift of the band maximum to larger wavenumbers and the absorption band became more symmetric as well as decreasing intensity [11]. However, in most reported spectroscopic studies of protein denaturation, the time-temperature history is unfortunately not specified. The absence of knowing the time-temperature history makes interpretation of the degree of thermal denaturation extremely difficult. Dong *et al.* developed a criteria for evaluating how successfully the spectra due to water may be subtracted from the observed spectrum in the amide I region and observed the precise movements of the absorption band as well as the intensity decreases [12]. Although this water subtraction technique from the observed spectrum is useful to recognize details of structural changes of macromolecules in our cartilage study, this application is limited to the use of a short (6-10 μm) path-length cell that could not be applied to our results because of the relatively thick path length of the samples (~100 μm). From our results in

Figure 2.8, the absence of macromolecule absorption bands below 1700 cm^{-1} upon heating may be due to the simultaneous substantial decreases in the background water bands within the spectral ranges as well as thermal denaturation of macromolecules. Therefore, quantitative analysis of the absorption bands of macromolecules may not be completed without subtraction of the water spectrum. Further studies with less than 10 μm thick cartilage samples produced by a microtome or proteoglycan solution in a very short path-length cell should be investigated by applying the water spectrum subtraction technique.

The process of water movement in cartilage has long been recognized of great importance for controlling cartilage nutrition. Maroudas and Schneiderman concluded from their study that all water in cartilage is exchangeable [13]. However, Torzilli suggested the existence of a considerable fraction of 'trapped' water that does not participate in water movement through the biological tissue [13]. As seen in Figure 2.8, the water absorption peak of dehydrated cartilage after PBS solution heating around 3100 cm^{-1} shows dramatic decrease compared to the dehydrated cartilage without heating. This may be explained a 'trapped' water that does not participate in water movement but this water may be turned to an 'exchangeable' water due to the heating. Bagratashvili *et al.* explored the reversibility of drying and water absorption processes and the mechanism of water diffusion in cartilage [2]. They used the FT-IR spectra of water to estimate the water content in dried and heated cartilage

at the spectral range from 5,500 to 1,500 cm^{-1} and observed that the FT-IR spectrum of bound water in cartilage differs from that of free water in cartilage and that both show differences to the FT-IR spectrum of pure water [2]. The water absorption spectra changes both due to heating and dehydration were consistent with our results, but they did not investigate the absorption bands of macromolecules below 1700 cm^{-1}. The dehydration and thermal denaturation effects from our results indicate that FT-IR spectroscopy can monitor the reversibility of water movement and denaturation of macromolecules, respectively.

From the results of photothermal effects, the laser irradiance and exposure time are the important factors to identify when thermal denaturation of the tissue occurs. Further studies for the FT-IR measurements of cartilage are to analyze the changes in shapes and shifts in the absorption bands of water and macromolecules with different temperatures and correlate with a theoretical modeling so that we can compare the theoretical results with the experimental results.

The unwanted dehydration during the measurements because of the direct contact with air and relatively long time (about 2 minutes) of data acquisition and irregular water film deposition on the sample surface made the sample hard to maintain the original position and gave an error during the data acquisition. Use of an IR window and optical coherence tomography measurement during laser

irradiation can overcome the dehydration problem and monitor water film thickness, respectively. The combination of laser heating setup within the FT-IR spectroscopy system will give a better understanding of the photothermal kinetics of macromolecular modification at different sample temperatures.

Using FT-IR spectroscopy, the photothermal effects in response to laser irradiation of cartilage were investigated and identified as dehydration and thermal modification of macromolecules. The reversibility of the drying process is also confirmed by the FT-IR spectra recorded after rehydration of the sample. Different degrees of photothermal modification of cartilage macromolecules were observed depending on the incident laser dose. This study may be used to investigate the spatial distribution of collagen and proteoglycans and their interactions with water molecules in response to laser irradiation. Because proteoglycans are responsible for the maintenance of internal stress in cartilage, refinements in the methodology may allow quantitative investigation of the relationship between the kinetics of proteoglycan denaturation and accelerated stress relaxation.

2.6. REFERENCES

1. Camacho N. P., West P., Torzilli P. A., Mendersohn R., "FTIR Microscopic Imaging of Collagen and Proteoglycan in Bovine Cartilage", *Biopolymers (Biospectroscopy)*, **62**:1-8, 2001

2. Bagratashvili V. N, Sobol E. N, Sviridov A. P, Popov V. K, Omel'chenko A. I, Howdle S. M, "Thermal and Diffusion Processes in Laser-Induced Stress Relaxation and Reshaping of Cartilage", *J. Biomech.*, **30(8)**: 813-817, 1997

3. Sobol E. N., *"Phase Transformations and Ablation in Laser-Treated Solids"*, John Wiley & Sons, New York, 1998

4. Hale G. M., Querry M. R., "Optical Constants of Water in the 200-nm to 200-mm Wavelength Region", *Applied Opt*., **12(3)**: 555-563, 1973

5. ThermoNicohlet Corp., "Introduction to Fourier Transform Infrared Spectroscopy", *Product manual*, 2001

6. Sobol E. N., Sviridov A., Omel'chenko A., Bagratashivili V., Kitai M., Harding S. E., Jones N., Jumel K., Mertig M., Pompe W., Ovchinnikov Y., Shekhter A., Svistushkin V., "Laser Reshaping of Cartilage", *Biotech. Gene. Eng. Rev*., **17**: 539-564, 2000

7. Krimm S., Bendekar J., "Vibrational Spectroscopy and Conformation of Peptides, Polypeptides, and Proteins", *Adv. Protein Chem.*, **38**:181-364, 1986

8. Carroll R. J., Ard J. S., Susi H., "The Infrared Spectrum and Water Binding of Collagen as a Function of Relative Humidity", *Biopolymers*, **10**:1597-1604, 1971

9. Doyle B. B., Bendit E. G., Blout E. R., "Infrared Spectroscopy of Collagen and Collagen-Like Polypeptides", *Biopolymers*, **14**:937-957, 1975

10. Fabian H., Mantsch H. H., "Ribonuclease A Revisited: Infrared Spectroscopic Evidence for Lack of Native-like Secondary Structures in the Thermally Denatured State", *Biochemistry*, **34**:13651-13655, 1995

11. Panick G., Winter R., "Pressure-Induced Unfolding/Refolding of Ribonuclease A: Static and Kinetic Fourier Transform Infrared Spectroscopy Study", *Biochemistry*, **39**:1862-1869, 2000

12. Dong A., Randolph T. W., Carpenter J. F., "Entrapping Intermediates of Thermal Aggregation in a-Helical Proteins with Low Concentration of Guanidine Hydrochloride", *J. Biol. Chem.*, **275**:27689-27693. 2000

13. Maroudas A., Schneiderman R., "Free and Exchangeable or Trapped and Non-Exchangeable Water in Cartilage", *J. Orthoped. Res.*, **5**:133-138, 1987

14. Torzilli P. A., “Water Content and Equilibrium Water Partition in Immature Cartilage”, *J. Orthoped. Res.*, **6**: 766-769, 1988

CHAPTER 3: DEPTH-RESOLVED PHASE RETARDATION MEASUREMENTS USING POLARIZATION SENSITIVE OPTICAL COHERENCE TOMOGRAPHY

3.1. ABSTRACT

Thermally induced changes in phase retardation of nasal septal cartilage following Nd:YAG laser irradiation were investigated using a polarization-sensitive optical coherence tomography (PS-OCT) system. A PS-OCT system and infrared imaging radiometer were used to record, respectively, depth-resolved images of the Stokes parameters of light backscattered from *ex vivo* porcine nasal septal cartilage and radiometric temperature changes following laser irradiation. PS-OCT images of cartilage were recorded before (control), during, and after laser irradiation. From the measured Stokes parameters (I, Q, U, and V), an estimate of the relative phase retardation between two orthogonal polarizations was computed to determine birefringence in cartilage. Phase retardation images of light backscattered from cartilage show significant changes in retardation following laser irradiation. To investigate the origin of retardation changes in response to local heat generation, we differentiated two possible mechanisms:

dehydration and thermal denaturation. PS-OCT images of cartilage were recorded after dehydration in glycerol and thermal denaturation in heated physiological saline. From our experiments, we think observed retardation changes in cartilage are primarily due to dehydration. Since dehydration is the principal source for changes in retardation in cartilage, use of PS-OCT as a feedback control methodology for non-ablative cartilage reshaping is sensitive to detection of water loss rather than thermal denaturation.

3.2. INTRODUCTION

Polarization sensitive optical coherence tomography (PS-OCT) has been used to characterize the polarization state of light backscattered as a function of optical path length in birefringent biological tissues such as muscle, skin and cornea [1, 2]. De Boer *et al.* demonstrated the application of PS-OCT to biological materials and determined the optical axis in rodent muscle and *in vivo* rodent skin [1]. They demonstrated that the coherent detection of the interference fringe intensity in orthogonal polarization channels allows determination of the depth-resolved Stokes parameters of light backscattered from tissue [1]. In another study, Ducros *et al.* used PS-OCT to observe birefringence in the rabbit eye and measured the thickness of the birefringent retinal nerve fiber layer that was in relatively good agreement with values determined from histology [2].

Birefringence in cartilage is due to the asymmetrical collagen fibril structure and may change if the underlying structure is disrupted due to local heat generation by absorption of laser radiation. Limited studies have been reported investigating birefringence in cartilage. Yarker *et al.* measured birefringence of the deep zone of pig tibial plateau cartilage using polarized light microscopy and provided information on collagen fibril orientation in the tissue [3]. Using quantitative microscopic methods Kiraly *et al.* also investigated birefringence changes in the articular cartilage collagen network and proteoglycans due to the deterioration associated with joint disease [4]. Kiraly *et al.* exposed tissue plugs to cyclic loading and observed that birefringence increased in the superficial zone and decreased in the deep zone [4].

Since PS-OCT is emerging as a new technique to determine phase retardation between orthogonal polarization modes of light propagating in biological materials, we attempted to measure thermodynamically induced changes of phase retardation in cartilage for application to laser assisted cartilage reshaping. In cartilage, the asymmetrical collagen fibril structure gives a difference in phase delay between light oscillations polarized along two orthogonal axes and may change if the underlying structures are disrupted due to local heat generation by absorption of laser radiation. Local heat generation can result in water movement (e.g. dehydration) and possible thermal denaturation of the constituent proteins. Although mechanisms underlying laser assisted

cartilage reshaping are incompletely understood, thermodynamic measurements of phase retardation changes in cartilage may find laboratory and clinical applications to characterize internal dynamics of macromolecules such as collagen and proteoglycans during laser irradiation. Moreover, active monitoring of phase retardation changes in cartilage may find application as a feedback control methodology in non-ablative laser assisted cartilage reshaping procedures.

3.3. EXPERIMENTAL METHODS

To investigate the thermodynamically induced phase retardation changes following laser irradiation, a polarization sensitive optical coherence tomography (PS-OCT) system [2] combined with a Nd:YAG laser as a heating source and infrared imaging radiometer was used (Fig. 3.1). Light from a super luminescent diode (SLD) (0.8 mW, λ=859 nm, FWHM=18 nm) is linearly polarized along the horizontal axis and then divided into reference and sample paths by a nonpolarizing beam splitter (BS). In the reference path, after reflection from a reference mirror moving at respectively 5 Hz and double passage through a polarizer at 45^{o}, the light is linearly polarized at 45° with respect to the horizontal. In the sample path, a quarter wave plate (QWP) transforms light incident onto the sample into a right circularly polarized state. Interference fringes between the

light backscattered from a reference mirror and sample are split into two orthogonal polarization components by a polarizing beam splitter (PBS). The vertical and horizontal polarization components are detected by photodiodes D1 and D2, respectively.

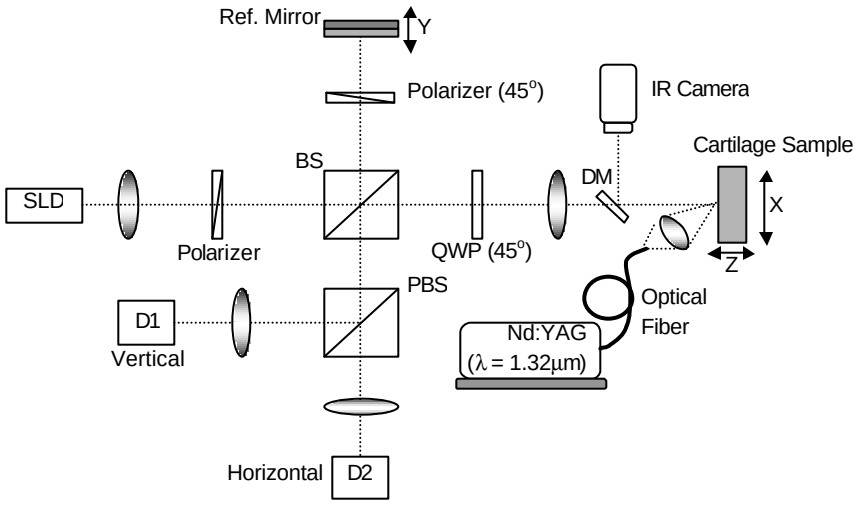

Figure 3.1: Schematic diagram of PS-OCT system combined with a Nd:YAG laser as a heating source (λ = 1.32 μm) and an infrared imaging radiometer. SLD: Super Luminescent Diode, BS: non-polarizing Beam Splitter, PBS: Polarizing Beam Splitter, QWP: Quarter Wave Plate, DM: Dichroic Mirror

At positions above the cartilage surface the signal is zero and $\Phi = 90^{o}$ is the mean phase. Once light reflects from the surface, the phase indicates the

polarization state due to specularly reflected light. Values of Φ for specularly reflected light vary due to speckle at the cartilage surface.

We used a Nd:YAG laser (New Star, Auburn CA) as a heating source (6W, λ=1.32 μm, D=4 mm, Pulse duration=6 s) and an infrared imaging radiometer to measure temperature changes during laser irradiation. Infrared blackbody emission from the cartilage sample is reflected by a dichroic mirror (DM) positioned between the focusing lens and sample and detected by an InSb imaging radiometer (Merlin, Indigo Systems Inc., 320 × 240 pixels) (Fig. 3.1).

Coherent detection of the amplitude and phase of the interference fringes in orthogonal polarization channels allows imaging the Stokes parameters (*I, Q, U, V*), and the degree of polarization, *P*. The intensity based image (*I*) is similar to that which conventional OCT provides. The parameter *I* represents total intensity of light backscattered from the cartilage sample (3.1a), *Q* represents the difference between intensities of light linearly polarized at 0° and 90°, normalized to total intensity (3.1b). Similarly, parameters *U* and *V* represent the differences between intensities of light linearly polarized at +45° and –45°, right circularly polarized (3.1c) and left circularly polarized (3.1d), respectively [1].

$$I = I_0{}^{o} + I_{90}{}^{o} \quad (3.1a), \qquad Q = \frac{I_{0^o} - I_{90^o}}{I} \quad (3.1b), \qquad U = \frac{I_{45^o} - I_{-45^o}}{I} \quad (3.1c),$$

$$V = \frac{I_{rc} - I_{lc}}{I} \quad \text{(3.1d)}, \quad P = \sqrt{Q^2 + U^2 + V^2} \quad \text{(3.1e)} \qquad \text{(Eq. 3.1)}$$

The computed *Q, U, V* Stokes parameters represent the polarization state of light backscattered from the sample, transmitted through a quarter wave plate and incident onto the detectors. For example, the Stokes parameters for the light specularly reflected from the surface of the sample are $Q = -1$, $U = 0$, and $V = 0$.

From this knowledge, we calculated phase retardation, Φ:

$$\Phi = arccos\,(-Q) \qquad \text{(Eq. 3.2)}$$

In the Poincaré sphere representation (Fig. 3.2) [5], parameter Φ is the angle between the Stokes vectors on the Poincaré sphere of light backscattered from inside the cartilage specimen and the front surface of the sample ($Q = -1$, $U = V = 0$). In this representation, Φ represents the phase retardation between vertical and horizontal polarization components of light backscattered from the user-specified region inside the cartilage sample relative to incident light. We obtain information about birefringence changes by calculating phase retardation, Φ, at each pixel representing a discrete position in the cartilage. When the backscattered light is unpolarized or when the intensity is lower than the system noise level, Φ varies uniformly between 0° and 180° and averages 90°.

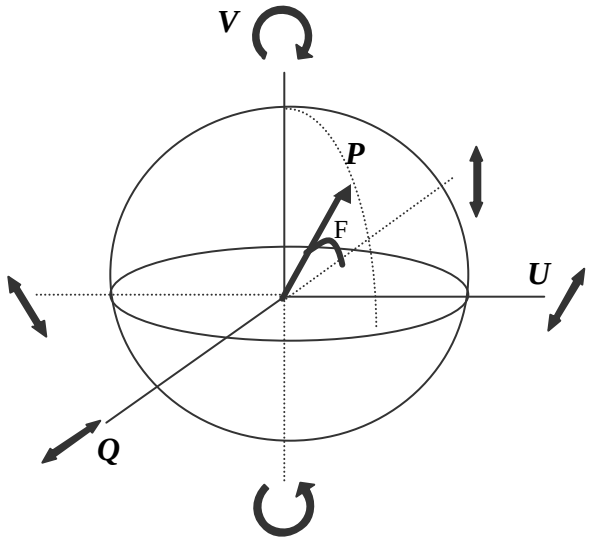

Figure 3.2: Schematic illustration of Poincaré sphere representation of polarization [5]. Four Stokes parameters, *I*, *Q*, *U*, *V*, represent total intensity and differences between intensities of linearly polarized light at 0° and 90°, 45° and –45°, right circularly polarized and left circularly polarized light, respectively. In this representation, Φ represents the phase retardation between two orthogonal polarization components of light backscattered from the sample relative to incident light.

After extraction, the cartilage specimen was sliced into six rectangular parallelepiped shapes and the prepared sample was placed in the sample path of the PS-OCT system. A red aiming beam co-aligned with the imaging beam was used to insure the scanning position of PSOCT and laser heating position were overlapped. Also, the IR imaging was aligned to PSOCT scanning position by

firing the laser several times with cartilage sample. Two PS-OCT images (2 mm wide × 1 mm deep) centered on the irradiated area were acquired before and after Nd:YAG laser irradiation. In the PS-OCT images recorded during laser irradiation, successive depth scans (5 scans per second) were recorded at a stationary lateral position at the center of the irradiation beam over a period of 10 seconds. Simultaneously, radiometric temperature was measured using an IR camera at a 60 Hz frame rate. After recording infrared imaging data, a calibration procedure was performed for the IR camera using a blackbody source with a thermocouple attached to the surface.

3.4. RESULTS

Figure 3.3 shows recorded PS-OCT images scanned spatially (2 mm width × 1 mm depth) for phase retardation, Φ, before and after laser irradiation. Incident light that is right circularly polarized at the air-tissue interface and polarization state of light propagating through the sample varies with depth and lateral position. Although the light incident on the sample is right circularly polarized, polarization state of recorded data is displayed as detected by the photodiodes. Circularly polarized light becomes vertically polarized after passing through the quarter wave plate in the sample path (Fig. 3.1). The Φ image changes before and after laser irradiation as seen in Figure 3.3.

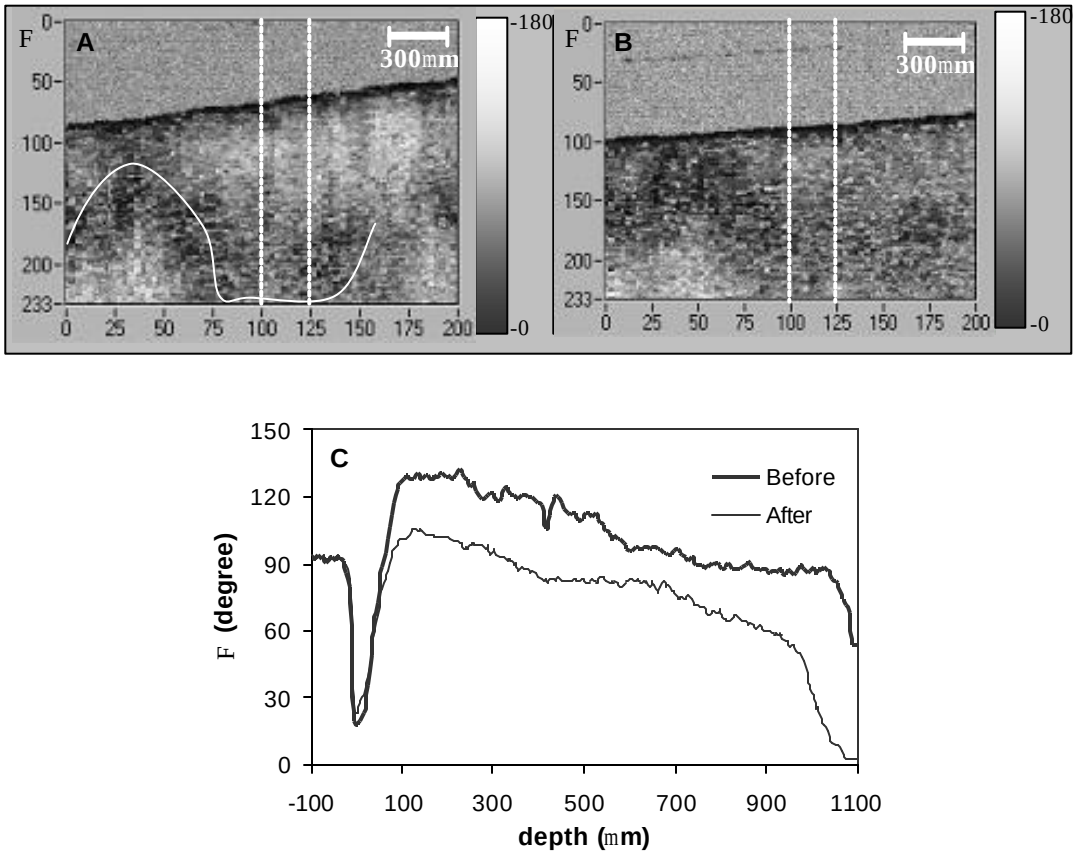

Figure 3.3: Phase retardation (Φ) images (2 mm × 1.4 mm), i.e. (Eq. 3.2), in the cartilage sample (A) before laser irradiation (the solid white line indicates an S-shaped structural pattern), (B) after laser irradiation and (C) the plot of phase retardation versus depth before and after laser irradiation of A-scans between dotted lines. Scale bar is 300μm and the laser irradiation spot size on the sample surface is 4 mm.

An S-shaped structural pattern in Figure 3.3(A) is modified following laser irradiation (Figure 3.3(B)) indicating that the scattering properties and phase

retardation of cartilage have changed in response to laser irradiation. To observe quantitatively the phase retardation before and after laser irradiation, we averaged phase retardation values in the dotted region and plotted phase retardation versus depth before and after laser irradiation (Figure 3.3(C)). As seen in Figure 3.3(C), the major phase retardation changes occur from the surface (depth = 0 μm) to about 100 μm in depth. No significant bulk changes in phase retardation were observed in the 100 μm to 1,000 μm depths.

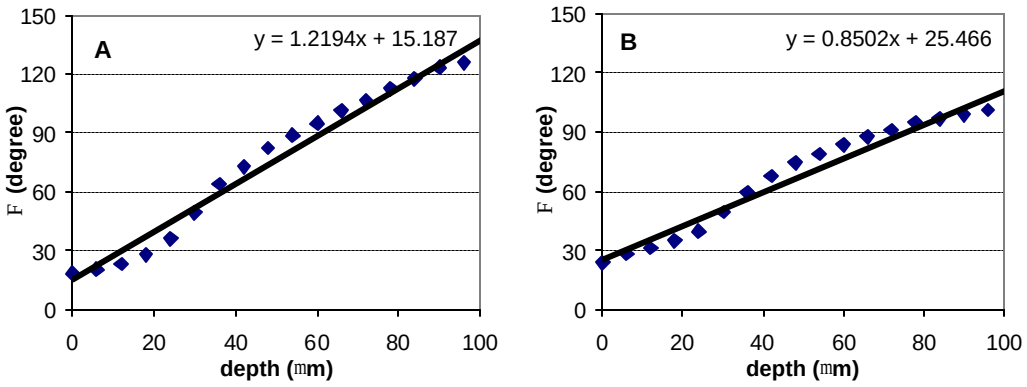

Figure 3.4: Phase retardation slope calculation before (A) and after (B) laser irradiation from the surface to 100 mm in depth.

To observe the changes at the sample surface giving major phase retardation changes, slope of the accumulated phase retardation with depth was calculated in Figure 3.4 since the phase retardation slope represents the

birefringence changes. The calculated slopes before (Figure 3.4(A)) and after (Figure 3.4(B)) laser irradiation from the surface to 100 μm in depth were 1.22 (degrees/micron) and 0.85 (degrees/micron), respectively, so the phase retardation gradient decreases after laser irradiation.

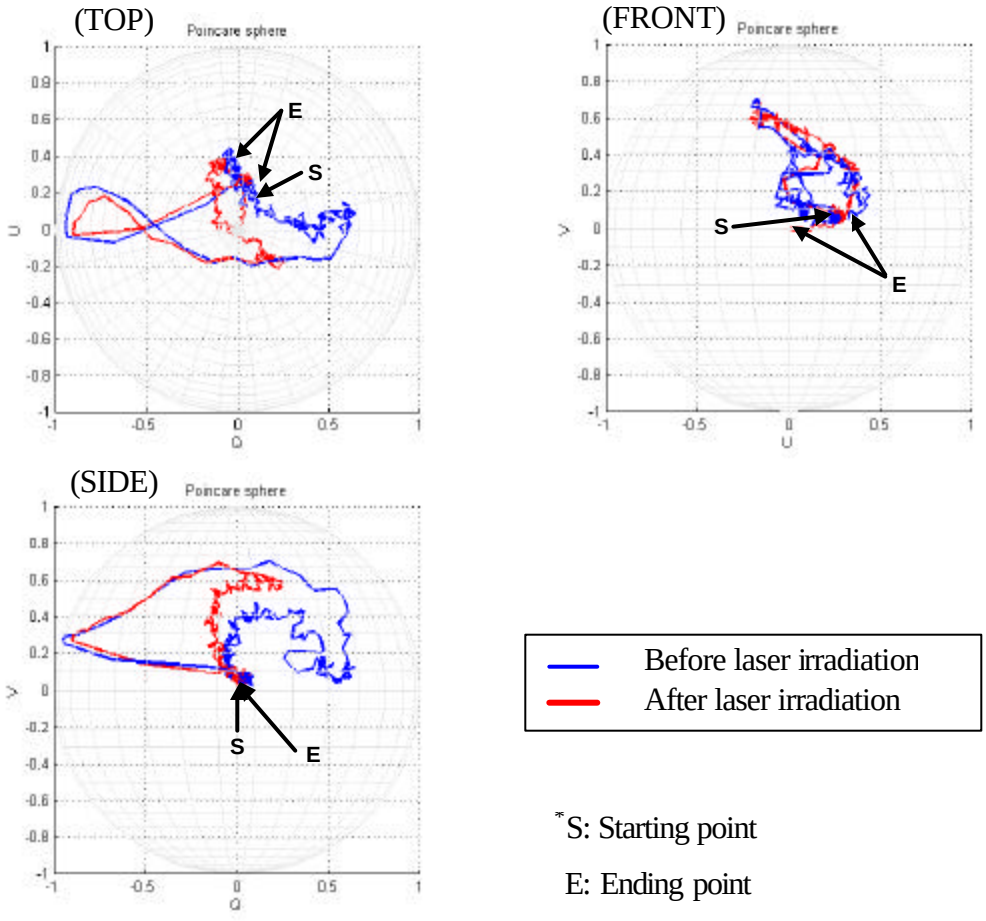

Figure 3.5: Poincare sphere of Stokes parameters before and after laser irradiation.

Figure 3.5 shows three orthogonal perspectives of the Stokes parameters, Q, U, and V on the Poincare sphere. For these results, we re-registered and averaged the 200 A-scans for each Stokes parameter and plotted versus depth. Because the data we obtained contained speckle noise, averaging 200 A-scans for each parameter reduced this noise. In the Stokes parameters before laser irradiation versus depth, the polarization state of light backscattered from the cartilage sample begins linearly polarized vertically ($Q = -1$, $U = V = 0$) below the air-tissue interface and transforms to right elliptically polarized ($Q = 0.7$, $U = 0$, $V = 0.7$), and then V rapidly decreases whereas Q begins to increase and decreases as the depth increases. After laser irradiation, the light begins linearly polarized vertically ($Q = -1$, $U = V = 0$) below the air-tissue interface and becomes right elliptically polarized ($Q = U = 0$, $V = 0.7$). These results show that retardation of light in the cartilage sample is changed in response to laser irradiation.

The Φ image recorded during laser irradiation is shown in Figure 3.6(A) and compared with the corresponding radiometric temperature changes (Figure 3.6(B)). The x-axis represents time, while the y-axis represents depth. The left side of the image corresponds to the beginning of laser irradiation. Upon heating the cartilage sample, structural optical property changes are observed at approximately the 20^{th} A-scan or about 4 seconds (~75 ^{o}C) after beginning laser irradiation.

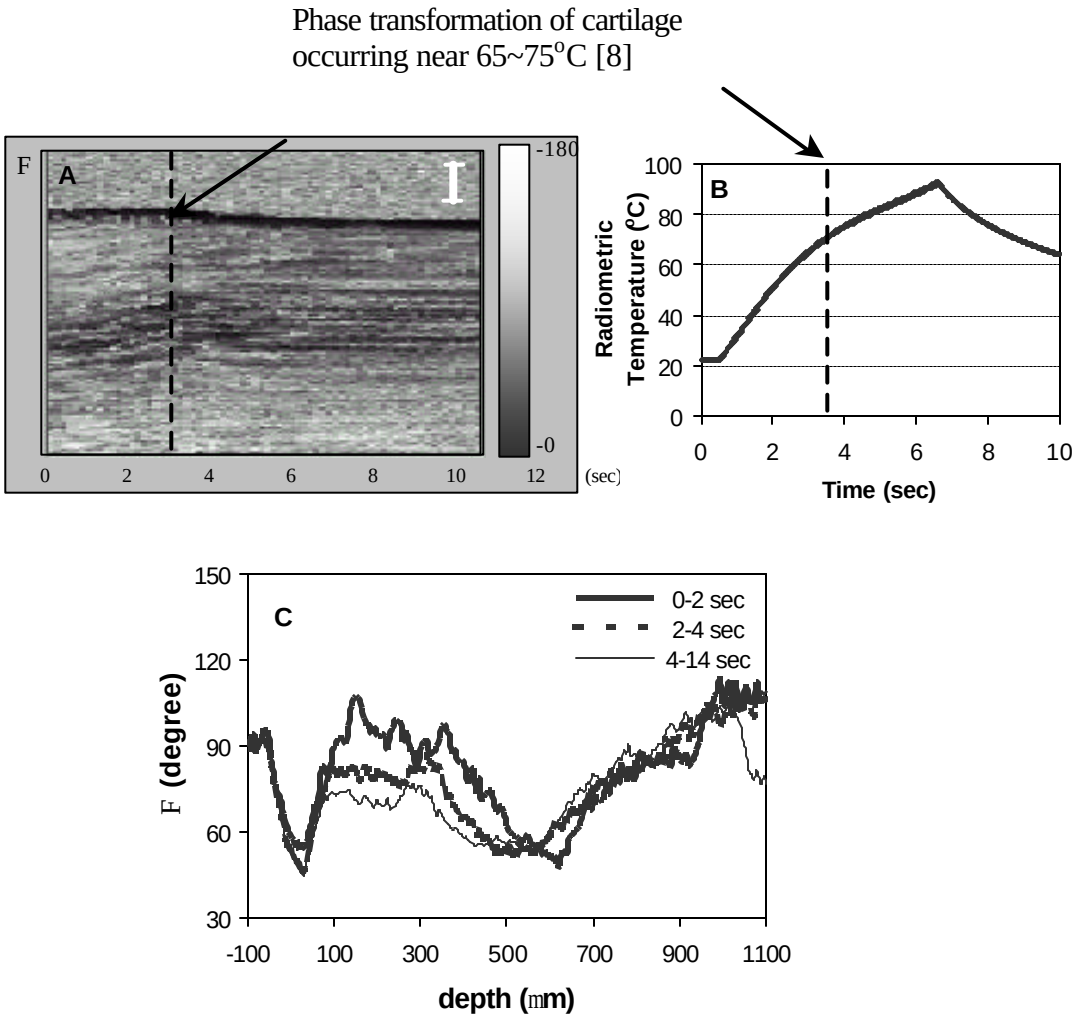

Figure 3.6: Phase retardation (Φ) images in cartilage sample (Scale bar is 300μm) (A), radiometric temperature change (B), and plot of phase retardation versus depth during laser heating (C). The horizontal dimension is time (s) in both A and B, and reported results represent data recorded during laser irradiation. The radiometric temperature was plotted by averaging values in pixels over a 2 mm × 2 mm area on the cartilage surface.

To investigate the thermodynamically induced changes quantatively, plot of phase retardation (Fig. 3.6(C)) is given versus depth during laser irradiation. Inasmuch as data during laser irradiation was scanned in time at a fixed position, we grouped recorded A-scans into three groups: (1) early laser irradiation (10 A-scans, 0-2 seconds, 20 ^{o}C – 50 ^{o}C) (2) transition (10 A-scans, 2-4 seconds, 50 ^{o}C – 78 ^{o}C) (3) post transition (40 A-scans, 4-14 seconds). Radiation from the Nd:YAG laser was utilized as a heating source and applied for 6 seconds and the PS-OCT imaging process started simultaneously with laser irradiation. From the plot in Figure 3.6(C), the slope of phase retardation from the surface to 100 μm in depth is calculated over three time intervals to observe the birefreingence changes of cartilage during laser irradiation in Figures 3.7(A)-(C). The major phase retardation changes occur at the surface as seen in Figure 3.7, but no significant changes in phase retardation are observed at depths greater than 100 μm. The calculated slopes show the decreases from 0.43 (degrees/micron) to 0.27 (degrees/micron) during laser irradiation. Thess calculated slopes are less than those of before and after laser irradiation because the phase retardation data during laser irradiation was scanned in time at a single fixed point instead of scanning spatially for before and after laser irradiation. Furthermore, the sample variation may give rise the slope differences.

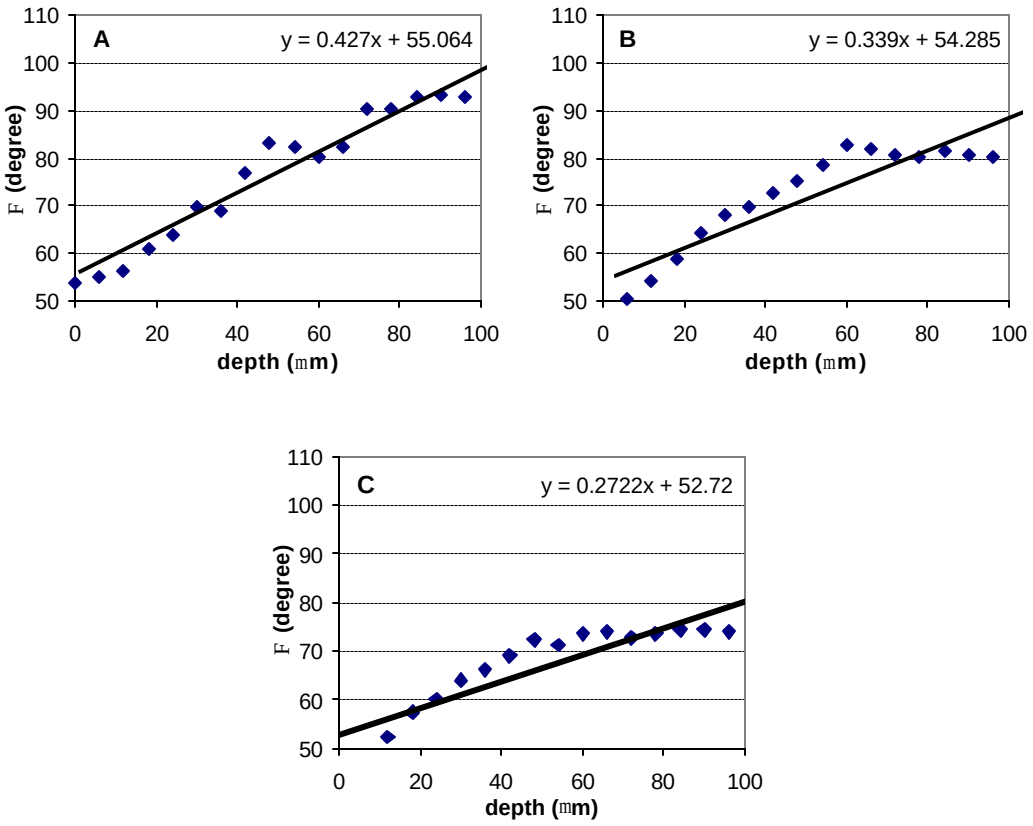

Figure 3.7: Phase retardation slope calculations during laser irradiation ((A): early laser irradiation, (B): transition, (C): post transition).

When the radiometric temperature reaches 65 ^{o}C – 75 ^{o}C, protein systems in tissue begin to undergo thermal denaturation and dehydration and the observed changes signal the initial stages of thermal denaturation of collagen and other macromolecules within cartilage [6-11]. When the thermal denaturation of

collagen or other macromolecules occurs, the helices may unwind and then recoil as the tissue is allowed to cool [11]. Also, fibrils in the tissue may move closer together as water is lost because of the heat generation and then rehydrate when the tissue is imbibed into PBS solution [12]. The retardation changes accompanying laser irradiation may be used to identify the biophysical transformation responsible for stress relaxation in cartilage.

3.5. DISCUSSION AND CONCLUSIONS

To understand the origin of the phase changes of light propagating in biological materials, two types of birefringence should be considered: form and intrinsic birefringence. Intrinsic birefringence is due to molecular anisotropy (e.g., tropocollagen molecule) while form birefringence is due to structural anisotropy [12,13]. The relation between the volume fraction of fibrils in biological tissue and form birefringence (Δn) may be derived analytically [14] (Eq. 3.3). The calculated variation of form birefringence with increasing fractional fibril volume is shown in Figure 3.8.

$$\Delta n = n_e - n_o = (f_1 n_1^{\,2} + f_2 n_2^{\,2})^{1/2} - \left(\frac{f_2 n_2^{\,4} + (1+f_1) n_1^{\,2} n_2^{\,2}}{f_2 n_1^{\,2} + (1+f_1) n_2^{\,2}} \right)^{1/2} \qquad \text{(Eq. 3. 3)}$$

where n_e and n_o are the refractive indices of extraordinary and ordinary waves, f_1 and f_2 ($=1 - f_1$) are the volume fraction of fibril and surrounding medium, and n_1 and n_2 are the refractive indices of fibril and medium, respectively.

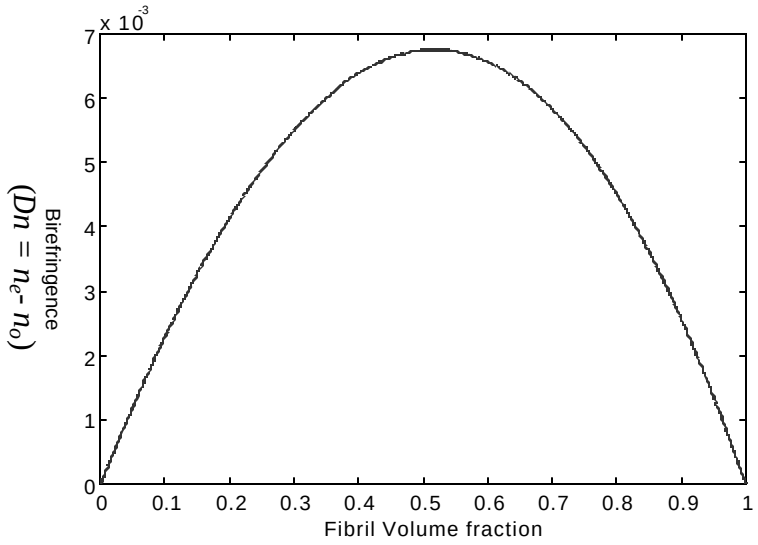

Figure 3.8: Plot of the calculated variation of form birefringence versus volume fraction of fibrils in tissue. Fibril and medium refractive indices are 1.53 and 1.34, respectively.

When local heat generation is produced in the tissue, two effects occur; dehydration and thermal denaturation. In dehydration, form birefringence changes since the surface shrinkage occurs and fibrils move closer as water is lost and the volume fraction of fibrils increases (Fig. 3.9(A)). For thermal denaturation, the fibrils in tissue occupy a larger volume due to unraveling of the

underlying structures (Fig. 3.9(B)). Form birefringence can increase or decrease depending on the starting volume fraction of tissue [13].

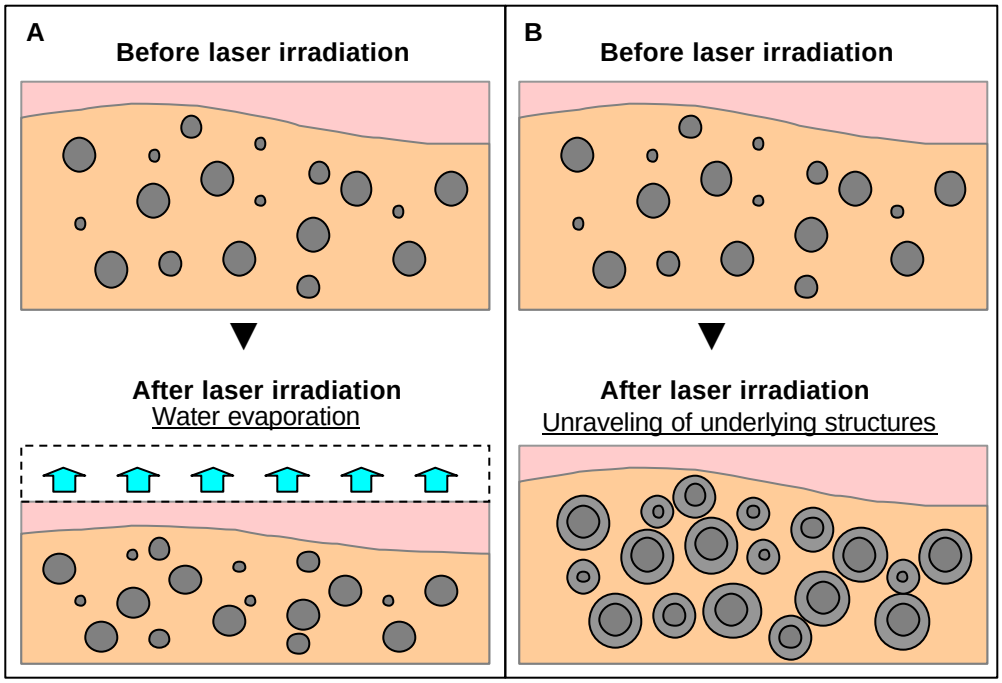

Figure 3.9: Dehydration (A) and thermal denaturation effects (B) before and after laser irradiation.

Since few studies have reported measurements of the volume fraction of biological materials, two native cartilage samples were placed into a desiccator for two weeks and allowed to dehydrate to determine approximate volume fraction of fibril and medium. The table 3. 1 shows the mass changes of cartilage before and after dehydration.

Table 3.1: Volume fraction measurements of cartilage. m_{total} is controlled total mass, V_{total} is controlled total volume, and m_f is dehydrated mass of cartilage sample.

	m_{total} (g) (V_{total} (ml))	m_f (g)
Sample 1	0.5878 (0.5026)	0.3616
Sample 2	0.6466 (0.6068)	0.3978

The fibril volume fraction (f_1) can be calculated by

$$f_1 = 1 - \frac{V_{solution}}{V_{total}} = \frac{V_{total} - (m_{total} - m_f)/r_{solution}}{V_{total}} \qquad \text{(Eq. 3.4)}$$

where $V_{solution}$ is solution volume and $r_{solution}$ ($\approx$ 1.0) is solution density. Since the solution mass substantially decreases when the sample is dehydrated, we assume the measured values of dehydration mass approximates fibril mass (m_f). Using Eq. 3.4, the fibril volume fractions for two samples were calculated to f_1 = 0.55 and 0.59, respectively. From these calculations, the controlled fibril volume fraction of cartilage starts at greater than 0.5 in Figure 3.8. Therefore, the phase retardation results show that when water evaporates from cartilage due to laser irradiation, the fibrils may move closer together and the volume fraction

of fibrils is increased and this phenomenon causes a decrease in form birefringence as well as surface shrinkage [12, 13]. In thermal denaturation, the birefringence may decrease since fibrils occupy a larger volume due to unraveling of the underlying structures and the refractive index ratio between the fibril and extracellular matrix also decreases as seen in Figure 3. 10 [12,13].

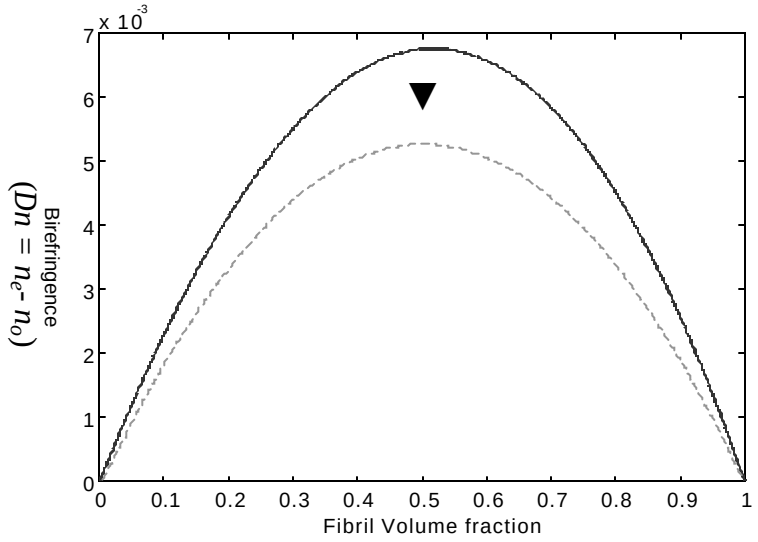

Figure 3.10: Plot of form birefringence changes with the decrease of the refractive index of fibrils (n_1 = 1.53 → 1.50 (---)).

To reduce the uncertainty for the volume fraction measurements of cartilage, the two types of water within cartilage should be considered: these include trapped water that does not participate in water movement and exchangeable water that evaporates when the tissue is dehydrated [15].

Therefore, the measured fibril volume fraction of cartilage may include trapped water even though a desiccator extracted water from cartilage over a two-week time interval. This may result in an overestimate of the fibril volume fraction. If the fibril volume fraction is greater than 0.5, form birefringence gradually decreases following laser irradiation. Otherwise, the slight increase of form birefringence may be observed before the decrease of form birefringence. Since the trapped water within cartilage can be turned to exchangeable water when moderate heating is applied to the sample, the additional measurements of the fibril volume fraction combined with a heating source should be performed [15].

We investigated these two effects by conducting experiments using glycerol and heated saline at 63 ^{o}C. For dehydration measurements, cartilage was imbibed into glycerol (GX0185-6, EM Science, NJ) for 20 minutes and PS-OCT images recorded every 5 minutes. After dehydration, the samples were rehydrated at room temperature in saline for 10 minutes and PS-OCT images recorded again. Figure 3.11 shows the phase retardation changes versus depth in glycerol to investigate the dehydration process. The major phase retardation changes occur at the surface. In addition, phase retardation in cartilage substantially decreased with increasing time. After rehydration for 10 minutes in room temperature saline, the phase retardation increased and returned to original values.

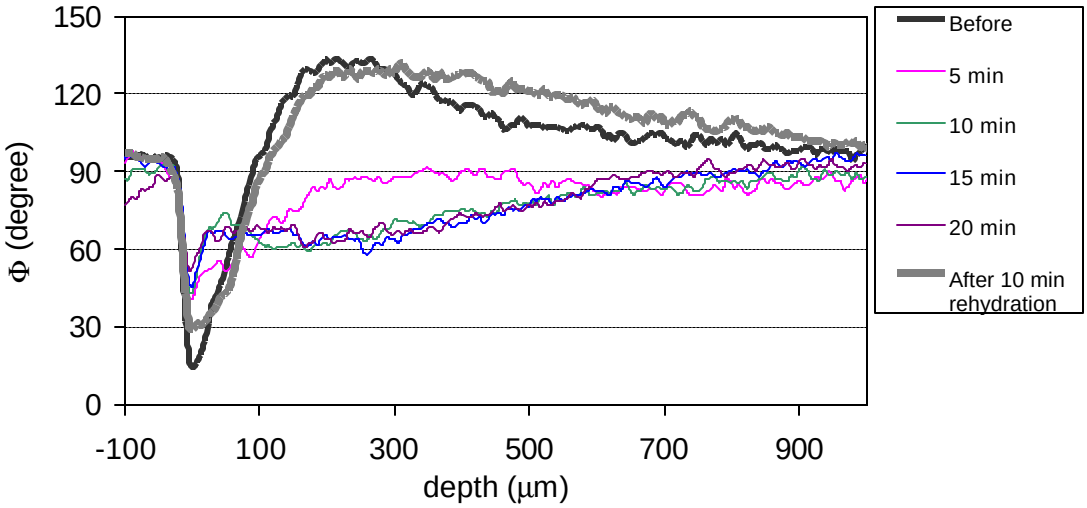

Figure 3.11: Plots of phase retardation versus depth for cartilage in glycerol for dehydration effects.

For thermal denaturation measurements, cartilage was immersed at 63 ^{o}C in heated saline for 20 minutes after which PS-OCT images were recorded every 3 minutes. After rehydration for 10 minutes in room temperature saline, PS-OCT images of the sample were recorded again. As seen in Figure 3.12, no phase retardation changes were observed in cartilage over the time. Although the heating may have been insufficient to result in substantial or near complete thermal denaturation, a calculation of damage integral indicates the collagen should have been denatured.

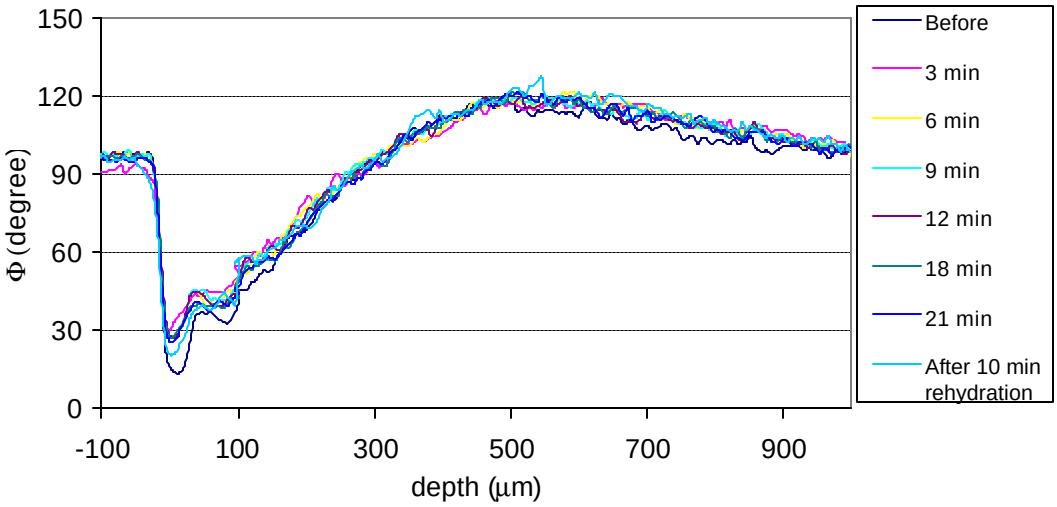

Figure 3.12: Plots of phase retardation versus depth for cartilage in heated saline for thermal denaturation effects. The temperature was maintained at 63 ^{o}C during measurements.

From our experiments, we conclude phase retardation changes observed in cartilage are primarily due to dehydration. Since dehydration is the principal source for changes in birefringence in cartilage, use of PS-OCT as a feedback control methodology for non-ablative cartilage reshaping is primarily sensitive to detection of water loss rather than thermal denaturation.

Thermally induced changes in birefringence of porcine nasal septal cartilage (extracted 2-hours postmortem) following Nd:YAG laser irradiation were investigated using a polarization sensitive optical coherence tomography (PS-OCT) system combined with an infrared imaging radiometer. We observed

surface shrinkage following laser irradiation using PS-OCT imaging, and an S-shaped structural pattern could be differentiated using a phase sensitive contrast variable on the Stokes parameters of backscattered light. Phase retardation was observed to decrease following laser irradiation indicating that the scattering properties of cartilage vary and the birefringence decreases following laser irradiation. Since dehydration is the principal source for changes in birefringence in cartilage, use of PS-OCT as a feedback control method for non-ablative cartilage reshaping must rely on detection of water loss rather than thermal denaturation.

3.6. REFERENCES

1. De Boer J. E., Milner T. E., Nelson J. S., "Determination of the Depth Resolved Stokes Parameters of Llight Backscattered from Turbid Media using Polarization Sensitive Optical Coherence Tomography", *Optics Letters*, **24**: 300-302, 1999

2. Ducros M. G., De Boer J. E., Huang H. E., Chao L. C., Chen Z., Nelson J. S., Milner T. E., Rylander III H. G., "Polarization Sensitive Optical Coherence Tomography of the Rabbit Eye", *IEEE J. of Selected Topics in Quantum Elec.*, **5(5)**: 1159-1167, 1999

3. Yarker Y. E., Aspden R. M., Hukins D. W. L., "Birefringence of Articular Cartilage and the Distribution of Collagen Fibril Orientations", *Connective Tissue Research*, **11**: 207-213, 1983

4. Kiraly K., Hyttinen M., Parkkinen J., Arokoski J., Lapvetelainen T., Torronen K., Kiviranta I., Helminen H. J., "Articular Cartilage Collagen Birefringence is Altered Concurrent with Changes in Proteoglycan Synthesis during Dynamic In Vitro Loading", *The Anatomical Record*, **251**: 28-36, 1998

5. Brosseau C., "*Fundamentals of Polarized Light: A Statistical Optics Approach*", John Wiley & Sons, New York, NY, 1998

6. Sobol E. N., Bagratashvili V., Sviridov A., Omel'chenko A., Kitai M., Jones N., Zenger V., Nasedkin N., Isaev M., Karlov V., Schechter A., "Study of Cartilage Shaping with Holmium Laser ", *Proceedings of SPIE*, **2623**: 544-547, 1996

7. Sobol E. N., Bagratashvili V., Sviridov A., Omel'chenko A, Schechter A., Jones N., Howdle S., Helidonis E., "Phenomenon of Cartilage Shaping using Moderate Laser Heating and Its Application in Otorhinolaryngology", *Proceedings of SPIE*, **2623**: 548-552, 1996

8. Wong B. J. F., Milner T. E., Kim H. K., Telenkov S., Chew C., Kuo T., Smithies D. J., Sobol E. N., Nelson J. S., "Critical Temperature Transitions in Laser Mediated Cartilage Reshaping", *Proceedings of SPIE*, **3425**: 161-172, 1998

9. Wong B. J. F., Milner T. E., Anvari B., Sviridov A., Omel'chenko A., Bagratashvili V. V., Sobol E. N., Nelson J. S., "Thermo-Optical Response of Cartilage during Feedback Controlled Laser-Assisted Reshaping", *Proceedings of SPIE*, **2970**: 380-391, 1997

10. Wong B. J. F., Milner T. E., Anvari B., Sviridov A., Omel'chenko A., Bagratashvili V. V., Sobol E. N., Nelson J. S., "Measurements of Radiometric Surface Temperature and Integrated Backscattered Light Intensity during Feedback Controlled Laser-Assisted Cartilage Reshaping", *Lasers in Med. Sci.*, **13**: 66-72, 1998

11. Wong B. J. F., Milner T. E., Kim H. H., Nelson J. S., Sobol E. N., "Stress Relaxation of Porcine Septal Cartilage during Nd:YAG (λ = 1.32mm) Laser Irradiation: Mechanical, Optical, and Thermal Response", *J. Biomed. Opt.*, **3(4)**: 409-414, 1998

12. Bragg W. L., Pippard A. B., "The Form Birefringence of Macromolecules", *Acta Cryst*, **6**: 865-867, 1953

13. Maitland D. J., Walsh Jr. J. T., "Quantitative Measurements of Linear Birefringence during Heating of Native Collagen", *Laser Surg. Med.*, **20**: 310-318, 1997

14. Born M., Wolf E., *"Principles of Optics"*, 7th edi., Cambridge Univ. Press, 1999

15. Torzilli P. A., "Water Content and Equilibrium Water Partition in Immature Cartilage", *J. Orthoped. Res.*, **6**: 766-769, 1988

CHAPTER 4: ELECTROKINETIC MEASUREMENT OF CARTILAGE USING DIFFERENTIAL PHASE OPTICAL COHERENCE TOMOGRAPHY

4.1. ABSTRACT

When an electric field is applied to cartilage, current-generated stress gradients are produced and stress deformation occurs. Since differential phase optical coherence tomography (DP-OCT) is sensitive to electrokinetic-induced surface displacement, we stimulated cartilage electrically and detected electric-current induced stress gradients. The electrokinetic surface displacement of cartilage was characterized by applying sinusoidal voltages with two amplitudes (5 V and 10 V) and frequencies (1 Hz and 0.5 Hz). The results show that by application of DP-OCT the surface displacement increased with increasing applied voltage and decreased with increasing excitation frequency. In the electrokinetic response of cartilage, measured optical phase delay between the surface displacement response and excitation waveform varies inversely to the excitation frequency. Since the streaming potential and other electrokinetic effects in cartilage are directly proportional to proteoglycan density, application of an

electric field in cartilage combined with DP-OCT measurements may provide a sensitive indicator of cartilage viability.

4.2. INTRODUCTION

Osteoarthritis, also called degenerative and heterogeneous disease of the joints, is the most common joint disorder and characterized by progressive loss of cartilage [1]. The earliest biochemical features, which precede gross pathological changes, include non-uniform loss of proteoglycans associated with increase of water content in tissue and finally, increased fibrillation of the tissue's collagen network [2].

Over the decades, investigators have found that electromechanical interactions are an important element in the physiology of connective tissue. Frenkel first introduced the application of porous media models to describe a streaming potential in the area of soil mechanics [3]. He applied electrokinetic theory to quasistatic Poiseuille flow in charged, cylindrical capillaries to model the induced 'seismoelectric potentials' [3]. In the case of connective tissue, Matijevic studied electrokinetic models formulated on 'microcontinuum' and 'macrocontinuum' spatial scales [4]. Figure 4.1 shows the microcontinuum approach including the cylindrical pore model (Fig. 4.1A) and exterior flow through a bed of charged rods (Fig. 4.1B) [4].

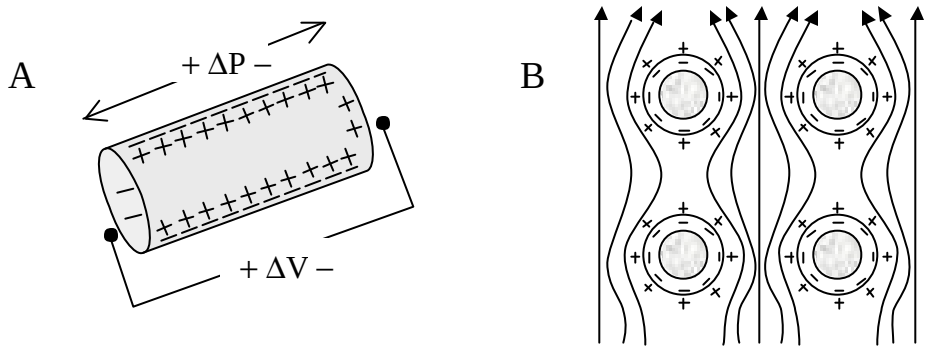

Figure 4.1: Microcontinuum models of electrokinetics. (A) Fluid flow through the interior of a charged rod. (B) Exterior fluid flow in an array of charged rods.

Matijevic hypothesized that the immobilized molecular charge groups and their surrounding counter ion atmospheres generate an intense "double layer" electric field that imparts a large electrical energy density storage to the double layer [4]. As seen in Figure 4.1A, the wall is charged negatively, while the diffuse part of the double layer is correspondingly positive [4]. Matijevic recognized that a fluid flow driven by pressure difference *DP* through a cylindrical pore whose walls support a surface charge, produces a streaming potential *DV* given by

$$\Delta V = \frac{ez}{hK}\Delta P \qquad \text{(Eq. 4.1)}$$

where ε is the fluid dielectric constant, η the fluid viscosity, K the specific conductivity of the fluid, and ζ is the 'zeta' potential at the electrokinetic slip plane related to the pore wall surface charge [4]. Fluid flow through a charged cylindrical rod gives rise to a streaming potential via convective charge separation (Fig 4.1A). The molecular mechanisms that underlie electrokinetic phenomenon have also been characterized and theoretically modeled in a variety of colloidal and polymeric gel systems [5,6]. When exterior fluid flows through the negatively charged solid matrix, fluid convection of positive mobile counter-ions tends to separate them from the immobilized negative charge groups (Fig. 4.1B) [7,8].

In cartilage, proteoglycan aggrecans with abundant negatively charged groups attract mobile cations such as Na^+ and Ca^+ in the interstitial fluid to maintain electroneutrality of the tissue [1,10]. The electromechanical properties are dependent upon the relative amount of the solid matrix and the mechano-electrical interaction of the components within the extracellular matrix. Since electrokinetic transduction in cartilage has its origin in the fixed charged groups, primarily the proteoglycans, either mechanical deformation or streaming fluid tends to separate and entrain the mobile ions from the fixed negatively charged side chain groups. This charge separation creates an electric field collinear to the fluid flow and proportional to the fluid velocity at each position within the extra cellular matrix. The resulting electric field gives rise to a voltage

difference called a streaming potential [7-10]. Conversely, when a current-generated stress is applied to cartilage, an applied electric field can exert a force on the ionic space charge in the fluid phase and produce concomitant electrophoretic motion of the proteoglycans. These electroosmotic and electrophoretic effects can result in mechanical deformation and stress within the tissue [7-10]. Frank and Grodzinsky observed the changes in the streaming potential that resulted from modification of bath ionic strength and pH and stated that the results can provide additional insights into the molecular origins of the electrokinetic (or streaming) transduction processes [7]. Frank and Grodzinsky also completed studies to compare the experimentally observed frequency response of the streaming potential, oscillatory mechanical stiffness, and current-generated stress to that predicted by theory to characterize a wide range of electrokinetic phenomena in charged biological tissues [8].

Lai *et al.* studied the nature of electric fields inside articular cartilage by accounting for both streaming and diffusion potentials [11]. Lai *et al.* hypothesized that there exist two sources for the electric potential in a charged soft hydrated biological tissue such as cartilage: streaming and diffuse flows [11]. The streaming potential is due to movement of ions being convected by interstitial fluid flow and the diffusion potential is caused by the tendency of the ions to diffuse from a region of higher concentration to a region of lower concentration, thus, causing a separation between the positive and the negative charges [11].

Lai *et al.* demonstrated that the streaming and diffusion potentials are in opposite directions and the magnitude and polarity of the resulting electric field are dependent upon the relative magnitude of these two effects [11]. Lai *et al.* solved coupled tissue mechano-electrochemical equations using Van Mow's triphasic theories and showed that the diffusion potential competes against the streaming potential for dominance inside the tissue [11].

Loss of proteoglycans decreases the ability of cartilage to withstand compressive loading and makes the tissue softer and more susceptible to wear and fibrillation [2]. If the early loss of proteoglycans is detectable by a non-invasive optical technique, progression of the disease may be arrested using, for example, change of lifestyle, pharmacologic or possibly surgical interventions. When an electric field is applied to cartilage, current-generated stress gradients are produced and stress deformation occurs. Since DP-OCT is sensitive to surface displacement resulting from an electrokinetic response, cartilage samples were stimulated electrically and electromechanical stress gradients were detected. Since electrical stimulation is one of many possible mechanisms to probe cartilage, a variety of energy sources may serve as a stimulating agent. For example, non-contact photo-thermal stimulation by absorption of incident laser radiation produces thermoelastic deformation that may be observed with DP-OCT.

4.3. EXPERIMENTAL METHODS

Differential Phase Optical Coherence Tomography (DP-OCT) System

A fiber-based dual channel optical low-coherence reflectometer that is capable of differential phase measurement between light backscattered from two spatially separated sites in a sample is used to investigate electromechanical stress changes induced by applying an electrical current to a cartilage sample (Fig. 4.2).

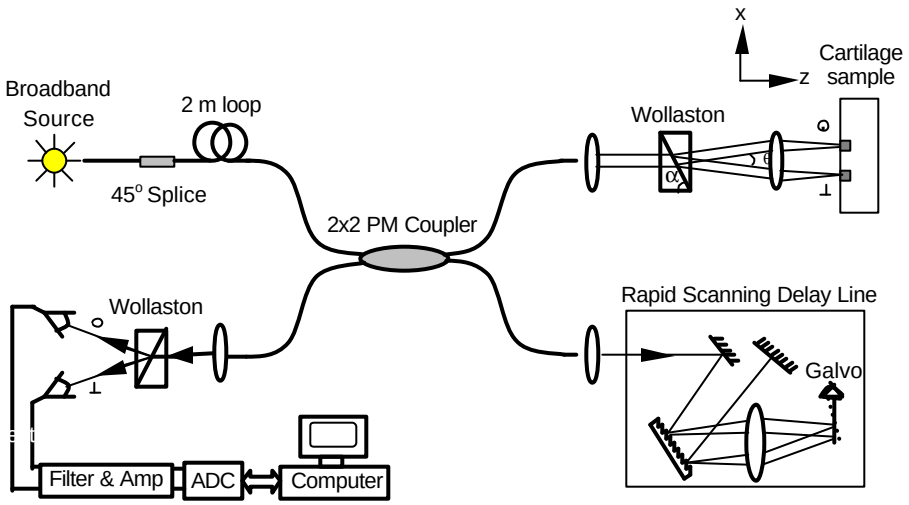

Figure 4.2: Schematic of differential phase optical coherence reflectometer.

Since the elimination of phase noise in the dual-channel fiber interferometer is performed by differential phase measurement, accurate depth-resolved phase detection of the interference signal can be achieved [12]. Partially polarized light emitted from an optical semiconductor amplifier (AFC

technologies, λ = 1.3 μm, FWHM = 60 nm) as an input source is depolarized by splicing together two segments of birefringent fiber. The orthogonal birefringent axes of the two fibers are oriented at 45^{o} with respect to each other and ensures that equal amplitude of each linearly polarized component of the incident source light is coupled along the birefringent axes of the second fiber. The two polarization modes become decorrelated after a short propagation distance because of the high birefringence of the fiber (beat length 1.6mm) and short coherence length (15 μm) of the source. At the input to the 2×2 polarization maintaining (PM) coupler (Canadian Instrumentation) two independent and decorrelated linearly polarized modes propagate along the birefringent axes of the fiber, forming two signal channels. Light splits equally into reference and sample paths at the 2×2 PM coupler. In the reference path, an adjustable rapid-scanning delay line and collimating lens were used [13].

In the sample path, the linearly polarized mutually orthogonal polarization modes of the birefringent fiber split in the Wollaston prism and the diverging beams from the prism are made parallel to each other and focused on the cartilage. Backscattered light waves from the cartilage in both paths of the interferometer recombine and interfere at the 2×2 PM coupler. In the detection path, interfering light is split into two mutually orthogonal linearly polarized waves from each channel by a large angle Wollaston prism and detected by two photodetectors. Each interference signal is bandpass filtered and digitized by a

12-bit analog-digital converter. Since the two polarization modes are totally decorrelated, no cross interference occurs between light waves in channels 1 and 2 [12]. The optical scanning system in the sample path of DP-OCT was designed and the detailed description is in Appendix B.

Surface Displacement Measurements

Description of experiments

Platinum was selected as a stimulating electrode since the material does not corrode inside the body, and allergic reactions to platinum are extremely rare. Moreover, the material has good electrical conductivity, which makes it an ideal stimulating electrode material.

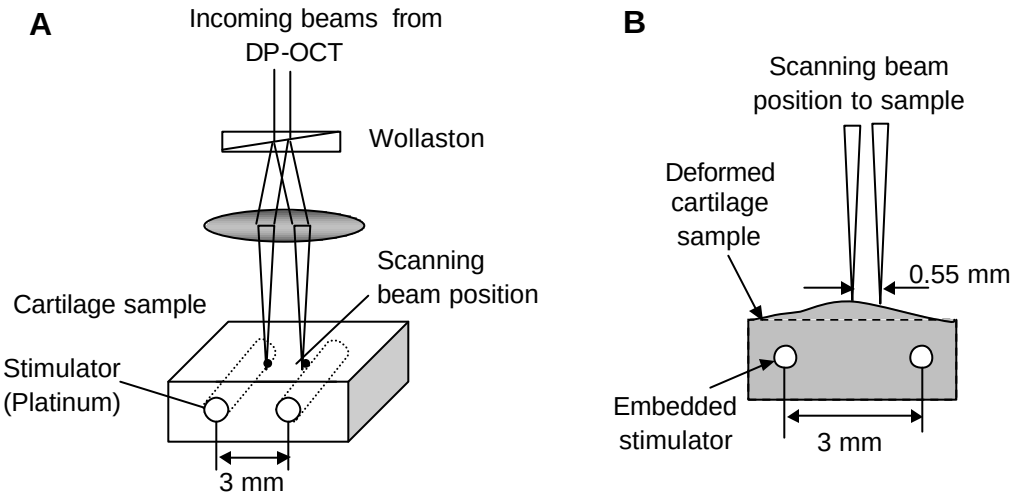

Figure 4.3: Schematic of the sample path of DP-OCT instrument and the sample (A), and the physically deformed cartilage in response to stimulation (B).

Two platinum electrodes (ϕ = 1.5 mm) were used to stimulate cartilage electrically to induce electrokinetic surface displacement for observation using DP-OCT (Fig. 4.3).

Figure 4.4 shows a timing diagram indicating how data were collected by the high-speed 12-bit A/D converter (Gage®) versus the stimulating waveform. A 2-cycle sinusoidal waveform (SRS, DS 345) was applied to the platinum stimulation electrodes with peak amplitude voltages of 5 and 10 volts at excitation frequencies of 1.0 and 0.5 Hz. A square waveform (500 cycles) (Hewlet-Packard, 33120A) was applied to trigger and acquire the data. Acquisition of the fringe data by the DP-OCT system was triggered at the rising edge of each square wave and 2,048 points were recorded following each trigger event. Table 4.1 shows the four cases of electrokinetic measurements conducted with different excitation voltages and frequencies.

Table 4.1: The applied parameters for cartilage electrokinetic measurements. Two samples were used for each case to record data.

	Case I	Case II	Case III	Case IV
Applied Peak amplitude Voltage	5 V	5 V	10 V	10 V
Applied Excitation Frequency (2-cycle sinusoidal waveform)	0.5 Hz	1.0 Hz	0.5 Hz	1.0 Hz
Acquisition Frequency	125 Hz	250 Hz	125 Hz	250 Hz
Total acquisition time	4 sec	2 sec	4 sec	2 sec
Number of acquisition	500	500	500	500
Number of points per acquisition	2,048	2,048	2,048	2,048

The separation between the two beams on the cartilage sample was 550 μm, the carrier frequency for the DP-OCT fringes was 50 KHz, and the sampling rate set at 5 M samples/sec.

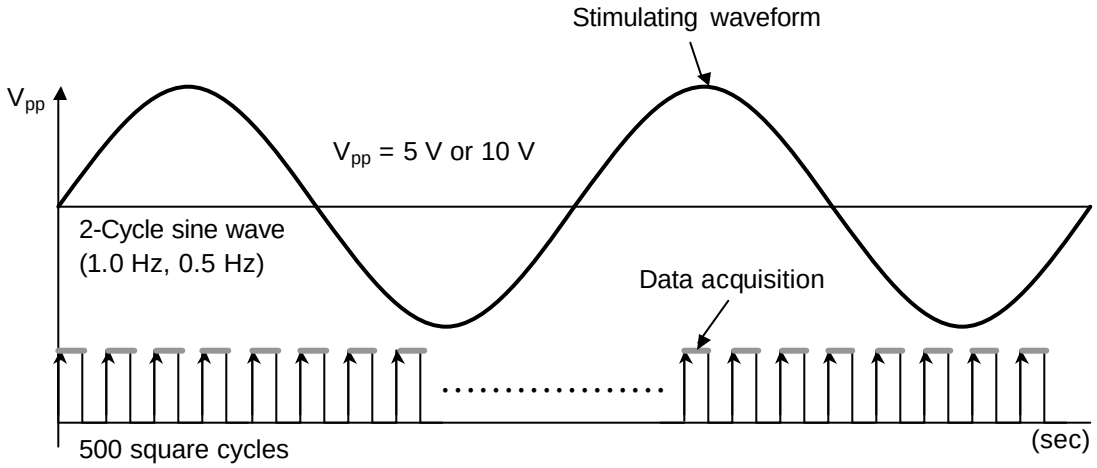

Figure 4.4: Schematic of stimulating waveform (top) and trigger sequence for data acquisition (bottom).

Data analysis

The two interference signals were recorded from channels 1 and 2 as shown in Figure 4.5. Since the two fringe patterns recorded by DP-OCT system are correlated with each other, the absolute values of lags at the maximum correlation represent relative surface displacement between the two scanning beams.

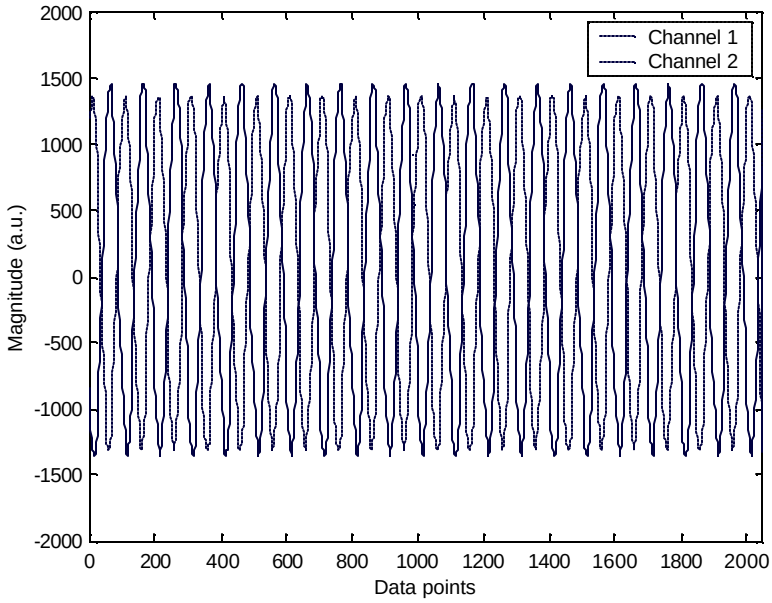

Figure 4.5: Recorded interference signals in channels 1 and 2.

The cross correlation function used for the data analysis is a standard method of estimating the degree to which two time series are correlated (Eq. 4.2).

$$R_{xy}(t) = \lim_{T\to\infty} \frac{1}{T} \int_0^T x(t)y(t+t)dt \qquad \text{(Eq. 4.2)}$$

where *x* and *y* are the two time series separated by a delay of t [14]. As a simple example of a cross-correlation function (Eq. 4.2) we consider two sine wave forms, *x* and *y*, shown in Figure 4.6A where *x(i) = sin (t)* and *y(i) = sin (t + t)*.

The cross-correlation, $R_{xy}(i)$, is shown in Figure 4.6B and a peak correlation is observed at a delay of t = 3.

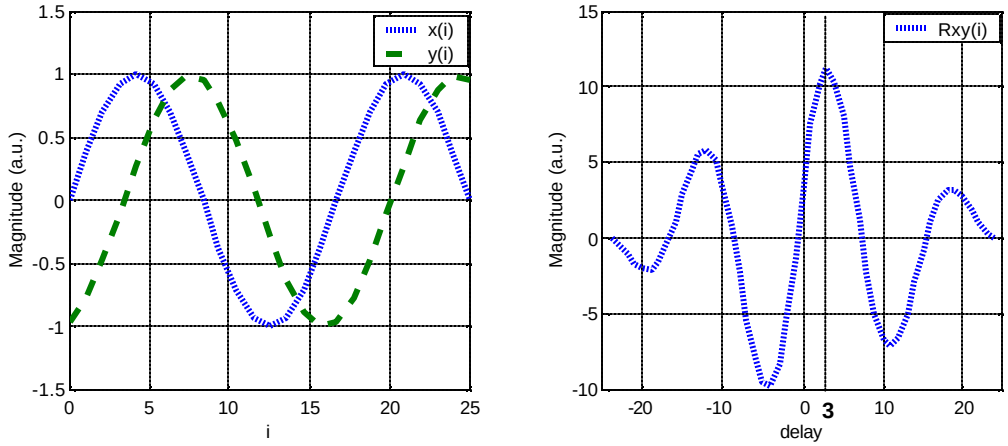

Figure 4.6: Example of cross-correlation. (A) two sine waves, and (B) cross-correlation series.

The cross-correlation function is applied to the interference fringe signals recorded by the DP-OCT system and the maximum correlation of each data set was calculated. The indices corresponding to maximum correlation of each 500-recorded data sets were plotted versus time. The plot of these indices measures relative surface displacement between the two probe beam positions versus time. Figure 4.7 shows the flow chart of data analysis used to compute the relative surface displacement measurements of cartilage at the probe beam.

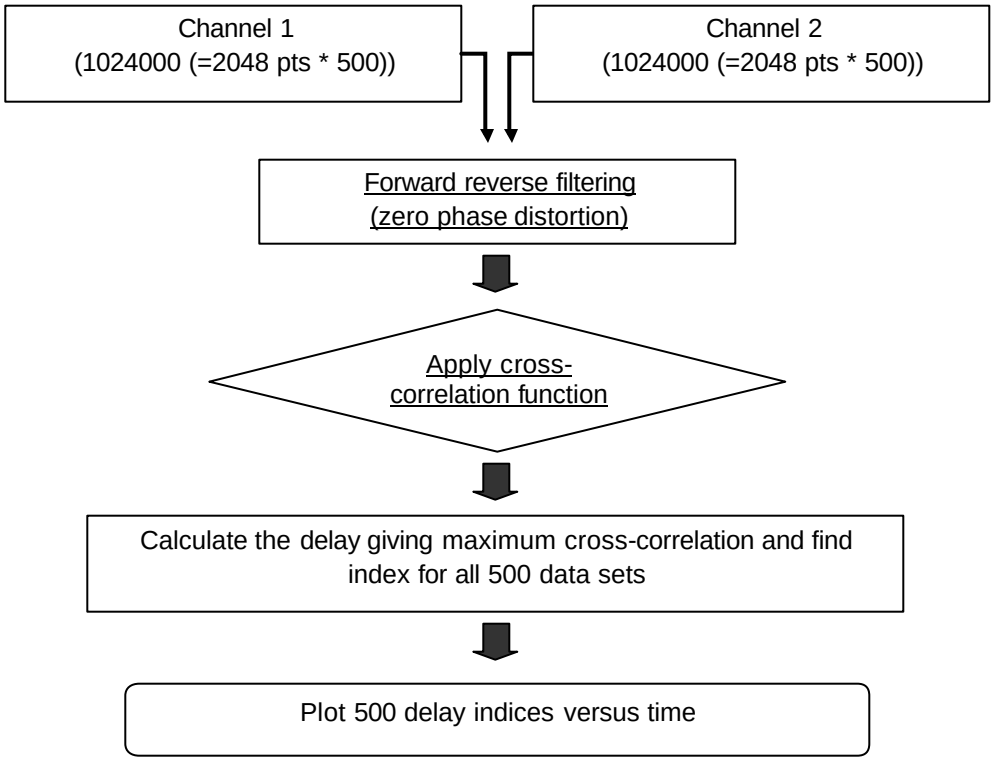

Figure 4.7: Flow chart for data analysis of electrokinetic surface displacement measurements of cartilage.

4.4. RESULTS

The profiles induced by 5 V and 10 V stimulation waveforms indicate that cartilage surface displacement gradually increases over time (2 or 4 seconds) and greater relative displacements are observed with increased applied voltages and lower excitation frequencies as seen in Figure 4.8.

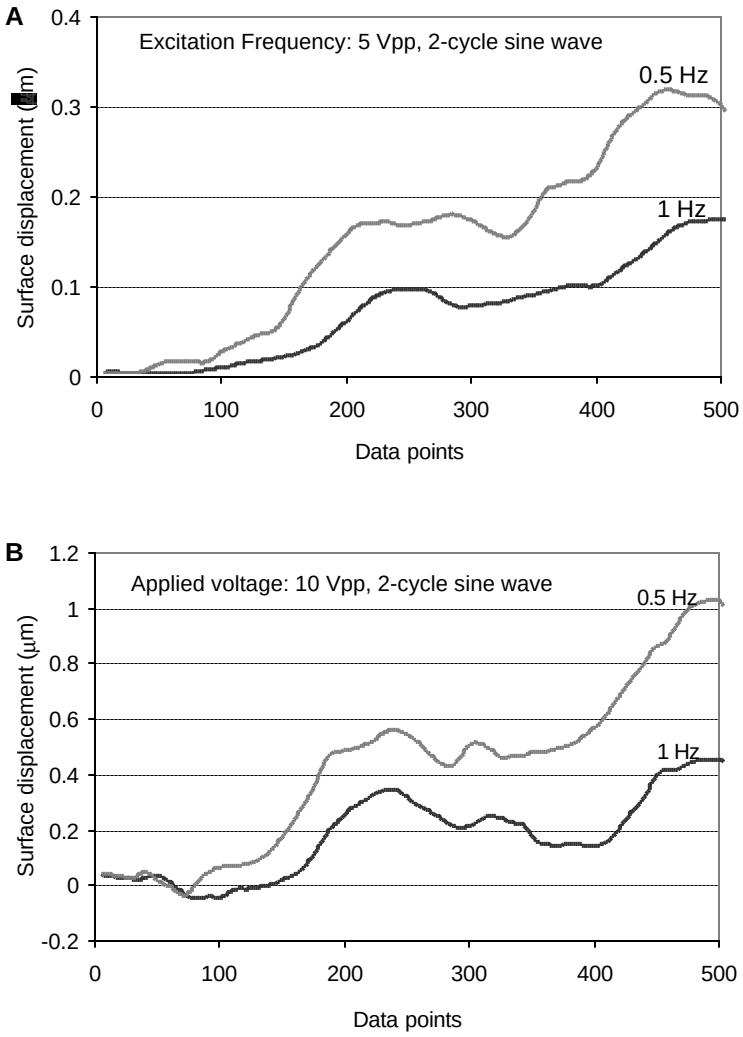

Figure 4.8: Surface displacement amplitude within cartilage generated by 1, and 0.5 Hz excitation frequencies with 5 V (A) and 10 V (B) amplitudes.

The monotonic increase in surface displacement observed over time was due to thermal expansion by ohmic heating. The thermal expansion coefficient gives a linear related volume expansion and surface displacement as temperature

increases linearly. To remove the effect of ohmic heating and observe the oscillating component, a 'Detrend' function (MATLAB®) is used to remove the best-fit linear trend from the data. With the detrended data, non-linear fitting to a sinusoidal waveform ($y = A_o \cdot sin(f_o t + t)$) with free parameters A_o and t was applied to estimate surface displacement amplitude and phase delay at a specific excitation frequency.

Figures 4.9 and 4.10 show the detrended data from the measured surface displacement profiles (Figure 4.8). To observe the relationship between the electrokinetic responses versus applied excitation frequencies, at 5 V excitation amplitude (Figure 4.9), the phase delay is larger when a higher frequency is applied to cartilage (1 Hz → 2.21 *rad*, and 0.5 Hz → 1.92 *rad*). Magnitude of surface displacement increases with lower frequencies. The phase delay at 10 V excitation is also larger with a higher frequency as seen in Figure 4.10 (1 Hz → 2.21 *rad*, and 0.5 Hz → 2.08 *rad*) and magnitude of surface displacement increases with lower frequencies. From the measured phase delays of the detrended data, the magnitude of surface displacement electrokinetic response by electric stimulation varies inversely to the excitation frequency as seen in the excitation voltage of both 5 V and 10 V. Overall, the measured surface displacement increases with increased applied excitation voltage and decreases with increasing excitation frequency. Furthermore, the electrokinetic response from the measured phase delay varies inversely to the excitation frequencies.

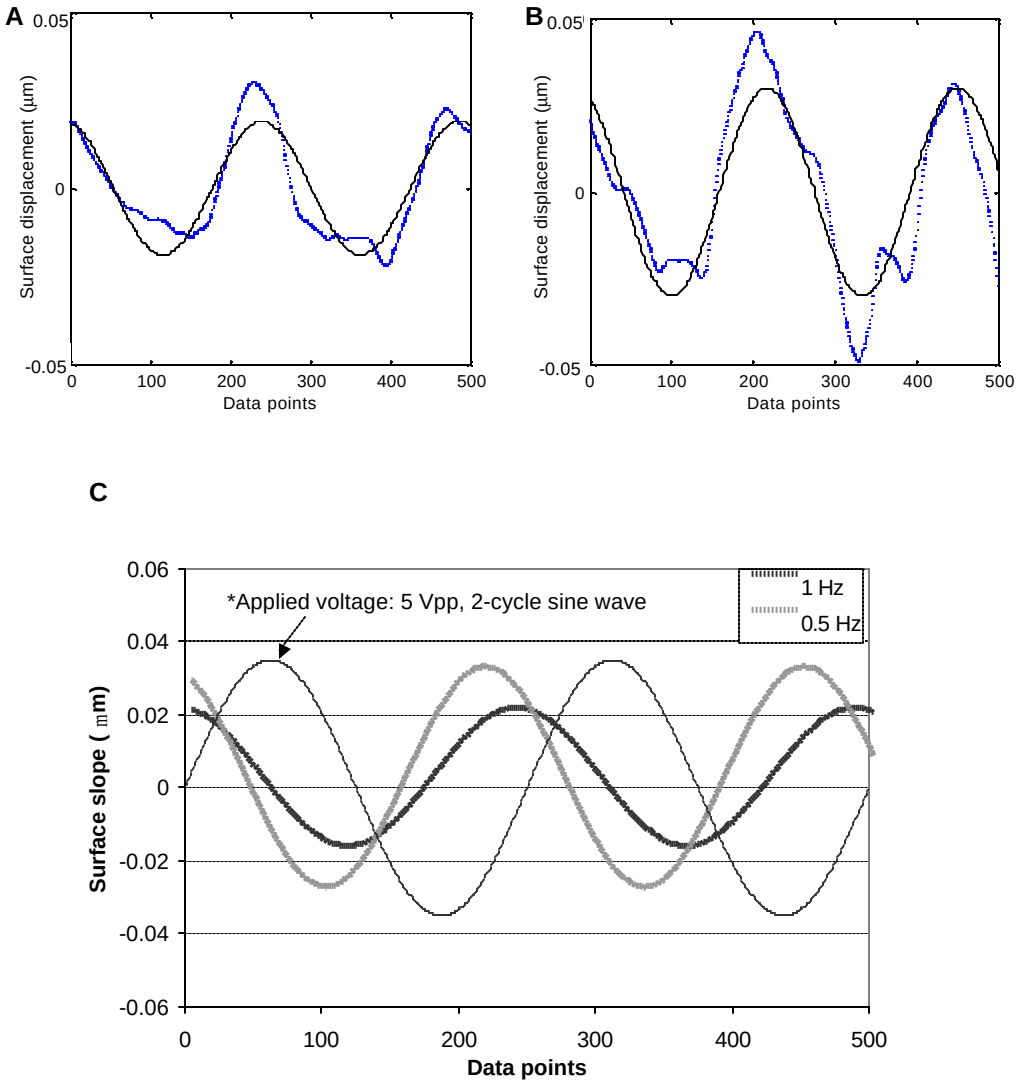

Figure 4.9: Detrended data (thick dotted line) and non-linear fitted data (thin line) with excitation frequency of 1 Hz (A) and 0.5 Hz (B), and phase delays and slope amplitudes at 5 V excitation (C).

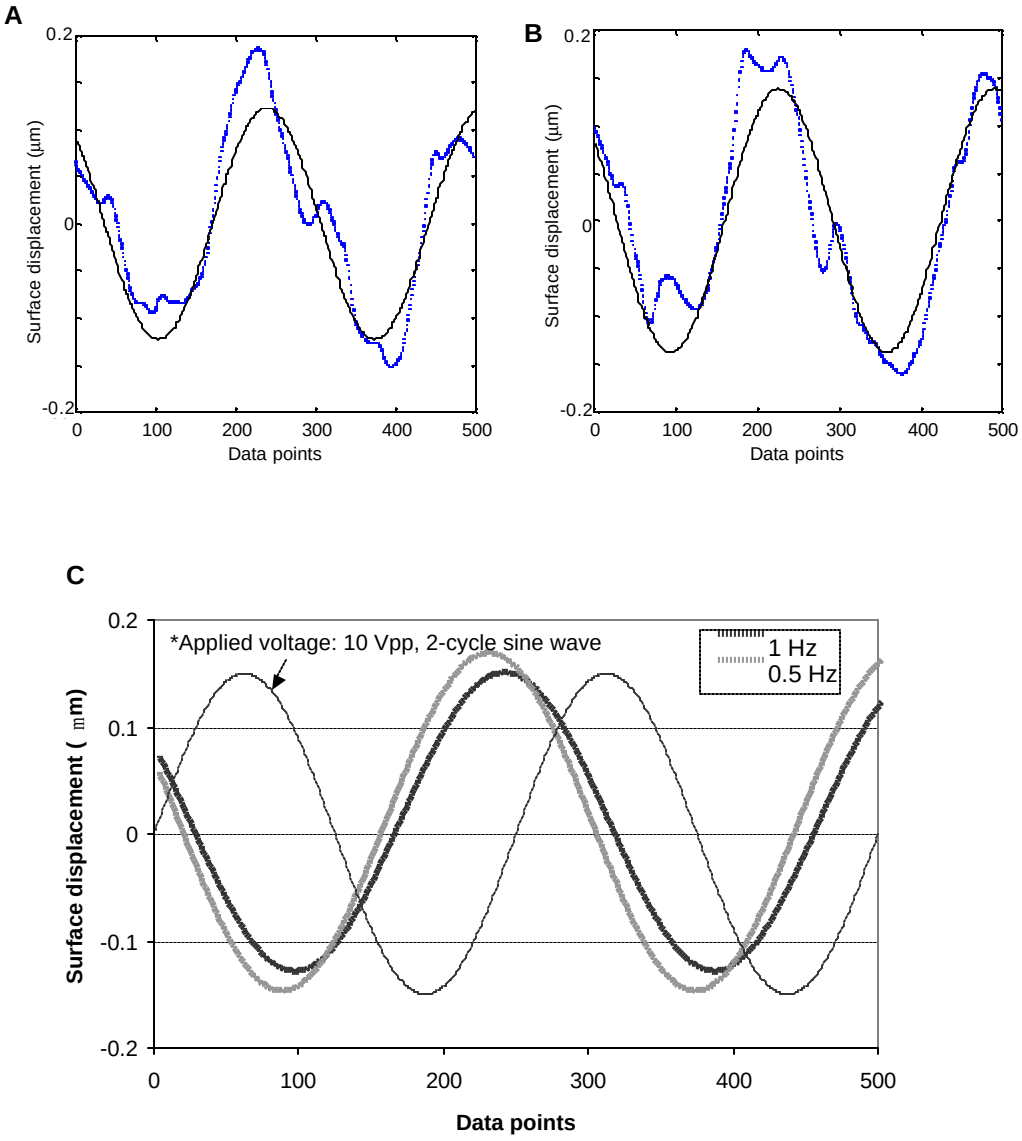

Figure 4.10: Detrended data (thick dotted line) and non-linear fitted data (thin line) with excitation frequency of 1 Hz (A) and 0.5 Hz (B), and phase delays and slope amplitudes at 10 V excitation (C).

4.5. DISCUSSION AND CONCLUSIONS

Frank *et al.* proposed a continuum model for linear electrokinetic transduction in cartilage and experimentally observed the streaming potential and current-generated stress responses [8]. The experimental results from Frank *et al.* showed the surface displacement amplitude increases at lower frequencies and a linear relationship between the stimulus amplitude and the transduction response amplitude that is consistent with a theoretical model [8]. Berkenblit *et al.* [15] constructed an electrokinetic surface probe capable of applying small sinusoidal currents at the surface of articular cartilage and measuring the current-generated stress with a centrally placed piezoelectric sensor. The technique was entitled "electromechanical surface spectroscopy" because the electrical frequency of the applied sinusoidal currents is varied during the measurement. They observed that the measured stress amplitude is proportional to the applied current density and inversely proportional to the excitation frequency. Results of their experiment support the feasibility of surface measurements as a means of assessing electromechanical transduction in cartilage [15]. The surface displacement measurements using DP-OCT are consistent with the experimental and theoretical results that demonstrated by Frank *et al.* [8] and Berkenblit *et al.* [15]. In addition to the surface displacement, DP-OCT was able to measure the optical phase delays that showed the larger phase delay with a higher frequency at both 5 V and 10 V excitation amplitudes. With piezoelectric sensors that Berkenblit *et al.* used, one has to correct for phase response of the measurements while DP-OCT is not required to this correction. The results show the

electrokinetic response varies inversely to the excitation frequencies. Furthermore, DP-OCT is a non-contact instrument and allows fast imaging in comparison to a contact measurement.

The gradual increase in the measured surface displacement using DP-OCT with increasing excitation voltage amplitudes may be due to the thermal expansion by ohmic heating effect. By applying an electric current through the electrodes in cartilage, heat is generated and this ohmic heating will give rise to thermal expansion that produces in part the observed monotonic increase in surface displacement. Since depth-resolved DP-OCT is also able to detect subsurface electromechanical stress gradients and provide a sensitive indicator of subsurface molecular-level cartilage degeneration, further investigation of volumetric stress gradients combined with DP-OCT lateral and depth scanning should be performed.

Depth-resolved interrogation of the electrical potential inside cartilage if a disease process begins should be performed in addition to measurements of surface displacement and electrokinetic response. Furthermore, the electrical potential in healthy cartilage should be compared with diseased cartilage using depth-resolved DP-OCT. Numerical modeling of the current-generated stress, a finite element model, using for example Femlab® software should be performed to compare experimental results with model predictions.

Since the current generated stress also depends on the fixed space charge density that is a function of intra-tissue pH as well as applied current density, the

depth-resolved observation of electrokinetic behavior with variable pH may be useful to investigate the relationship between space charge density and mechanical deformation effects.

For the analysis of acquired DP-OCT data, the investigation of deeper depths with different filtering techniques should be performed since the backscattered light waves contain increased noise as the window size for a desired depth increases. For improvement of signal-to-noise ratio of the fringe amplitude, optimization of reference intensity and source power should be achieved. Furthermore, to correlate the morphological features within cartilage to measured phase variations, histological assessment should be performed.

Since electrical stimulation is one of many possible mechanisms to excite cartilage, other energy sources for stimulation can be used such as non-contact photo-thermal stimulation by absorption of laser radiation that produces thermoelastic deformation. Combination of photothermal excitation with DP-OCT may provide a useful combination for clinical screening the mechanical response of cartilage.

The current-generated stress measurements were performed in nasal septal cartilage using DP-OCT and the dependence of the measured stress on the amplitude and frequency of the applied current was characterized. Since the streaming potential and other electrokinetic effects in cartilage are directly related to proteoglycan density, application of an electric field in cartilage combined with

DP-OCT measurements may provide a sensitive indicator of cartilage viability on the molecular-level.

4.6. REFERENCES

1. Mow V. C., *"Injury and Repair of the Musculoskeletal Soft Tissues"*, American Academy of Orthopaedic Surgeons, 1988

2. Maroudas A., "Physicochemical Properties of Articular Cartilage", *Adult Articular Cartilage*, Freeman, M.A.R. ed., Pitman Medical, Kent, England, 2nd ed., 215-290, 1979

3. Frenkel J., "On the Theory of Seismic and Seismoelectric Phenomena in a Moist Soil", J. Phys. U.S.S.R. **8**: 230-241, 1944

4. Matijevic E., *"Surface and Colloid Science"*, Wiley-Interscience, New York, 49-272, 1974

5. Overbeek J. T. G., *"Electrokinetic Phenomena"*, Colloid Science, vol. 1, Elsevier Publishing Co., Amsterdam, 194-244, 1952

6. Levich V. G., *"Physicochemical Hydrodynamics"*, Prentice-Hall, Englewood Cliffs, NJ, 1962

7. Frank E. H., Grodzinsky A. J., "Cartilage Electromechanics I: Electrokinetic Transduction and the Effects of Electrolyte pH and Ionic Strength", *J. Biomechanics*, **20**: 615-627, 1987

8. Frank E. H., Grodzinsky A. J., "Cartilage Electromechanics Ⅱ: A Continuum Model of Cartilage Electrokinetics and Correlation with Experiments", *J. Biomechanics*, **20**: 629-639, 1987

9. Bassett C. A. L., Pawluk R. J., "Electrical Behavior of Cartilage during Loading", *Science*, **178**: 982-983, 1972

10. Lotke P. A., Black J., Richardson S. J., "Electromechanical Properties in Human Articular Cartilage", *J. Bone Joint Surg*., **56-A**: 1040-1046, 1974

11. Lai W. M., Mow V. C., Ateshian G. A., "On the Electric Potentials Inside a Charged Soft Hydrated Biological Tissue: Streaming Potential Versus Diffusion Potential", *Trans. ASME*, **122**: 336-346, 2000

12. Dave D. P., Milner T. E., "Optical Low-Coherence Reflectometer for Differential Phase Measurement", *Opt. Lett*., **25**: 227-229, 2000

13. Tearney G. J., Bouma B. E., Fujimoto J. G., "High-speed Phase- and Group-delay Scanning with a Grating-based Phase Control Delay Line", *Opt. Lett*., **22**: 1811-1813, 1997

14. Beauchamp K. G., Yuen C. K., "*Digital Methods for Signal Analysis*", George Allen & Unwin, London, UK, 1979

15. Berkenblit S. I., Frank E. H., Salant E. P., Grodzinsky A. J., “Nondestructive Detection of Cartilage Degeneration using Electromechanical Surface Spectroscopy”, *Trans. ASME*, **116**: 384-392, 1994

CHAPTER 5: SUMMARY AND FUTURE DIRECTIONS

5.1. SUMMARY

Throughout my dissertation, I have endeavored to identify and characterize the physiological transformation in cartilage accompanying laser irradiation. The purpose of these studies is to provide a scientific and engineering basis to improve the laser-assisted cartilage reshaping procedure. Moreover, results from Chapter 4 may provide preliminary data to detect the electrokinetic response in cartilage for screening of osteoarthritis.

In Chapter 2, photothermal effects following laser irradiation of cartilage are investigated using a Fourier transform infra-red (FT-IR) spectrometer and an infrared focal plane array (IR-FPA) camera. The reversibility of the drying process was confirmed by FT-IR absorption spectra recorded after rehydration of the sample. In response to Ho:YAG laser irradiation ($\lambda = 2.1\ \mu m$), infrared absorption peaks of water and macromolecules decrease, respectively, due to dehydration and thermal denaturation. Different degrees of photothermal modification of cartilage macromolecules were observed depending on the incident laser dose. From the results of these studies, we identified that the laser irradiance and exposure time are the important factors to identify when thermal

denaturation of the tissue occurs. This study may be used to investigate the spatial distribution of collagen and proteoglycans and their interactions with water molecules in response to laser irradiation. The methodology may be useful for quantitative investigation of the relationship between the clinically important phenomenon of accelerated stress relaxation and the kinetics of macromolecular denaturation.

In Chapter 3, polarization sensitive optical coherence tomography (PS-OCT) and infrared imaging radiometry were used to investigate the phase retardation changes following Nd:YAG laser (λ = 1.32 μm) irradiation. Since phase retardation measured by PS-OCT has been a tool for the identification of thermal damage in tissue, the monitoring of phase retardation changes in cartilage during non-ablative laser heating can be a possible feedback control methodology in laser-assisted cartilage reshaping procedure. From the measured Stokes parameters (I, Q, U, and V) using PS-OCT, an estimate of the relative phase retardation between orthogonal polarizations was computed to determine birefringence in cartilage. Phase retardation images of light backscattered from cartilage show significant changes following laser irradiation. To investigate the origin of birefringence changes in response to local heat generation, two possible mechanisms, dehydration and thermal denaturation, were identified. PS-OCT images of cartilage were recorded after dehydration in glycerol and thermal denaturation in physiological saline. The results show that phase retardation

decrease observed in cartilage in response to laser irradiation is primarily due to dehydration. Since dehydration is the principal source for the observed changes of phase retardation in cartilage, use of PS-OCT as a feedback control methodology for non-ablative cartilage reshaping is primarily sensitive to the detection of water loss rather than thermal denaturation. The retardation changes accompanying laser irradiation may be used to identify the biophysical transformation related to water loss that are responsible for stress relaxation in cartilage.

In Chapter 4, detection of the electrokinetic response and surface displacements in cartilage using differential phase optical coherence tomography (DP-OCT) were performed to monitor cartilage degeneration for detection and screening of osteoarthritis. The measured surface displacement increased with increasing applied voltage and decreases with increasing excitation frequency. Besides the surface displacements, the measured phase delay between the surface displacement response and excitation waveform was larger with a higher frequency that shows the electrokinetic response varies inversely to the excitation frequency. Since the streaming potential and other electrokinetic effects in cartilage are directly proportional to proteoglycan density, application of an electric field in cartilage combined with DP-OCT measurements may provide a sensitive indicator of cartilage viability on the molecular-level.

5.2. FUTURE DIRECTIONS

In optical diagnosis for laser-assisted cartilage reshaping, optimization of the reshaping process requires feedback control methods by understanding both the time and temperature dependent dynamic changes in optical, thermal, mechanical, and biophysical properties of cartilage accompanying local laser irradiation. While two non-invasive optical diagnostics, FT-IR spectroscopy (Chapter 2) and PS-OCT (Chapter 3), are being developed to improve the laser-assisted cartilage reshaping procedure, rigorous evaluation of cartilage viability by using histological and biochemical techniques. Furthermore, theoretical analysis of the space-time temperature distribution and time-dependent thermal denaturation kinetics should be investigated.

For FT-IR measurements (Chapter 2), although the isolated constituents of cartilage have unique spectral features, their spectra are considerably overlapped and it may be difficult to determine quantitatively the changes in the spectra of the individual constituents and their interactions due to photothermal modification of the macromolecules without application of a more sophisticated model-based spectral analysis. Quantitative analysis of the absorption bands of macromolecules may not be completed without subtraction of the water spectrum with a short path-length cell. Further studies using 10 μm thick cartilage samples produced by a microtome or proteoglycan solution in a very short path-length cell should be investigated by applying the water spectrum subtraction

technique. Additional studies are to analyze the changes in shapes and shifts in the absorption bands of water and macromolecules with different temperatures and correlate with theoretical modeling so that comparison between model predictions and experimental results can be made.

For PS-OCT measurements (Chapter 3), the uncertainty for the fibril volume fraction measurements of cartilage should be reduced. Since the trapped water within cartilage can be turned to exchangeable water when moderate heating is applied to the sample, the additional measurements of the fibril volume fraction combined with a heating source should be performed.

There is an additional study that may improve the laser-assisted cartilage reshaping procedure. A candidate feedback control method is optoacoustic monitoring of cartilage correlated with mechanical stress measurements using a load cell. The correlation between temporal acoustic signal changes and decrement of cartilage internal stress during laser irradiation can be applied to investigate internal dynamics of macromolecules and interactions with water molecules. Preliminary results not reported in my dissertation show the scaling of acoustic signal spectrum that may explain the dehydration of cartilage and presence of harmonics that may be due to multiple reflections. Further investigations with a short-pulsed laser source and interpretation of experimental results with visco-elastic modeling to verify the results should be done.

For optical diagnosis of osteoarthritis (Chapter 4), a theoretical model for electromechanical effects in cartilage should be correlated with the experimental results. Furthermore, the physiological mechanisms responsible for the electromechanical behavior and their relationship to the biochemical composition should be investigated with comparing normal and degenerated cartilage. The electrokinetic behavior in cartilage has its origin in the fixed charge groups, primarily the proteoglycans and these groups are ionized under physiological conditions. Therefore, the measurements of electrokinetic behavior as a function of the concentration of an ionic solution bath to see the effect of bath ionic strength and pH may also provide information an basic interactions between the fluid, macromolecules, and ionic constituents of cartilage. Since electrical stimulation is one of many possible mechanisms to probe cartilage, a variety of energy sources can be used such as non-contact photo-thermal stimulation by absorption of incident laser radiation that produces thermoelastic deformation that may be observed with DP-OCT.

APPENDIX A

< Nomenclatures >

Symbol	Description	Definition	Units
I	Total intensity of light		-
$I_0{}^o$	Intensities of light linearly polarized at 0°	$I = I_0{}^o + I_{90}{}^o$	-
$I_{90}{}^o$	Intensities of light linearly polarized at 90°		-
Q	Difference between intensities of light linearly polarized at 0° and 90°	$Q = \frac{I_{0^\circ} - I_{90^\circ}}{I}$	-
U	Difference between intensities of light linearly polarized at +45° and -45°	$U = \frac{I_{45^o} - I_{-45^o}}{I}$	-
V	Difference between intensities of light right circularly and left circularly polarized	$V = \frac{I_{rc} - I_{lc}}{I}$	-
P	Degree of polarization of light	$P = \sqrt{Q^2 + U^2 + V^2}$	°
F	Phase retardation	$\Phi = arccos\ (-Q)$	°

Symbol	Description	Definition	Units
Δn	Form birefringence		-
n_e	Refractive index of extra-ordinary wave		-
n_o	Refractive index of ordinary wave	$\Delta n = n_e - n_o$ $= (f_1 n_1^{\ 2} + f_2 n_2^{\ 2})^{1/2}$	-
f_1	Volume fraction of fibril	$-\left(\frac{f_2 n_2^{\ 4} + (1+f_1) n_1^{\ 2} n_2^{\ 2}}{f_2 n_1^{\ 2} + (1+f_1) n_2^{\ 2}} \right)^{1/2}$	-
f_2	Volume fraction of surrounding medium		-
n_1	Refractive index of fibril		-
n_2	Refractive index of medium		-
m_{total}	Controlled total mass of cartilage		g
V_{total}	Controlled total volume of cartilage	$f_1 = 1 - \frac{V_{solution}}{V_{total}}$	ml
m_f	Dehydrated mass of cartilage	$= \frac{V_{total} - \frac{(m_{total} - m_f)}{r_{solution}}}{V_{total}}$	g
$V_{solution}$	Cartilage solution volume		ml

$r_{solution}$	Cartilage solution density	$r_{solution} = \frac{m_{total} - m_f}{V_{solution}}$	g/ml
DV	Streaming potential	$\Delta V = \frac{ez}{hs}\Delta P$	-
DP	Pressure through a cylindrical pore		-
ε	Fluid dielectric constant		-
η	Fluid viscosity		-
σ	Fluid conductivity		-
ζ	'zeta' potential at the electrokinetic slip plane related to the pore wall surface charge		-

APPENDIX B

DP-OCT OPTICAL SCANNING SYSTEM

Abstract

An optical scanning system has been widely used for many applications such as in optical coherence tomography, confocal microscopy, and digital imaging system. This term project was attempt to design and build an optical scanning system, a pre-objective scanning, to improve an existing instrument, differential phase sensitive optical coherence reflectormeter, in our laboratory since the reflectormeter performs only depth-resolved scanning. To build the optical scanning system that allows us to the lateral scanning as well as depth scanning in the reflectormeter, the scanning lenses were determined by considering all possible aberrations and the opto-mechanical parts were designed to mount the lenses on the optical table. To verify the scanning lens system, a simple test was performed both computationally and experimentally. For computational analysis, an optical design program, ZEMAX®, was used to demonstrate the scanning system and measure spot diameters for 1 mm scanning length. The numerical estimate for the spot diameter was approximately 24 μm and the spot diameter was not changed at the overall scanning positions. For experimental analysis, a collimated broadband laser source (λ = 1.32 μm) and Galvanometer scanning system was used to measure spot diameters by moving 1 μm slit attached to a photodetector longitudinally. The experimental values of the spot

diameters were approximately 26 μm. From overall the results that acquired both computationally and experimentally, the spot diameters were relatively consistent. Integration of the optical scanning system in the sample path of the differential phase sensitive optical coherence reflectormeter will allow us to lateral scanning as well as depth scanning. Overall this term project was provided me to the understanding of optical lens design and optomechanical design criteria for the optical scanning system.

1. Introduction

There are numerous ways to scan an optical beam using a mirror and lens. In general, there are three common types of the optical scanning system depending on the applications as seen in Figure A.1; (1) Post-objective scanning: the mirror component is used after the beam passes through the lens. This is less demand on the lens meaning that a simple plano convex lens can be used for the scanning system, but has a disadvantage that the material to be scanned has to be on curved surface.

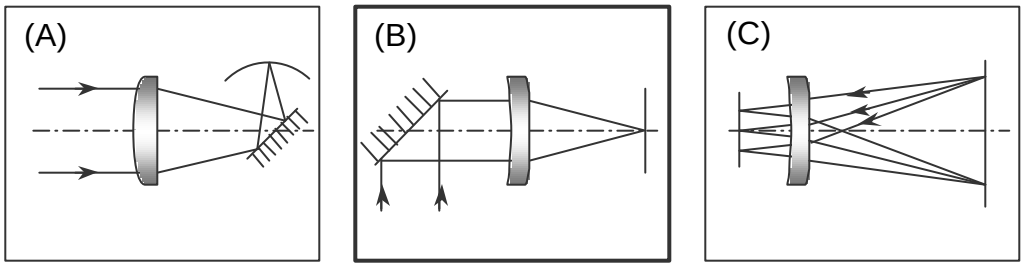

Figure A.1: The optical scanning systems; (A) Post-objective scanning (B) Pre-objective scanning (C) Double-pass scanning [1].

(2) Pre-objective scanning system: The scanning mirror is placed in front of the lens. This configuration is the most commonly used and good for flat surface of the sample. Disadvantage of this system is that there are many requirements of the scanning lens design. (3) Double-pass scanning (also called a retrofocus scanning system): This system can be compact because it does not need a collimating lens for the source. It is collimated as it passes through the lens, and then is redirected back through the lens at the angle determined by the mirror. However, this system is not quite as symmetrical as it appears, because the feed beam enters from the edge of the lens and operating field. This causes any additional aberrations mainly coma and distortion errors at all the field angles in the scan [1].

Typically, a pre-objective lens requires that the design meet the f-theta ($f\theta$) condition, in which equal angle increments at the scan deflector result in equal displacements in the focal plane. In addition, there are many considerations to design the pre-objective scanning such as setting up the initial design configuration with a reasonable Petzval field curvature by continuously checking the ratio of the Petzval radius to the focal length and minimizing primary and secondary chromatic aberrations [1].

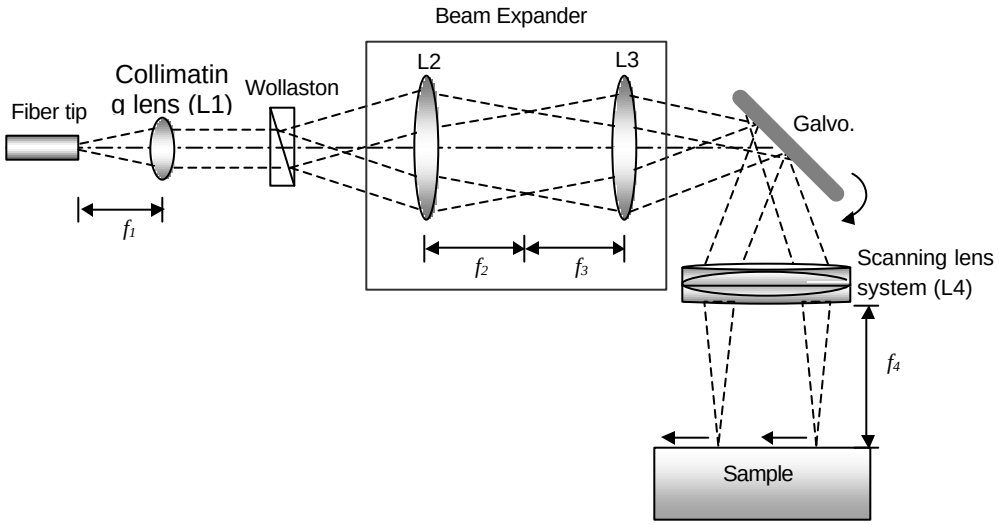

Figure A.2: Schematic of optical scanning system

Figure A.2 shows the proposed schematic of the pre-objective scanning system. Spatially coherent light emitted from a broadband laser source (λ = 850 nm) passing through a fiber is collimated by L1 and split in the Wollaston prism. The diverging beams from the prism are then expanded by a beam expander and reflected by a mirror in Galvanometer scanner system. The reflected beams are made to parallel to each other and focused on the sample. With rotating the mirror that attached on the galvanometer scanning system, the lateral scanning can be achieved.

The limitation of DP-OCT system is that the only depth-resolved measurement can be achieved. Therefore, the integration of the optical scanning

system in the sample path of the differential phase sensitive optical coherence reflectometer will allow us to lateral scanning as well as depth scanning.

2. Optical Scanning Lens Design

Since the optical scanning system should have a high resolution, all possible aberrations need to be considered. There are several types of aberration that are contributing to the poor image quality. The most common aberrations are the monochromatic (also called spherical aberration) and chromatic aberration. In spherical aberration, when the surface of a lens is spherical-shaped, the center of the lens focuses an image farther from the lens than the edge. The higher refractive index or the higher entry angle the more the rays will bend from Snell's law. In chromatic aberrations, different colors, wavelengths have different speed and hence different refractive indices for the same material. Therefore, the focal length of the lens will be slightly different for different colors. By using achromat lens, these aberrations can be partially corrected and yields about 75 to 80% of their numerical aperture with practical resolution. To correct more of these aberrations, an apochromat, also called a triplet, can be used. The beauty of the apochromat is that virtually the entire numerical aperture is corrected, resulting in a resolution that achieves what is theoretically possible as predicted by Abbe equation [4].

There are other monochromatic aberrations that deteriorate the image, making it unclear, also called first-order or primary aberrations such as coma, astigmatism, Petzval field curvature, and distortion. Comatic aberrations are

similar to spherical aberrations, but they are mainly encountered with off-axis light fluxes (Figure A.3(A)). Light that goes through the center of a lens can be focused to a point. If the light goes through the lens off-axis at an angle, the light will not focus to a point and look like a fuzzy circle. The farther off axis, the larger the circle, giving objects a comet-like look to the image (hence the name "coma"). For a single lens, coma can be partially corrected by bending the lens. More complete correction can be achieved by using a combination of lenses such as apochromat that is symmetric about a central stop. Astigmatism aberrations are similar to comatic aberrations, however these artifacts are not as sensitive to aperture size and depend more strongly on the oblique angle of a specimen point appearing as a line or ellipse instead of a point (Figure A.3(B)). Depending on the angle of the off-axis rays entering the lens, the line image may be oriented in either of two different directions, tangentially or sagitally. The intensity ratio of the unit image will diminish, with definition, detail, and contrast being lost as the distance from the center is increased. For Petzval field curvature, the planer object is not image at a plane, but a curved surface (Figure A.3(C)). Distortion is a unique aberration in that it does not affect the quality of the image in terms of sharpness or focus (Figure A.3(D)). Rather, distortion affects the sharp of the image, causing it to depart from a true-scaled duplicate of the object. Therefore, the magnification of image points is different at off-axis position due to the difference in focal lengths and magnification through the various parts of the lens [4,5].

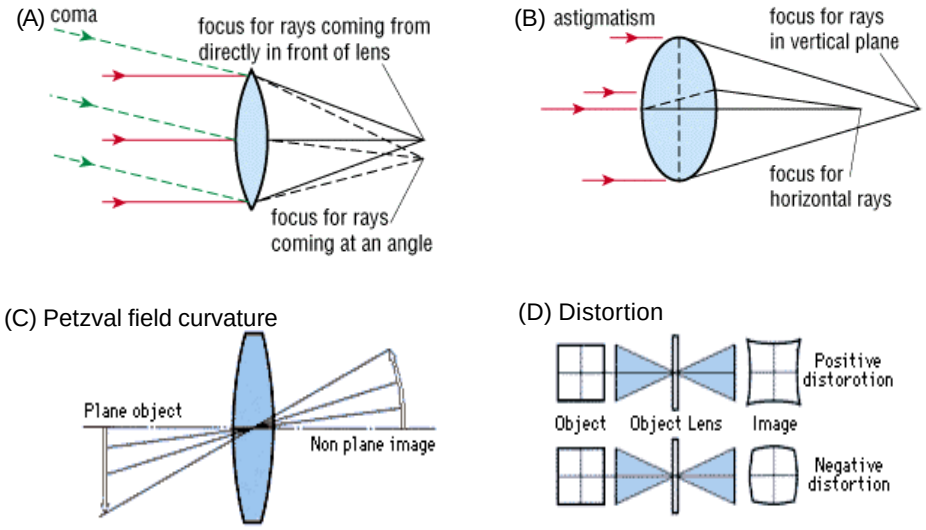

Figure A.3: Primary aberrations; (A) coma, (B) astigmatism, (C) Petzval field curvature, and (D) distortion

There are several steps to minimize these aberrations for the optical scanning lens design. First of all, the focal lengths and positioning of the lenses for the optical scanning system in the entire system should be determined. Then, It needs to be considered to select a positive and negative lens such that the Petzval curvature (C_p) is nearly zero as seen in the equation below.

$$C_p = -\left(\frac{1}{f_1 n_1} + \frac{1}{f_2 n_2}\right) \cong 0 \qquad \text{(Eq. A.1)}$$

where f_1, f_2 and n_1, n_2 are the refractive indices and focal lengths of the lenses, respectively. Secondly, Using the computed Abbe numbers (ν), the separation between positive and negative lenses (t) needs to be computed.

$$t = \frac{f_1 n_1 + f_2 n_2}{n_1 + n_2}, \quad \text{where} \quad n_d = \frac{n_d - 1}{n_F - n_C} \qquad \text{(Eq. A. 2)}$$

Finally, the net power (ϕ) of the combination and simulation of the performance of the combined lens system in ZEMAX®, optical design software, can be achieved.

$$f = \frac{f_1 n_1 + f_2 n_2}{n_1 + n_2} \qquad \text{(Eq. A.3)}$$

3. Opto-Mechanical Designs

There are a variety of common techniques for mounting optical components such as individual and multiple lenses, windows, domes, filters, small mirrors, and prisms [6]. To achieve the high precision of the optical scanning lens assembly, the thickness of the lenses that is selected by previous considerations and other additional components such as a spacer and O-rings were accurately measured with a caliper and the length of a lens holder was determined. The use of O-rings in the upper and bottom sides can protect the lenses from possible scratches

in the lens holder. The aluminum was used for the material of the lens holder and retaining ring. For convenience to mount the lens assembly on the optical table, 6-holes for 8-32 and ¼ -20 screws were drilled on each side of the holder as seen in Figure A.4.

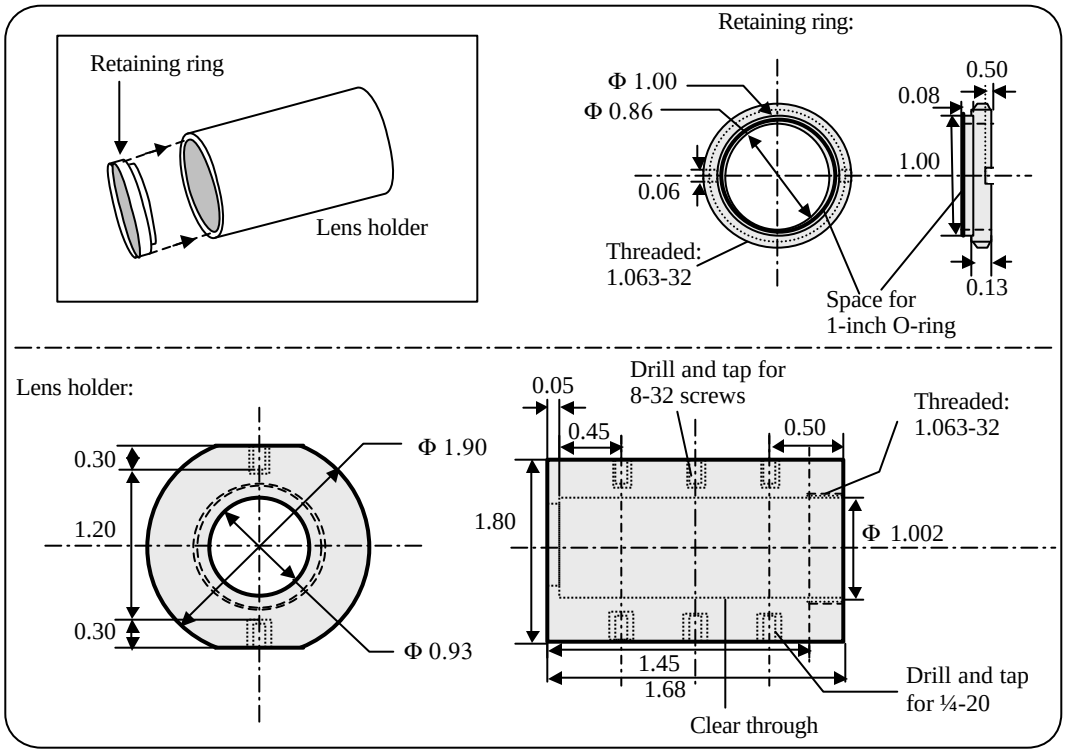

Figure A.4: The schematic layout of the opto-mechanical design.

4. Results: Computational Simulation Analysis

Figure A.5 shows ZEMAX simulations by using the selected lenses, one triplet (TRP14365, JML Direct) and one singlet (CPV10874, JML Direct). In Figure A.5(A), the mirror component is placed in front of the lens assembly with the tilt of 45 degree so that the same condition can be achieved as Galvanometer scanning system. The wavelength is selected as 1.32 micron because the application for the optical scanning system, differential phase sensitive optical coherence reflectometer, has the wavelength of 1.32 micron. Figure A.5(B) shows the spot diagram at different wavelengths (λ = 1.27, 1.32, and 1.37 μm). The size of the simulated spot diameter without the tilt of the mirror in that t he beam is focused on the center position is less than 4 micron. In Figure A.5(C), the fraction of enclosed energy versus radius from centroid is shown. When the fraction of enclosed energy is 0.5, which means the FWHM (Full-Width Half-Max) of the spot intensity, the diameter of the spot is approximately 24 μm.

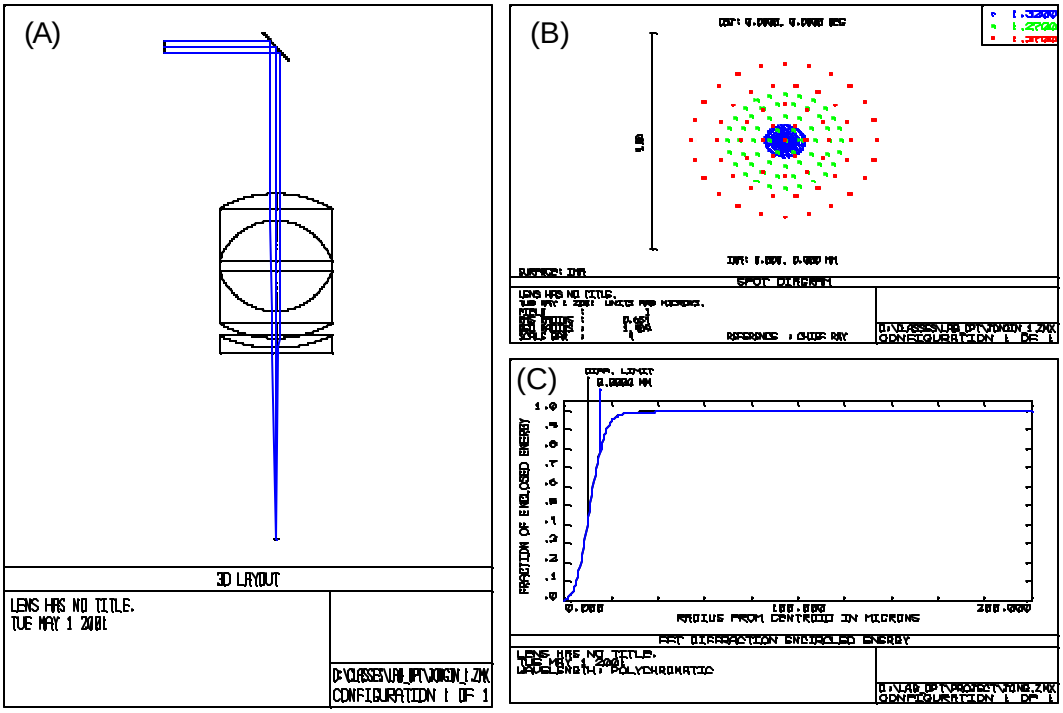

Figure A.5: The ZEMAX simulations; (A) 3-D layout of the scanning lens system, (B) the spot size of the system at the center position (no mirror tilt), and (C) the fraction of enclosed energy versus radius from centroid

There are several options to analyze the aberrations in the optical scanning system in the optical design program, ZEMAX. Figure A.6(A) shows the ray aberrations as a function of pupil coordinate (PX or PY) for the system. The vertical axis scale is given at the bottom of the graph and shows the maximum scale of ± 2 micron. In Figure A.6(B), the field curvature and f-theta distortion is seen. The field curvature plot shows the distance from the currently defined focal (image) plane to the paraxial focal plane as a function of field coordinate.

The tangential data are the distances measured along the Z-axis from the currently defined focal plane to the paraxial focal plane measured in the tangential (YZ) plane. The sagittal data are the distances measured in the plane orthogonal to the tangential plane. The base of the plot is on axis, and the top of the plot represents the maximum field (angle or height). There are no units on the vertical scale because the plot is always normalized to the maximum radial field [7]. In tangential plane, the maximum field curvature is 0.425 degree at the wavelength of 1.32 micron. However, the sagittal plane has less field curvature. In the plot of f-theta distortion (Figure A.6(A)), less than 0.02 percent is occurred.

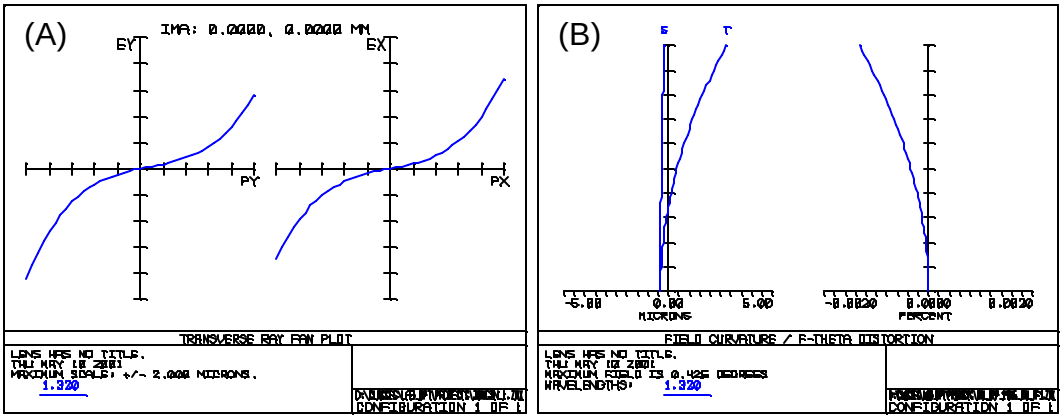

Figure A.6: ZEMAX analysis; (A) Transverse ray fan plot (B) Field curvature and f-theta distortion

Figure A.7(A) displays the longitudinal aberration as a function of pupil height at the wavelength of 1.32 micron. This feature computes the distance from the image surface to where a zonal marginal ray "focuses", or crosses the optical axis.

The computation is performed only for the on axis field point, and only for zonal marginal tangential rays as a function of pupil zone. The base of the plot is on axis, and the top of the plot represents the maximum entrance pupil radius. There are no units on the vertical scale because the plot is always normalized to the maximum entrance pupil radius. The horizontal scale is in lens units, and represents the distance from the image surface to the point where the ray crosses the optical axis [7].

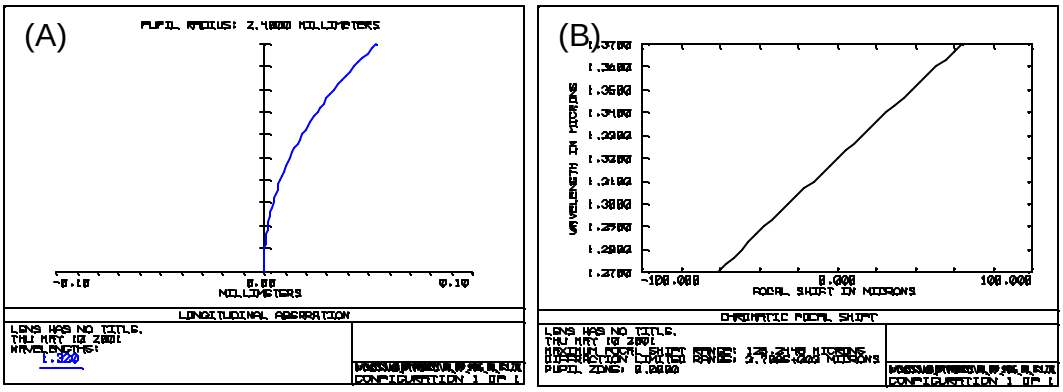

Figure A.7: ZEMAX analysis; (A) Longitudinal aberration (B) chromatic focal shift

In Figure A.7(B), this is a plot of the shift in back focal length with respect to the primary wavelength, 1.32 micron. At each plotted wavelength, the shift in the image plane required to reach paraxial focus for that color marginal ray is computed [7]. The maximum chromatic focal shift is approximately 125.24 micron in the wavelength from 1.27 micron to 1.37 micron.

To demonstrate the movement of a mirror in the Galvanometer scanning system, the mirror is tilted in the ZEMAX software and each spot diagram is acquired from – 0.5 to + 0.5 mm at the interval of 0.1 mm. As seen in Figure 4.4, the spot diameter is not changed over the scanning positions, but the coma effect occurs when the beam is positioned to both edge scanning positions.

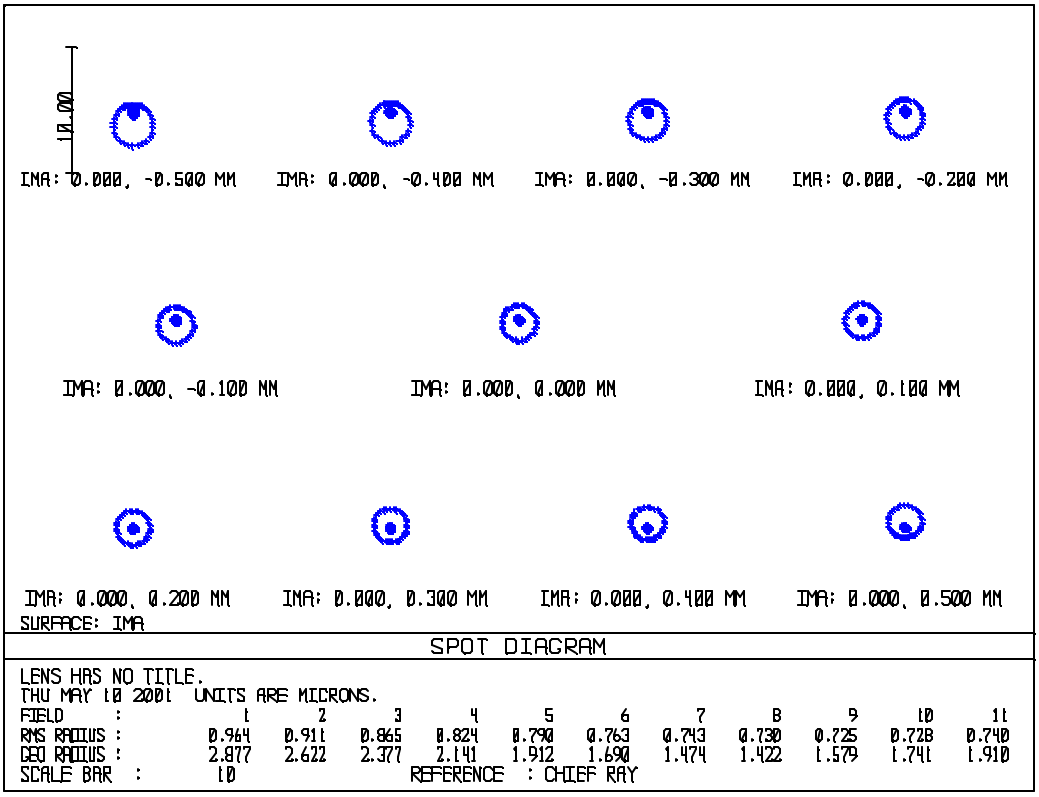

Figure A.8: Various spot diameters over the scan length (1 mm) at the interval of 0.1 mm

With putting all the fractions of enclosed energy distribution at different scanning positions as seen in Figure A.9, the spot diameters at FWHM which has the 50 percent enclosed energy were about 24 micron and did not changed at different scanning positions with the input wavelength of 1.32 micron. "Diff. Limit" in the figure means that a horizontal line indicating the diffraction limited response is drawn on the plot. For RMS radius, x, or y; the diffraction limit is assumed to be 1.22 times the working F/# times the wavelength (primary wavelength if polychromatic) on axis. The change in the diffraction limit due to changes in F/# with field are ignored; a single value is used across the range of the plot. For Strehl ratio, 0.8 is used, and for RMS wavefront, 0.072 waves is used. These are all approximate indicators for convenience only; the actual meaning of "diffraction limited" may be open to interpretation [7].

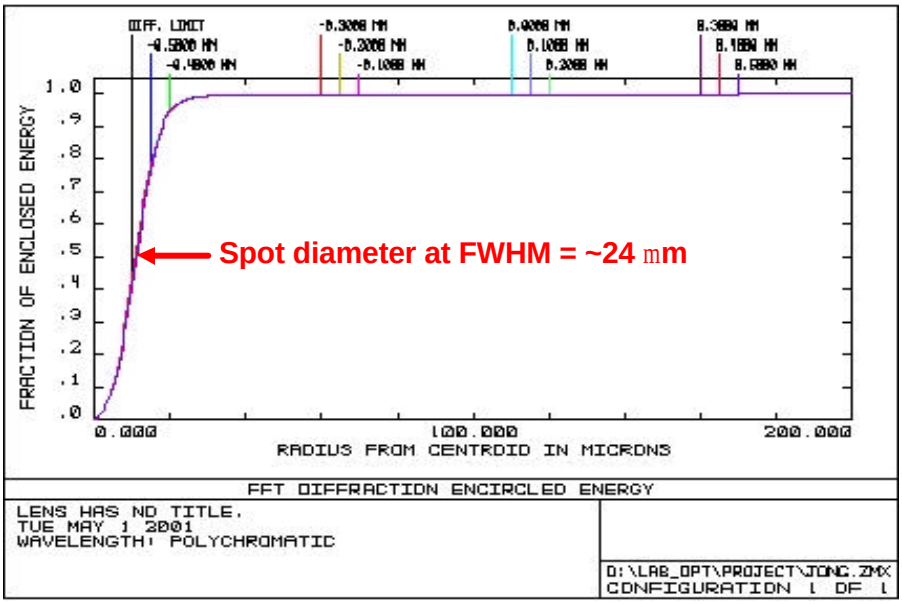

Figure A.9: The fraction of enclosed energy versus radius from centroid in micron over the scan distance, 1 mm at the interval of 0.1 mm

5. Results: Experimental Analysis

For the Scanning lens test experimentally, the setup as seen in Figure A.10 was built to investigate the spot diameters at each scanning position to compare with the computational results. The Galvanometer scanning system is used to tilt a mirror at a certain angle. To set the scanning length of 1 mm, the voltage of 156 mV_{pp} and the frequency of 20 Hz are driven to the Galvanometer using a function generator. With moving the 1 micron slit attached by a broadband photodetector laterally with the xyz translational stage, the gaussian shaped intensity profiles at each position of the scanning length is acquired by a digital oscilloscope. The distance of the FWHM for each gaussian profile over the scanning length is measured.

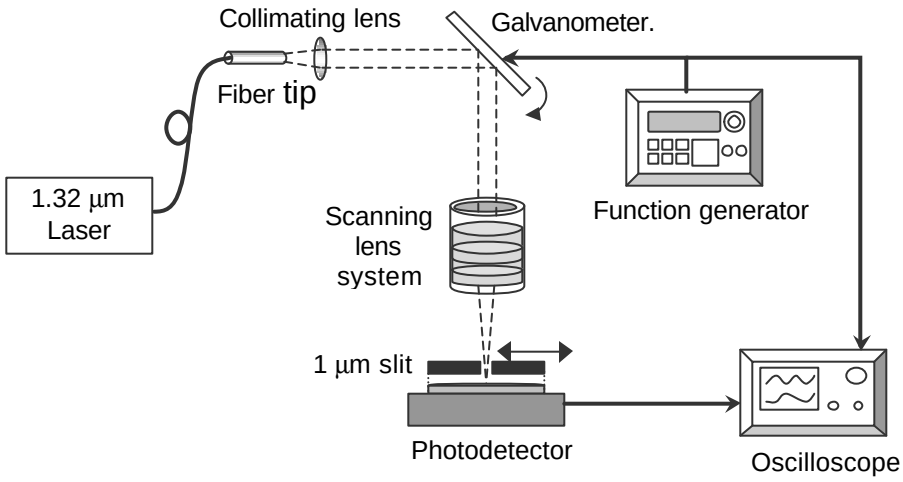

Figure A.10: The schematic of the scanning lens test setup

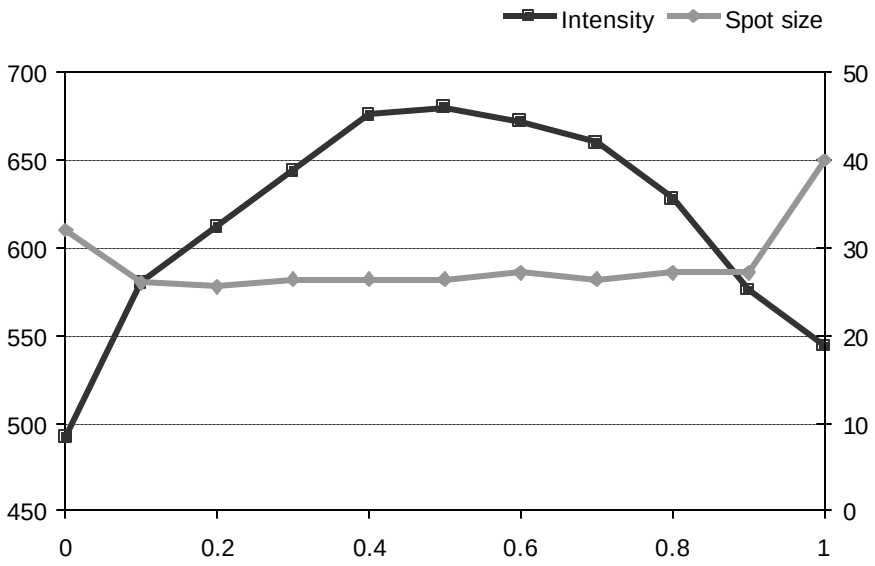

Figure A.11: The intensities and spot diameters over the scanning positions, 1 mm at the interval of 0.1 mm

As seen in Figure A.11, the spot diameters are approximately 26 micron in the middle scanning positions (0.1 ~ 0.9 mm), but somewhat bigger diameters at the edges are observed. This may be due to the mechanical vibration of the Galvanometer scanning system at the edges or other possible aberrations. In the intensity profile, it's parabolic shape over the scanning distance.

6. Summary and Conclusions

For computational analysis, an optical design program, ZEMAX®, was used to demonstrate the optical scanning system and measure spot diameters for 1 mm

scanning length. The numerical estimate for the spot diameter was approximately 24 μm and the spot diameter was not changed at the overall scanning distance. For experimental analysis, a collimated broadband laser source (λ = 1.32 μm) and Galvanometer scanning system was used to measure spot diameters by moving 1 μm slit attached to a photodetector longitudinally. The experimental values of the spot diameters were approximately 26 μm. From overall the results that acquired both computationally and experimentally, the spot diameters were relatively consistent.

For the future work, building a beam expander that needs to be placed in front of the Galvonometer and testing the optical scanning system should be performed. The integration of the optical scanning system to the sample path of the phase sensitive optical coherence reflectometer will allow us to lateral scanning as well as depth scanning.

6. References

1. Marshall G. F., "*Optical Scanning*", Marcel Dekker, Inc., New York, 1991
2. Hecht E., "*Optics*", 2nd edi., Addison-Wesley, Mass., 1987
3. Dave DP., Milner TE., "Optical low-coherence reflectometer for differential phase measurement", *Opt. Lett.*, vol.25, 227-229, 2000
4. Tearney G. J., Bouma B. E., Fujimoto J. G., "High-speed Phase- and Group-delay Scanning with a Grating-based Phase Control Delay Line", *Opt. Lett.*, 22, 1811-1813, 1997
5. Wolf E., Born M., "*Principles of Optics*", 7th edi., Cambridge university press, Cambridge, MA, 1999
6. Ahmad A., "*Optomechanical Engineering Handbook*", CRC Press, 1999
7. Software manual, "ZEMAX: Optical Design Program", User's Guide, ver. 9.0, Focus Software Inc., 2000

BIBLIOGRAPHY

Ahmad A., *"Optomechanical Engineering Handbook"*, CRC Press, 1999

Bagratashvili V. N, Sobol E. N, Sviridov A. P, Popov V. K, Omel'chenko A. I, Howdle S. M, "Thermal and Diffusion Processes in Laser-Induced Stress Relaxation and Reshaping of Cartilage", *J. Biomech.*, **30(8)**: 813-817, 1997

Bassett C. A. L., Pawluk R. J., "Electrical Behavior of Cartilage during Loading", *Science*, **178**: 982-983, 1972

Beauchamp K. G., Yuen C. K., *"Digital Methods for Signal Analysis"*, George Allen & Unwin, London, UK, 1979

Berkenblit S. I., Frank E. H., Salant E. P., Grodzinsky A. J., "Nondestructive Detection of Cartilage Degeneration using Electromechanical Surface Spectroscopy", *Trans. ASME*, **116**: 384-392, 1994

Bigio I. J., Mourant J. R., "Ultraviolet and Visible Spectroscopies for Tissue Diagnostics: Fluorescence Spectroscopy and Elastic-scattering Spectroscopy", *Phys. Med. Biol.*, **42**: 803-814, 1997

Born M., Wolf E., *"Principles of Optics"*, 7th edi., Cambridge Univ. Press, 1999

Bragg W. L., Pippard A. B., "The form birefringence of macromolecules", *Acta Cryst*, **6**: 865-867, 1953

Brosseau C., *"Fundamentals of polarized light: A statistical optics approach"*, John Wiley & Sons, New York, NY, 1998

Camacho N. P., West P., Torzilli P. A., Mendersohn R., "FTIR Microscopic Imaging of Collagen and Proteoglycan in Bovine Cartilage", *Biopolymers (Biospectroscopy)*, **62**:1-8, 2001

Caplan A. I., "Cartilage", *Scientific American*, **251(4)**: 84-94, 1984

Carroll R. J., Ard J. S., Susi H., "The Infrared Spectrum and Water Binding of Collagen as a Function of Relative Humidity", *Biopolymers*, **10**:1597-1604, 1971

Cheong W. F., Prahl S. A., Welch A. J., "A Review of the Optical Properties of Biological Tissues", *IEEE J. Quant. Elec.*, **26(12)**: 2166-2184, 1990

Dave D. P., Milner T. E., "Optical Low-Coherence Reflectometer for Differential Phase Measurement", *Opt. Lett.*, **25**: 227-229, 2000

De Boer J. E., Milner T. E., Nelson J. S., "Determination of the depth resolved Stokes parameters of light backscattered from turbid media using polarization sensitive optical coherence tomography", *Optics Letters*, **24**: 300-302, 1999

Dong A., Randolph T. W., Carpenter J. F., "Entrapping Intermediates of Thermal Aggregation in a-Helical Proteins with Low Concentration of Guanidine Hydrochloride", *J. Biol. Chem.*, **275**:27689-27693. 2000

Doyle B. B., Bendit E. G., Blout E. R., "Infrared Spectroscopy of Collagen and Collagen-Like Polypeptides", *Biopolymers*, **14**:937-957, 1975

Ducros M. G, De Boer J. E., Huang H. E., Chao L. C., Chen Z., Nelson J. S., Milner T. E., Rylander III H. G., "Polarization sensitive optical coherence tomography of the rabbit eye", *IEEE J. of Selected Topics in Quantum Elec.*, **5(5)**: 1159-1167, 1999

Fabian H., Mantsch H. H., "Ribonuclease A Revisited: Infrared Spectroscopic Evidence for Lack of Native-like Secondary Structures in the Thermally Denatured State", *Biochemistry*, **34**:13651-13655, 1995

Frank E. H., Grodzinsky A. J., "Cartilage Electromechanics I: Electrokinetic Transduction and the Effects of Electrolyte pH and Ionic Strength", *J. Biomechanics*, **20**: 615-627, 1987

Frank E. H., Grodzinsky A. J., "Cartilage Electromechanics II: A Continuum Model of Cartilage Electrokinetics and Correlation with Experiments", *J. Biomechanics*, **20**: 629-639, 1987

Frenkel J., "On the Theory of Seismic and Seismoelectric Phenomena in a Moist Soil", J. Phys. U.S.S.R. **8**: 230-241, 1944

Gray H., "*Gray's Anatomy*", Gramercy Books, New York, 1977

Grodzinsky, A. J., "Electromechanical and Physicochemical Properties of Connective Tissue", *CRC Crit. Rev. Biomed. Eng.*, **9**: 133-199, 1983

Hale G. M., Querry M. R., "Optical Constants of Water in the 200-nm to 200-mm Wavelength Region", *Applied Opt.*, **12(3)**: 555-563, 1973

Hall B. K., *"Cartilage: Structure, Function, and Biochemistry"*, vol. 1, Academic Press, New York, 1983

Hecht E., "*Optics*", 2nd edi., Addison-Wesley, Mass., 1987

Kaplan P. D., Dinsmore A. D., Yodh A. G., Pine D. J., "Diffuse-Transmission Spectroscopy: A structural probe of opaque colloidal mixtures", *Phys. Rev.*, **50(6)**: 4827-4835, 1994

Khosrofian J. M., Garetz B. A., "Measurement of a Gaussian Laser Beam Diameter through the Direct Inversion of Knife-Edge Data", *Appl. Opt.*, **22**(21): 3406-3410, 1983

Kiraly K., Hyttinen M., Parkkinen J., Arokoski J., Lapvetelainen T., Torronen K., Kiviranta I., Helminen H. J., "Articular cartilage collagen birefringence is altered concurrent with changes in proteoglycan synthesis during dynamic in vitro loading", *The Anatomical Record*, **251**: 28-36, 1998

Kovach I. S., Athanasiou K. A., "Small-Angle He:Ne Laser Light Scatter and the Compressive Modulus of Articular Cartilage", *J. of Orthopaedic Res.*, **15**: 437-441, 1997

Krimm S., Bendekar J., "Vibrational Spectroscopy and Conformation of Peptides, Polypeptides, and Proteins", *Adv. Protein Chem.*, **38**:181-364, 1986

Lai W. M., Mow V. C., Ateshian G. A., "On the Electric Potentials Inside a Charged Soft Hydrated Biological Tissue: Streaming Potential Versus Diffusion Potential", *Trans. ASME*, **122**: 336-346, 2000

Levich V. G., *"Physicochemical Hydrodynamics"*, Prentice-Hall, Englewood Cliffs, NJ, 1962

Lotke P. A., Black J., Richardson S. J., "Electromechanical Properties in Human Articular Cartilage", *J. Bone Joint Surg.*, **56-A**: 1040-1046, 1974

Madsen S. J., Chu., Wong B. J. F., "The Optical Properties of Porcine Nasal Cartilage", IEEE J. Selected Topics Quantum Elec., **5**:1127-1133, 1999

Maitland D. J., Walsh Jr. J. T., "Quantitative measurements of linear birefringence during heating of native collagen", *Laser Surg. Med.*, **20**: 310-318, 1997

Manning G.S., "The Molecular Theory of Polyelectrolyte Solutions with Applications to the Electrostatic Properties of Polynucleotides", *Quart. Rev. Biophy. II*, **11**:179-246, 1978

Maroudas A., "Physicochemical Properties of Articular Cartilage", *Adult Articular Cartilage*, Freeman, M.A.R. ed., Pitman Medical, Kent, England, 2nd ed., 215-290, 1979

Maroudas A., Schneiderman R., "Free and Exchangeable or Trapped and Non-Exchangeable Water in Cartilage", *J. Orthoped. Res.*, **5**:133-138, 1987

Marshall G. F., "*Optical Scanning*", Marcel Dekker, Inc., New York, 1991

Matijevic E., "*Surface and Colloid Science*", Wiley-Interscience, New York, 49-272, 1974

Mourant J. R., Freyer J. P., Hielscher A. H., Eick A. A., Shen D., Johnson T. M., "Mechanisms of Light Scattering from Biological Cells relevant to Noninvasive Optical-Tissue Diagnostics", *Appl. Opt.*, **37**(16):3586-3593, 1998

Mourant J. R., Fuselier T., Boyer J., Johnson T. M., Bigio I. J., "Predictions and Measurements of Scattering and Absorption over Broad Wavelength Ranges in Tissue Phantoms", *Appl. Opt.*, **36**(4): 949-957, 1997

Mow V. C., *"Injury and Repair of the Musculoskeletal Soft Tissues"*, American Academy of Orthopaedic Surgeons, 1988

NIAMS, "Handout on Health: Osteoarthritis", NIH Publication No. 99-4617, June, 1999

Ovchinnikov Y., Sobol E. N., Shekhter A., Bagratashvili V., Svididov A., "Laser Septochondrocorrection", *Arch Facial Plast. Surg.*, **4**:180-185, 2002

Overbeek J. T. G., *"Electrokinetic Phenomena"*, Colloid Science, vol. 1, Elsevier Publishing Co., Amsterdam, 194-244, 1952

Panick G., Winter R., "Pressure-Induced Unfolding/Refolding of Ribonuclease A: Static and Kinetic Fourier Transform Infrared Spectroscopy Study", *Biochemistry*, **39**:1862-1869, 2000

Perelman L. T., Backman V., Wallace M., Zonios G., Manoharan R., Nusrat A., Shields S., Seiler M., Lima C., Hamano T., Itzkan I., Van Dam J., Crawford J. M., Feld M. S., "Observation of Periodic Fine Structure in Reflectance from Biological Tissue: A New Technique for Measuring Nuclear Size Distribution", *Phys. Rev. Lett.*, **80(3)**: 627-630, 1998

Reihanian H., Jamieson A. M., Tang L. H., Rosenberg L., "Hydrodynamic Properties of Proteoglycan Subunit from Bovine Nasal Cartilage. Self-Association Behavior and Interaction with Hyaluronate Studied by Laser Light Scattering", *Biopolymers*, **18**: 1727-1747, 1979

Setton L. A., Elliott D. M., Mow V. C., "Altered Mechanics of Cartilage with Osteoarthritis: Human Osteoarthritis and an Experimental Model of Joint Degeneration", *Osteoarthritis & Cartilage*, **7**:2-14, 1999

Sobol E. N., *"Phase Transformations and Ablation in Laser-Treated Solids"*, John Wiley & Sons, New York, 1998

Sobol E. N., Bagratashvili V., Omel'chenko A., Sviridov A., Hwlidonis E., Kawalos G., Christodoulou P., Naoumidi I., Velegrakis G., Ovchinnikov Y., Shechter A., "Laser Shaping of Cartilage", *Proc. SPIE*, **2128**: 43-49, 1994

Sobol E. N., Bagratashvili V., Sviridov A., Omel'chenko A., Kitai M., Jones N., Zenger V., Nasedkin N., Isaev M., Karlov V., Schechter A., "Study of Cartilage Shaping with Holmium Laser ", *Proceedings of SPIE*, **2623**: 544-547, 1996

Sobol E. N., Bagratashvili V., Sviridov A., Omel'chenko A., Schechter A., Jones N., Howdle S., Helidonis E., "Phenomenon of Cartilage Shaping using Moderate Laser Heating and Its Application in Otorhinolaryngology", *Proceedings of SPIE,* **2623**: 548-552, 1996

Sobol E. N., Kitai M., Jones N., Sviridov A., Milner T. E., Wong B. J. F., "Theoretical Modeling of Heating and Structure Alterations in Cartilage under Laser Radiation with regard of Water Evaporation and Diffusion Dominance", *Proc., SPIE*, **3254**: 54-63, 1998

Sobol E. N., Sviridov A., Bagratashvili V., Omel'chenko A., Ovchinnikov Y., Shechter A., Downes J., Howdle S., Jones N., Lowe J., "Stress Relaxation and Cartilage Shaping under Laser Radiation", *Proc. SPIE*, **2681**: 358-363, 1996

Sobol E. N., Sviridov A., Omel'chenko A., Bagratashivili V., Kitai M., Harding S. E., Jones N., Jumel K., Mertig M., Pompe W., Ovchinnikov Y., Shekhter A., Svistushkin V., "Laser Reshaping of Cartilage", *Biotech. Gene. Eng. Rev.*, **17**: 539-564, 2000

Software manual, "ZEMAX: Optical Design Program", User's Guide, ver. 9.0, Focus Software Inc., 2000

Sun D. N., Gu W. Y., Guo X. E., Lai W. M., Mow V. C., "A Mixed Finite Element Formulation of Triphasic Mechno-Electrochemical Theory for Charged, Hydrated Biological Soft Tissues", *Int. J. Numer. Meth. Eng.*, **45**: 1375-1402, 1999

Sviridov A., Sobol E. N., Jones N. S., Lowe J., "Effect of Holmium Laser Radiation on Stress, Temperature, and Structure Alterations in Cartilage", Lasers in Med. Sci., **13**:73-77, 1998

Tearney G. J., Bouma B. E., Fujimoto J. G., "High-speed Phase- and Group-delay Scanning with a Grating-based Phase Control Delay Line", *Opt. Lett.*, **22**: 1811-1813, 1997

ThermoNicohlet Corp., "Introduction to Fourier Transform Infrared Spectroscopy", *Product manual*, 2001

Torzilli P. A., "Water Content and Equilibrium Water Partition in Immature Cartilage", *J. Orthoped. Res.*, **6**: 766-769, 1988

Venn M., Maroudas A., "Chemical Composition and Swelling Pressure of Normal and Oseteoarthrotic Femoral Head Cartilage", *Ann. Rheum. Dis.*, **36**:121-129, 1977

Welch A. J., van Gemert M. J. C., *"Optical-Thermal Response of Laser-Irradiated Tissue"*, Plenum Press, New York, 1995

Wolf E., Born M., *"Principles of Optics"*, 7th edi., Cambridge university press, Cambridge, MA, 1999

Wong B. J. F., Milner T. E., Anvari B., Sviridov A., Omel'chenko A., Bagratashvili V., Sobol E. N., Nelson J. S., "Thermo-Optical Response of Cartilage During Feedback Controlled Laser-Assisted Reshaping", *Proceedings SPIE*, **2970**: 380-391, 1997

Wong B. J. F., Milner T. E., Anvari B., Sviridov A., Omel'chenko A., Bagratashvili V. V., Sobol E. N., Nelson J. S., "Measurement of Radiometric Surface Temperature and Integrated Back-Scattered Light Intensity During Feedback Controlled Laser-Assisted Cartilage Reshaping", *Lasers in Med. Sci.*, **13**: 66-72, 1998

Wong B. J. F., Milner T. E., Anvari B., Sviridov A., Omel'chenko A., Bagratashvili V., Sobol E. N., Nelson J. S., "Thermo-Optical Response of Cartilage During Feedback Controlled Laser-Assisted Reshaping", *Proceedings SPIE*, **2970**: 380-391, 1997

Wong B. J. F., Milner T. E., Anvari B., Sviridov A., Omel'chenko A., Bagratashvili V. V., Sobol E. N., Nelson J. S., "Measurements of Radiometric Surface Temperature and Integrated Backscattered Light Intensity During Feedback Controlled Laser-Assisted Cartilage Reshaping", *Lasers in Med. Sci.*, **13**: 66-72, 1998

Wong B. J. F., Milner T. E., Kim H. H., Nelson J. S., Sobol E. N., "Stress Relaxation of Porcine Septal Cartilage during Nd:YAG ($\lambda = 1.32\mu m$) Laser Irradiation: Mechanical, Optical, and Thermal Response", *J. of Biomed. Opt.*, **3(4)**: 409-414, 1998

Wong B. J. F., Milner T. E., Kim H. K., Telenkov S., Chew C., Kuo T., Smithies D. J., Sobol E. N., Nelson J. S., "Critical Temperature Transitions in Laser Mediated Cartilage Reshaping", *Proceedings SPIE*, **3425**: 161-172, 1998

Yarker Y. E., Aspden R. M., Hukins D. W. L., "Birefringence of articular cartilage and the distribution of collagen fibril orientations", *Connective Tissue Research*, **11**: 207-213, 1983

Youn J. I., Telenkov S. A., Kim E., Bhavaraju N. C., Wong B. J. F., Valvano J. W., Milner T. E., "Optical and Thermal Properties of Nasal Septal Cartilage", Lasers Surg. Med., **27**:119-128, 2000

VITA

Jong-In Youn was born on 22 November 1973 in Pusan, Korea, to Tae-Sun Youn and Wae-Soo Kim. Upon graduating from Chung-Ryeul High School in Pusan, Korea, in 1992, he enrolled at Inje University in Korea, and majored in Biomedical Engineering with a specialization in tissue engineering and controlled modification of biomaterials. During his junior year, he worked as a research assistant to Dr. Sung-Soo Kim in the Department of Biomaterials at the Korea Research Institute of Chemical Technology, and contributed to various projects investigating cell biocompatibility on the surface of polymers utilized for artificial vessels and other biological implants. After graduating from Inje University in 1997, he enrolled in the biomedical engineering graduate program at The University of Texas at Austin in the fall of 1997 to pursue a Master's and also Ph.D. degrees.

Since arriving at The University of Texas at Austin, he has been involved in laser-tissue interaction studies under the supervision of Dr. Thomas E. Milner. He earned M.S.E degree in the summer of 1999 entitled as "Laser-Mediated Cartilage Reshaping: Thermal, Optical, and Quasi-Elastic Light Scattering Studies. In his dissertation work, he studied non-invasive optical diagnostics of cartilage for laser-assisted cartilage reshaping and osteoarthritis disease.

Permanent Address: 1480 Hyundai Hometown 1 Cha, 107-803, Koje 1 Dong,
Yeonje-Gu, Pusan,
Korea, 613-071

This dissertation was typed by Jong-In Youn.